Heat-transfer modelling in freeze-drying and related processes

Rudolf Kohulák

A dissertation submitted in partial fulfillment

of the requirements for the degree of

Doctor of Philosophy

of

University College London

UCL Department of Mathematics

University College London

September 10, 2020

I, Rudolf Kohulák, confirm that the work presented in this thesis is my own. Where information has been derived from other sources, I confirm that this has been indicated in the work.

Abstract

Freeze-drying is a process extensively used in the pharmaceutical industry as a solution on how to reduce the water content of temperature-sensitive materials and increase their stability and shelf life. However, at the moment, freeze-drying remains the most expensive stage of pharmaceutical manufacturing, and hence further modelling is needed. To model the process, Stefan problems are considered. A numerical method based on the level set approach and compact finite differencing is developed and adapted for solidification scenarios. Various one and two-dimensional solidification problems are considered. These include solidification in a rectangle with Dirichlet and convective flux boundary conditions. To further investigate the behaviour of the model analytically, small time asymptotic solutions have been developed and used to start the numerical computation. The model is later extended to simulate the freezing process on multiple three-dimensional vials with simplified cuboid geometry. The extended model is used to investigate the 'edge vial' effect caused by non-symmetrical heat transfer inside the freeze-drying chamber. The results are presented that show that under certain conditions, the 'edge vial' effect can cause non-uniformity in freezing rates of the edge and corner vials when compared to the centre vials. Lastly, a novel heuristic model of freezing is developed based on dynamics of chemical reactions. The model is investigated analytically and asymptotic solutions are presented in different time scales and compared to full numerical simulations. The results show a good agreement between the asymptotic and numerical solutions.

Impact Statement

Freeze-drying or lyophilisation is a process widely using within the pharmaceutical industry. It is used to remove water content from the product hence greatly improving the stability and shelf life. Due to its very long duration and the environment in which it needs to be performed, freeze-drying is currently one of the most expensive stages during the whole manufacturing process. Therefore, there is great industry interest in understanding the underlying processes better to drive the manufacturing costs down.

From a physical standpoint, lyophilisation represents a complex heat and mass transfer problem. A lot of effort has been put into trying to experimentally determine the physical parameters of the procedure as well as the final outcomes. However, relying purely on experimental data perhaps provides only a limited understanding of the fundamental drivers and their interactions. Moreover, the optimisations of the process can only rely on costly trial-and-error methods.

Mathematical modelling is, therefore, a crucial element in determining optimal process parameters. There has been a significant amount of work done in modelling different aspects of freeze-drying. However, most of the current models do not take into consideration all the spatial variabilities both inside the vials where the product is stored during the process and across the whole freeze-drying chamber. What we are trying to understand in this work is how these variables might impact the final product.

The models and methods developed in this work can provide a useful tool for studying freezing stage of the freeze-drying processes, as well as other solidification scenarious such as casting of metals. In particular we have developed a

solidification model that is capable of capturing most of the important parameters of freezing pharmaceutical products in vials, whilst still being relatively simple and quick to run in comparison to commercial solvers.

It was observed in practice that sometimes the final freeze-dryer is not in a form of a flat porous cake, but instead it is skewed to one side. Better knowledge and more accurate modelling of all the temporal and spatial differences within the samples can provide a key understanding behind certain unusual shapes of the final product. Although, investigation of these phenomena is outside the scope of this work, different freezing rates could alter the crystal structure of the frozen product, resulting in different sublimation rates in subsequent stages. Furthermore, models presented here could be extended to study the drying stage of the process. Currently, a lot of product is discarded purely because it does not pass the quality control tests. Insights into whether or how non-uniform process parameters influence the final state of the finished product could also greatly reduce the waste and hence the costs.

Acknowledgements

Firstly, I would like to thank my two supervisors, Prof Frank Smith, from the UCL Department of Mathematics and Prof Ajoy Velayudhan from UCL Department of Biochemical Engineering for their help, guidance and patience throughout this project. Without their inputs and discussions, I do not think it would be possible to for this project to reach this stage.

I am also grateful to my parents Renata Kohuláková and Otto Kohulák for supporting me and providing me with the opportunities that eventually lead me here.

My gratitude also goes to my long-term girlfriend Steffi who stood by my throughout ups and downs of the PhD process.

Lastly, I would like to thank my colleagues and dear friends from the UCL Department of Mathematics. Especially, to the members of so-called "SuperKLB Group", Rafael, Pietro, Alex, Hugo, Mihai, Dimitris, Niki, and even Fabian, for their engaging discussions, heated constructive arguments and moral support.

Contents

1 Introduction **11**

1.1 Freeze-drying 14

1.2 Stages of Freeze-drying 15

1.3 Review of Literature 16

1.4 Stefan Problem 18

1.5 Formulation of Classical Stefan Problem 18

1.5.1 Non-dimensional form 20

1.6 Two-Phase Problem 21

1.7 Stefan Condition 21

1.8 Multiple Space Dimensions 22

1.9 Further Generalisations 23

1.10 Alternative Form of Stefan Condition 23

2 Level Set Method **26**

2.1 Introduction 26

2.2 Level Set Equation 28

2.3 Reinitialisation 29

2.4 Numerical Discretisation 31

2.4.1 Preliminaries 31

2.4.2 ENO Schemes 34

2.4.3 WENO Schemes 36

2.4.4 TVD Runge-Kutta 42
2.5 Other Level Set Schemes 45
2.5.1 Narrow Banding 45
2.5.2 Stationary Level Set Formulation 46
2.5.3 Fast Marching Level Set 46
2.6 Summary 48

3 Compact Finite Differencing 49
3.1 Boundary Interpolation Method 49
3.2 Compact Finite Difference Approximations 54
3.3 Boundary Conditions 57
3.3.1 Dirichlet Boundary Conditions 57
3.3.2 Neumann Boundary Conditions 58
3.3.3 Robin Boundary Conditions 59
3.4 Summary 60

4 Level Set Method and Solidification 62
4.1 Introduction 62
4.2 Solidification 63
4.3 Numerical Discretisation 65
4.4 Summary 67

5 Single Vial Model Discussion 69
5.1 Freezing of a Semi-infinite Slab 69
5.2 Cylinder Problem 71
5.2.1 Analytical Solution 72
5.3 Single Vial Model 74
5.3.1 Small Time Solution with Dirichlet Boundary Condition 75
5.3.2 Small Time Solution with Robin Boundary Condition . . 77
5.3.3 Single Vial Model Results 80
5.4 Volume Change 81
5.4.1 Mathematical Model with Density Change 85

5.4.2 Volume Change Model Results 87
5.5 Summary 88

6 Heat transfer modelling of a tray of vials 90
6.1 Introduction 90
6.2 Heat transfer inside the vial 92
6.2.1 Solving the field equation 95
6.2.2 Interior nodes 96
6.2.3 Boundary nodes: Dirichlet condition 97
6.2.4 Boundary nodes: Neumann/Robin condition 98
6.3 Time stepping 99
6.3.1 Basic derivation of ADI scheme 100
6.3.2 Compact ADI Scheme 103
6.4 Heat transfer between the vials 106
6.4.1 Radiation heat transfer 107
6.4.2 Solving the heat flux equation 109
6.5 Two-stage Model Results 112
6.6 Summary 124

7 Chemical Model of Freezing 125
7.1 Introduction 125
7.2 Chemical reactions 125
7.3 The model 126
7.4 Numerical results 128
7.5 Large β solution 134
7.5.1 Boundary layer 135
7.5.2 Comparison 138
7.6 Summary 140

8 Discussion and conclusions 141

Appendices 143

A Two-stage Model Additional Figures **144**

References **159**

Chapter 1

Introduction

In recent decades, the freeze-drying process has become increasingly popular in pharmaceutical manufacturing. It presents a simple answer on how to significantly decrease the water content of temperature-sensitive substances and hence increase their stability and shelf life. Nevertheless, at this stage, freeze-drying is one of the most expensive stages in the manufacturing of pharmaceuticals, and therefore, a further study of the underlying processes and better mathematical models are required.

Although there has been some research conducted in developing mathematical models for the freeze-drying processes, most of the practical applications and optimisation procedures still rely on a "trial and error" basis [59, 13].

We aim to explore the first stage of the process, the freezing stage. We are interested in determining the progression of the interface between the liquid and solidified regions. The objective here is to be able to predict the time taken to complete solidification and to develop a robust numerical method that is able to extend the work to complex or three-dimensional shapes of vial and shapes of the moving interface, which may include topological changes. The general problems of this type were extensively studied by Joseph Stefan in the 19th century and are now often referred to as Stefan problems.

Following some modelling and simplifications, we consider multiple solidification problems. The first one is a simpler model concerning solidification

in a rectangle with Dirichlet boundary conditions imposed on all sides, which resemble a simplified scenario for freezing a substance in a vial during freeze-drying. In the second model, the Dirichlet boundary conditions are replaced by convective heat flux conditions based on Newton's law of cooling.

Furthermore, we will develop a model that, as well as tracking the solidification interface inside a single vial, also takes into consideration heat transfer between vials that are placed on a tray inside the freeze-frying chamber. This will allow us to study the impact of different heat transfer rates experienced by the "edge vials" which are placed along the edges of the vial tray and "centre vials" positioned in the middle of the tray [43, 48].

We shall develop a numerical scheme based on the level set method and compact finite differencing and test it against analytical solutions for the freezing on a semi-infinite slab and inward solidification of a cylinder. Further, we present an extension of the model to include the effects of density change across the solidification interface.

The rest of the document is structured as follows. In the remaining sections of this chapter, we provide a more detailed introduction into free-drying processes followed by a brief discussion on Stefan problems; these form a mathematical model for solidification that will provide the basis of our own modelling. Here, we will also present an alternative form of the boundary condition on the solidification interface.

Chapter 2 provides a set-up for level set methods. We highlight the basic motivation for the level set method in section 2.1, as well as, we deriving the *level set equation* responsible for tracking the free boundary between the solid and the liquid regions in section 2.2. The *reinitialisation* procedures are covered in section 2.3. The remainder of the chapter 2 is concerned with the issues of numerical discretisation in section 2.4 and an introduction to different versions of level set methods in section 2.5, such are Fast Level Set methods or Narrow Banding.

In chapter 3 we develop a method based on compact differencing. The

main idea behind this approach is to create a numerical scheme capable of maintaining high accuracy in the neighbourhood of the moving boundary without the need of using finer computational grid or adaptive meshes. The section 3.3 deals with adapting this approach to different sets of boundary conditions.

The application of level set methods to solidification scenarios is discussed in chapter 4. In particular, we look at how the free boundary conditions from the solidification model can be implemented in the level set setting in section 4.2. Section 4.3 then deals with the numerical discretisation of the procedure. Finally, the whole algorithm is summarised in section 4.4.

In chapter 5 we apply the numerical procedure developed in chapter 4 to three solidification scenarios. Firstly, we use the method in two simple problems of freezing in a semi-infinite slab and inward solidification of a cylinder in section 5.1 and 5.2, respectively. We also compare the results to the analytical solutions. In section 5.2, we describe the first problem used to model the heat transfer and progression of the interface inside a single vial. We also present the asymptotic small-time solution to the problem used in starting the numerical procedure.

The chapter 6 introduces the second model used for computing the heat transfer on a tray of vials. A two-stage procedure is implemented. The first scale described in section 6.2 deals with the heat transfer inside a single vial. The model is similar to the single vial model implemented in chapter 5; however, the governing equation is slightly modified along with the boundary condition. This first scale model is applied to all of the vials on the tray. In section 6.2.1, we develop a new compact finite difference scheme to be applied to the governing equation for this particular single vial model. Section 6.3 discusses the ADI method applied to this specific compact differencing. The second scale of the two-stage model is developed in section 6.4. The model is summarised in section 6.5 along with the results.

Chapter 7 is a standalone chapter where we develop a model of solidification inspired by combustion theory. Here we model freezing as if it was a

chemical reaction between the solidified and liquid regions. Firstly the chemical model is solved numerically and subsequently, the numerics are compared to the asymptotic solution that is developed in section 7.5.

Finally, we provide some concluding remarks in chapter 8.

1.1 Freeze-drying

Freeze-drying or lyophilisation is a manufacturing process widely used for the dehydration of products via sublimation. In particular, it is used for materials of biological nature that are temperature sensitive. Although industry applications of freeze-drying are far-reaching, we are primarily interested in Lyophilisation applications in manufacturing pharmaceutical products in vials. The main advantages of the freeze-drying processes are increased stability of the product due to reduced water levels, cheaper transportation cost, more easily controlled environment and hence less chance of contamination and possibility of instant reconstruction by adding a diluent [40].

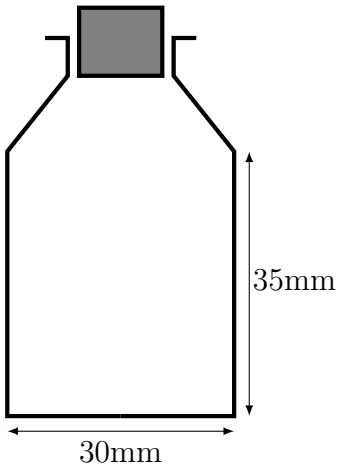

Figure 1.1: An illustration of a 20ml freeze-drying vial. The top of the vial is usually sealed with a rubber stopper (gray)

The main draw-backs of the freeze-drying lie in the very high cost and long time associated with the process. Depending on the size of the products, the whole process could take weeks. Moreover, not all products are suitable for freezing. Certain labile products such as liposomes or viruses can be damaged during freezing [55]. Some issues can also arise assurance of sterility of the freeze-drying chamber during loading and unloading of the product [55]. Moreover, there has been some stability problems associated with individual drugs [23].

Proteins, peptides and complex synthetic organic molecules are substances most frequently freeze-dried in the context of pharmaceutical industry [13]. In literature, 3%–5% solutions of mannitol or sucrose are usually used for experimental settings. We will base our mathematical models on 4% mannitol solution. The basic physical properties of this solution are taken from [46] and stated in table 1.1.

Density (kg/m^3)	Heat capacity (J/(kg K))	Thermal conductivity (W/(K m))
1001.5	3950	0.55

Table 1.1: Relevant physical properties of 4% mannitol solution.

Two main methods of freeze-drying are the bulk method and batch methods. In the bulk method, the product is poured into a pan and freeze-drying as a single unit [23]. The issue with this method is that the product cannot be sealed during the process. This method is usually reserved for a solution that is not sensitive to exposure to oxygen or moisture. Moreover, the sterility of the product is harder to maintain.

Therefore, pharmaceutical products are mostly freeze-dried using the batch method. During this procedure, the product is placed into similarly shaped vessels or vials, which are placed on a tray. Typical dimensions of these vials are depicted in figure 1.1.

1.2 Stages of Freeze-drying

The freeze-drying process consists of three main stages; Freezing stage and primary and secondary drying stages.

Freezing Stage

During the freezing stage, the vials are placed inside the freeze-drying chamber, and the temperature is gradually dropped below the triple point. The primary purpose of this stage is to separate the solvent from the solutes, prevention of the concentration of the drug during the drying stage, reduction of thermal degradation of product and prevention of foaming during drying when the

pressure is dropped [40].

In particular, the glass transition temperature of the solution to ensure the product is fully solidified. Depending on the solution, the temperature of the shelf is usually around -40°C.

Primary Drying Stage

After complete solidification of the product, the pressure in the freeze-drying chamber is lowered, and heat is applied to initiate the sublimation of ice [40]. During this stage, the temperature of the product is kept at around -15°C. The application of a partial vacuum grants movement of vapour from the solidified product [40]. During the primary drying stage, the temperature of the product will be significantly lower than that of the shelf due to the sublimation process and will only rise at the end of the stage [40].

Secondary Drying Stage

Upon the completion of the primary drying phase, there might still be some residual moisture left in the product. Although the water content has been significantly reduced, the moisture left can decrease the desired stability of the final product. The secondary drying stage is, therefore required. During this stage, the temperature of the shelf is increased (often above 0°C), and the partial pressure of water vapour is decreased so that the moisture is removed by desorption [40].

Although all of the stages of the freeze-drying process are of great importance, we will here solely focus on modelling the freezing stage only. This study might be particularly relevant to certain products that are not suitable for drying and are kept in the frozen state. In particular, we are interested in the solidification process of a single vial.

1.3 Review of Literature

The modelling freeze-drying is a complex problem. In order to model the procedure accurately, one needs to take into account all the stages simultaneously.

However, as mentioned previously, in this work, we shall solely focus on the freezing stage of the process. Nevertheless, even in this narrow focus, many approaches are worth exploring. For instance, one might take a "micro" level approach where the attention is focused on studying the nucleation stage of the freezing and the attention of devoted to calculating the shape and the average size on the ice crystals. Such studies were conducted by [17, 32, 24, 36].

The second approach, also employed in this work, to the problem, can be described as "macro" level. Here the attention is focused on calculating the overall shape and the progressing of the solidification interface, as well as the time taken to complete solidification.

From the macro-level perspective, the first stage of the freeze-drying process can also be referred to as an inward solidification problem. Due to their wide practical applications, these problems have been widely studied in the past. However, the complexity of the problems and non-linear nature of the condition on the moving boundary means that only very few analytical solutions have been found and they are usually restricted to fairly specific cases [42]. Numerical methods and approximations to exact solutions were therefore developed.

Generally, the numerical schemes can be divided into two categories. The strong numerical methods apply finite difference and finite element methods to the strong formulation of the problem [3]. The moving front is often immobilised by a change of the coordinate system or simply locating the moving boundary and temperature field distribution at each time step [3]. These methods are predominantly applied to one-dimensional cases, but they can be generalised to two-dimensional scenarios, as well.

Weak numerical methods allow us to track the moving boundary explicitly and are usually easily extended to multi-dimensional cases [3]. In this category fall the enthalpy methods which allow for a solution in the fixed domain with no modification of the numerical scheme (see, e.g. [67, 3]).

Approximate analytical methods were developed by Riley et al. [45],

who devised perturbation solutions in spherical and cylindrical coordinates. Assuming that ratio of latent heat and specific heat of the fusion (β) is large, [45] used asymptotic power series expansions of temperature field and time in β and later applied a two-region analysis near the complete solidification. Although these methods are strictly asymptotic in nature, they compared well with the full numerical methods used [45].

Tao in [61] devised general finite difference numerical schemes for freezing liquids contained in containers with spherical or cylindrical geometry. Poots [39] looked at applications of the integral methods comparable to those used in fluid mechanics in the solution of boundary layer equations.

Voller in [67] took the enthalpy methods used in one-dimensional problems and extended them to handle cylindrical and spherical coordinates. The enthalpy methods were later generalised by Cao et al. [3] and applied to multi-dimensional Stefan Problems (we will provide a more general discussion on Stefan Problems in sections 1.5 and 1.8).

1.4 Stefan Problem

We shall now introduce a general category of free-boundary problems called Stefan problems. The name is attributed to Joseph Stefan, who was interested in free-boundary problems when studying the melting of the polar caps in the early 1890s [7]. Stefan derived a large latent heat approximation for the problem. Later he adapted the solution to time-dependent surface temperature [7]. For single-phase problems, he developed a solution in terms of the error function and supplied second-order approximation, as well as [7].

1.5 Formulation of Classical Stefan Problem

Firstly, let us consider a simple one-dimensional freezing problem. Assume that a semi-infinite sheet of water is located in the region $x \in [0, \infty)$ and kept initially at fussion temperature. Let us, for simplicity, take the freezing temperature to be 0. At time $t = 0$ the surface of the water is lowered to a temperature $T = T_c$ with $T_c < 0$ at which it is subsequently maintained. Let

$x = f(t)$ be the position of the solidification interface that separates the liquid phase from the solid one. Assuming that heat flows by conduction only the temperature distribution $T(x,t)$ in the $x-t$ plane satisfies

$$k\frac{\partial^2 T}{\partial^2 x} = c\rho\frac{\partial T}{\partial t},\ 0 < x < f(t),\ t > 0 \tag{1.1}$$

subject to

$$T(0,t) = T_c,\ t > 0 \tag{1.2}$$

and

$$T(x,0) = 0,\ x > 0,\ f(0) = 0 \tag{1.3}$$

where c denotes the specific heat, ρ density and k heat conductivity.

Since the moving boundary $f(t)$ is unknown, two more conditions on the moving interface are needed. One gives another boundary condition for the temperature distribution while the second is required in order to determine the the solution for the moving boundary itself [7]. On top of the conditions 1.2 and 1.3, the problem 1.1 further satisfies

$$T(f(t),t) = 0,\ t > 0 \tag{1.4}$$

and

$$k\frac{\partial T}{\partial x}\bigg|_{x=f(t)} = H\rho\frac{df}{dt},\ t > 0. \tag{1.5}$$

Here H represents the latent heat of fussion. It describes the amount of heat released or absorbed in order for a unit mass of a substance to change phase. Condition 1.4 simply states that the freezing occurs at the freezing temperature $T = 0$. The condition 1.5 is also referred as the Stefan condition and we will explain the derivation of 1.5 in section 1.7. Let us first look at the non-dimensional form of a classical Stefan Problem.

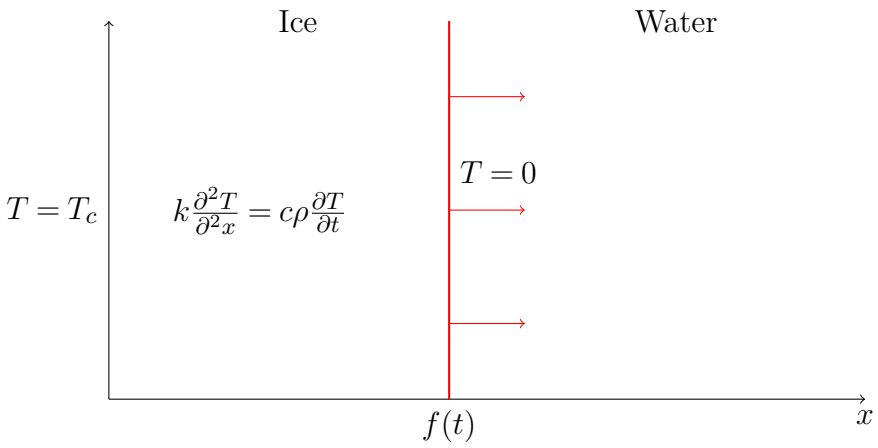

Figure 1.2: Illustration of a classical Stefan Problem at time $t > 0$. The red line corresponds to the position of the interface $f(t)$. The arrows indicate the movement of the interface.

1.5.1 Non-dimensional form

Let us scale all the quantities by introducing the non-dimensional variables

$$\tilde{x} = \frac{x}{L},\ \tilde{y} = \frac{y}{L},\ \tilde{f} = \frac{f}{L} \text{ and } \tau = \frac{tk\Delta T}{\rho H L^2}.$$

Moreover, let

$$\theta = \frac{T - T_c}{\Delta T},$$

then the initial governing equation reduces to

$$\frac{\partial^2 \theta}{\partial \tilde{x}^2} = \frac{1}{\beta}\frac{\partial \theta}{\partial \tau}. \tag{1.6}$$

Here β is a non-dimensional Stefan number given by

$$\beta = \frac{H}{c\Delta T}. \tag{1.7}$$

Furthermore, the Stefan condition on the moving boundary becomes

$$\left.\frac{\partial \theta}{\partial \tilde{x}}\right|_{\tilde{x}=\tilde{f}(\tau)} = \frac{d\tilde{f}}{d\tau}. \tag{1.8}$$

In freeze-drying applications β is relatively large $O(10^2)$. Therefore in the

single vial model in chapter 5 we will use a quasi-steady state approximation to (1.6) by using

$$\frac{\partial^2 \theta}{\partial \tilde{x}^2} = 0, \tag{1.9}$$

instead. We in the remaining sections of this chapter we will introduce different generalisations to the classical Stefan problem.

1.6 Two-Phase Problem

Let us consider a sheet of ice located in the region $x \in [0, l]$. The ice sheet is initially kept at temperature $T = T_a$ below the freezing temperature 0. Hence the heat flows in both the liquid and solid phases. Let T_1 and T_2 be the temperature distributions in the liquid and solid phases respectively and let $x = f(t)$ be the position of the interface between the two phases where the melting occurs. Then the problem 1.1 is generalised to

$$k_i \frac{\partial^2 T_i}{\partial x^2} = c_i \rho_i \frac{\partial T_i}{\partial t} \ \ i = 1, 2 \tag{1.10}$$

subject to the Stefan conditions

$$T_1(f(t), t) = T_2(f(t), t) = 0, \ t > 0, \tag{1.11}$$

$$k_2 \frac{\partial T_2}{\partial x}\bigg|_{x=f(t)} - k_1 \frac{\partial T_1}{\partial x}\bigg|_{x=f(t)} = H \rho \frac{df}{dt} \tag{1.12}$$

where c_i, H, ρ_i, k_i denote the specific heat, latent heat, density and heat conductivity in the liquid and solid phases respectively. Assuming the change in volume during melting is negligible, the density of the liquid and solid phases is the same at $x = f(t)$. Hence $\rho = \rho_1 = \rho_2$ [7].

1.7 Stefan Condition

We will now focus on derivation of the Stefan condition 1.12. The following derivation is adapted from [7]. Let us consider the problem 1.10.

At a general time $t > 0$ the interface point between the liquid and solid

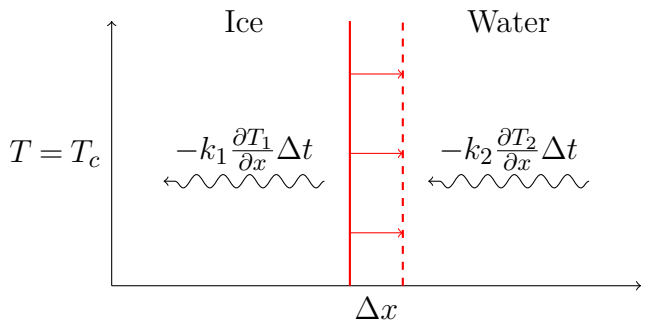

Figure 1.3: Illustration of the energy balance across the interface

regions is at $x = f(t)$. In order to move the interface by Δx, $H\rho\Delta x$ amount of heat is released. In time Δt, $-k_1\Delta t\frac{\partial T_1}{\partial x}$ amount of heat enters the $[x, x+\Delta x]$ region from the liquid phase and $-k_2\Delta t\frac{\partial T_2}{\partial x}$ leaves the $[x, x+\Delta x]$ region into the solid phase. Assuming the heat flows by conduction only, a heat balance requires that

$$-k_1\Delta t\frac{\partial T_1}{\partial x} + k_2\Delta t\frac{\partial T_2}{\partial x} = -H\rho\Delta x. \tag{1.13}$$

Hence on the moving interface $x = f(t)$, we get

$$k_2\frac{\partial T_2}{\partial x}\bigg|_{x=f(t)} - k_1\frac{\partial T_1}{\partial x}\bigg|_{x=f(t)} = -H\rho\frac{df}{dt} \tag{1.14}$$

1.8 Multiple Space Dimensions

In this section, we will extend the one-dimensionality of the problem formulated in sections 1.5 and 1.6 into two and more spatial dimensions.

Let $\mathbf{x}$ be the space coordinate vector. Let us consider domain $D = D_1 \cup D_2$ where D_i corresponds to the two domains of different phases. Moreover, instead of the position of the moving front being $x = f(t)$, we shall track the interface as a zero level-set of a function $g(\mathbf{x}, t)$. This formulation allows for more flexibility in terms of interface shapes and will be crutial later on during implementation of the numerical procedures. Then the problem 1.10 becomes

$$k_i\nabla^2 T_i = \rho_i c_i\frac{\partial T_i}{\partial t}, \quad \mathbf{x} \in D_i, \quad t > 0, \ i = 1, 2, \tag{1.15}$$

subject to the boundary conditions

$$T_i(\mathbf{x},t) = T_i^b,\ \mathbf{x} \in \partial D_i,\ t > 0,\ i = 1,2, \tag{1.16}$$

initial conditions

$$T(\mathbf{x},0) = T_0(\mathbf{x}), \tag{1.17}$$

$$g(\mathbf{x},0) = g_0(\mathbf{x}), \tag{1.18}$$

and Stefan condition

$$k_2 \frac{\partial T_2}{\partial n} - k_1 \frac{\partial T_1}{\partial n} = -\rho H v_n, \tag{1.19}$$

$$T_1(\mathbf{x},t) = T_2(\mathbf{x},t) = T_g, \tag{1.20}$$

on the moving interface $g(\mathbf{x},t) = 0,\ t > 0,$ where $\frac{\partial T}{\partial n}$ denotes the normal derivative and v_n the velocity in the normal direction.

1.9 Further Generalisations

Crank in [7] provided a wide range of further generalisations of classical Stefan problems. These include the formulations with non-linear heat parameters, density changes, and convection, inverse Stefan problems, problems with multiple phase transitions, formulations with implicit boundary conditions or concentrated heat parameters. There is a wide range of literature concerning these generalised Stefan problems (e.g. [7, 3]) but they shall be not covered in detail here.

1.10 Alternative Form of Stefan Condition

In the Stefan problem, as stated in the previous section, the interface is given as a zero level contour of the function $g(\mathbf{x},t) = 0$. Such a formulation does provide flexibility in the possible shapes of the solidification front. However, in certain situations, we can expect the interface to stay relatively simple. Therefore, we can restrict ourselves to interfaces that have the form $y = f(x,t)$.

In this section, we derive an alternative form of Stefan condition that

is valid for interfaces that can be described as graphs of a one-dimensional function. Let us also restrict to one-phase case where the domain D_2 is kept at the fusion themperature. Hence heat only flows in the domain D_1 and $\frac{\partial T_2}{\partial n} = 0$. Then from 1.19, and dropping the subscript we have that on $g(x,y,t) = 0$,

$$\frac{\partial T}{\partial n} = a v_n, \tag{1.21}$$

where $a = (\rho H)/k$. Let $\mathbf{n}$ be the outward pointing unit normal to g. Then

$$\mathbf{n} = \frac{\nabla g}{|\nabla g|}, \text{ hence} \tag{1.22}$$

$$v_n = \mathbf{v} \cdot \mathbf{n} = \frac{1}{|\nabla g|}(\mathbf{v} \cdot \nabla g). \tag{1.23}$$

From $g(x,y,t) = 0$ any change on g must satisfy

$$dg = \frac{\partial g}{\partial x}dx + \frac{\partial g}{\partial y}dy + \frac{\partial g}{\partial t}dt = 0, \text{hence} \tag{1.24}$$

$$\frac{\partial g}{\partial x}\frac{dx}{dt} + \frac{\partial g}{\partial y}\frac{dy}{dt} + \frac{\partial g}{\partial t} = 0. \tag{1.25}$$

Then from 1.23 and 1.25 it follows that

$$|\nabla g| v_n = \mathbf{v} \cdot \nabla g = \left(\frac{dx}{dt}, \frac{dy}{dt}\right) \cdot \left(\frac{\partial g}{\partial x}, \frac{\partial g}{\partial y}\right) = -\frac{\partial g}{\partial t}. \tag{1.26}$$

Since

$$\frac{\partial T}{\partial n} = \nabla T \cdot \mathbf{n} = \frac{1}{|\nabla g|}(\nabla T \cdot \nabla g), \tag{1.27}$$

then using 1.21 and 1.26 we obtain

$$\nabla T \cdot \nabla g = -a\frac{\partial g}{\partial t}. \tag{1.28}$$

Then again putting $g(x,y,t) = y - f(x,t)$ we obtain

$$\frac{\partial T}{\partial y} - \frac{\partial T}{\partial x}\frac{\partial f}{\partial x} = a\frac{\partial f}{\partial t}. \tag{1.29}$$

Since the derivatives with respect to x and y are related by

$$-\frac{\partial T}{\partial y}\sin\alpha = \frac{\partial T}{\partial x}\cos\alpha, \tag{1.30}$$

where α is the angle between the tangent of the curve $g(x,y,t)=0$ at a point (x_0,y_0) and the horizontal direction. We have that

$$\frac{\partial T}{\partial y} = a\frac{\frac{\partial f}{\partial t}}{1+\tan\alpha\frac{\partial f}{\partial x}}. \tag{1.31}$$

Since at a given point (x_0,y_0), $\partial f/\partial x = \tan\alpha$, the above condition can be rewritten as

$$\frac{\partial T}{\partial y} = a\frac{\frac{\partial f}{\partial t}}{1+\left(\frac{\partial f}{\partial x}\right)^2}. \tag{1.32}$$

We shall use 1.32 as the Stefan condition on the interface instead for certain simpler models, as well as when looking for the small time solution in the single vial model in chapter 5.

Chapter 2

Level Set Method

2.1 Introduction

A common method of solving moving boundary problems is referred to as *the front-fixing method*. It was used in [58, 53, 26] when developing models for primary and secondary drying stages of freeze-drying. The main idea is to introduce a new curvilinear coordinate system which immobilises the moving interface. It is a simple way of tackling moving boundary problems; however, the interface needs to be of a particular form, and any topological changes are cumbersome to implement. The initial shape of the interface is restricted to the form $y = f(x,t)$ and the solidification fronts have to remain graphs of a function as they propagate. Moreover, the front fixing methods do not allow for any topological changes to occur without significant alterations to the numerical schemes. We aim to develop a method that would be robust enough to allow for more general shapes of the solidification front, as well as, being able to tackle any changes in the topology of the free boundary during the process. This was the motivation behind developing the time-dependent level set method first introduced by [35].

Suppose that $\Gamma(t)$ corresponds to a one-parameter family of closed contours corresponding to the time evolution of the interface. The idea behind the level set methods is to capture the interface as a zero level set of some

implicit auxiliary function $\phi(\mathbf{x},t)$. Hence

$$\Gamma(t) = [\mathbf{x}|\phi(\mathbf{x},t) = 0]. \tag{2.1}$$

Then by evolving the function ϕ in time, we produce an *Eulerian* formulation of the propagation of the interface $\Gamma(t)$.

Apart from the condition stated in equation 2.1, we would like the function ϕ to remain relatively smooth and differentiable throughout the interface propagation. With these two conditions, there are many choices to pick from when defining the auxiliary function ϕ.

For a fixed t, let us define the *distance function* $d(\mathbf{x})$ as

$$d(\mathbf{x}) = \min_{\mathbf{x}^I}(|\mathbf{x} - \mathbf{x}^{\mathbf{I}}|), \text{ where } \mathbf{x}^{\mathbf{I}} \in \Gamma(t). \tag{2.2}$$

The contour Γ separates the computational domain into two regions: the interior and exterior of Γ, denoted Γ_{INT} and Γ_{EXT} respectively. Then for a fixed t, we can define ϕ to be the *signed distance function* given by

$$\phi(\mathbf{x},t) = \begin{cases} -d(\mathbf{x}), & \text{if } \mathbf{x} \in \Gamma_{INT} \\ d(\mathbf{x}), & \text{if } \mathbf{x} \in \Gamma_{EXT} \end{cases} \tag{2.3}$$

The function ϕ defined by 2.3 will have the desired property that the zero level set will correspond to the position of the contour Γ. Moreover, the sign of $\phi(\mathbf{x},t)$ determines whether the point $\mathbf{x}$ is located in the solid or liquid region.

For a general implicit function $\psi(\mathbf{x})$, the unit normal vector $\mathbf{n}$ is given by

$$\mathbf{n} = \frac{\nabla\psi}{|\nabla\psi|}, \tag{2.4}$$

and the curvature κ is defined as

$$\kappa = \nabla \cdot \left(\frac{\nabla\psi}{|\nabla\psi|}\right). \tag{2.5}$$

Since $d(\mathbf{x})$ is a Euclidean norm, one has that $|\nabla d| = 1$. Hence in the case of a signed distance function, the equations 2.4 and 2.5 simplify to

$$\mathbf{n} = \nabla\phi \tag{2.6}$$

and

$$\kappa = \nabla \cdot \nabla\phi. \tag{2.7}$$

Osher and Fedkiw in [34] point out that the property

$$|\nabla\phi| = 1 \tag{2.8}$$

is only true in a general sense and it is not valid for points that are equidistant from at least two points on the interface. However, if an equation is true in a general sense and fails only in a few particular cases, it will not cause the overall deterioration of the numerical scheme [34].

2.2 Level Set Equation

As mention in the previous section, the progression of the interface is captured by the evolution of the implicit function ϕ. In this section, we derive the governing equation for the level set method. Proceeding along [52], let us suppose that F is the velocity field that moves the contour in the direction normal to itself. For a fixed time t, let us parametrise $\Gamma(t)$ by $\mathbf{x}(t)$. Then from the definition of F,

$$\dot{\mathbf{x}} \cdot \mathbf{n} = F(\mathbf{x}(t)). \tag{2.9}$$

The position of the interface is given by

$$\phi(\mathbf{x}(t), t) = 0. \tag{2.10}$$

Then by the chain rule,

$$\phi_t + \nabla\phi(\mathbf{x}(t), t) \cdot \dot{\mathbf{x}} = 0. \tag{2.11}$$

Hence using 2.9 and

$$\mathbf{n} = \frac{\nabla\phi}{|\nabla\phi|},$$

we obtain the *level set equation*

$$\phi_t + F|\nabla\phi| = 0. \tag{2.12}$$

Equation 2.12 is called the level set equation that governs the propagation of the free boundary. At this point, nothing has been said about the function F. The role of F is to advect the interface "correctly", in the sense that its position will be a good approximation to the physical phenomena that we are trying to model. Hence the form and construction of F depend on the particular problem at hand. We shall see a more detailed discussion on this in chapter 4.

2.3 Reinitialisation

The issue with the level set equation 2.12 is that the implicit function ϕ fails to be a signed distance function even after one time step. We shall see in section 4.3 that the choice of the signed distance function for ϕ has certain desirable properties as far as the numerical discretisation is concerned. Moreover, marching the equation 2.12 forward in time can cause steepening and flattening of the local gradients of the level set function in certain regions, which in turn can increase the numerical errors in the calculations [34]. Therefore Chopp in [5] proposed that it is desirable to reinitialise the function ϕ after certain time intervals.

A trivial way to reinitialise the level set function ϕ would be to find the position of the interface and then recompute the shortest distances to the moving front. However, this is computationally very costly. Given the level set function ϕ, one only needs to solve for $|\nabla\phi| = 1$ to again convert it to a signed distance function. In [47] Rouy and Tourin proposed a numerical

method for solving

$$|\nabla\phi| = f(\mathbf{x}) \tag{2.13}$$

for a general function f. They achieved it by evolving

$$\phi_t + |\nabla\phi| = f(\mathbf{x}) \tag{2.14}$$

until steady state.

For the level set formulation, however, the issue with the equation 2.14 lies in the fact that the information propagates from smaller values of ϕ to larger values of ϕ. Hence the position of the zero level set is not guaranteed to stay stationary since it will be influenced by the negative values of ϕ [34]. Hence Sussman, Smereka and Osher in [57] proposed the *reinitialisation equation*

$$\phi_t + S(\phi_0)(|\nabla\phi| - 1) = 0. \tag{2.15}$$

Here $S(\mathbf{x})$ is a *sign function* defined as

$$S(\mathbf{x}) = \begin{cases} -1, & \text{if } \mathbf{x} \in \Gamma_{INT} \\ 1, & \text{if } \mathbf{x} \in \Gamma_{EXT} \\ 0 & \text{if } \mathbf{x} \in \Gamma \end{cases} \tag{2.16}$$

and ϕ_0 is the initial value of the function ϕ, which is not necessarily a signed distance function but has the correct zero level set. When solving the equation 2.15 for points in Γ_{INT} that are close to the interface, one uses the points adjacent to the interface in Γ_{EXT} as boundary conditions and vice versa. This circular dependence eventually balances out and one obtains the steady state solution [34].

From numerical simulations, it has been shown that better results were obtained when the function $S(\phi_0)$ is numerically smeared out [34]. Hence Sussman, Smereka and Osher in [57] used the following as a numerical approx-

imation of $S(\phi_0)$

$$S(\phi_0) = \frac{\phi_0}{\sqrt{\phi_2^2 + (\Delta x)^2}}. \tag{2.17}$$

During the reinitialisation process, one would hope for the interface to remain stationary. However, numerical errors might cause a certain degree of distortion [34]. Therefore, in [50] Sethian and Semerka warn about too frequent reinitialisation of the implicit level set function ϕ. Hence in practical applications, it is advised to reinitialise either after a pre-set number of time steps or when the function ϕ is far away from being a signed distance function.

2.4 Numerical Discretisation

This section is dedicated to the study of the numerical discretisation of the level set method.

Let us focus on a general *Hamilton-Jacobi Equation* given by

$$\phi_t + H(\nabla\phi) = 0, \tag{2.18}$$

where the function H is known as the *Hamiltonian* and, generally, can be a function of both space and time. Therefore in the case of the equation (2.12) $H(\nabla\phi) = F|\nabla\phi|$ and in the case of equation (2.15) the Hamiltonian is given by $H(\nabla\phi) = S(\phi_0)(|\nabla\phi| - 1)$.

2.4.1 Preliminaries

To illustrate the basic methods of discretising the equation (2.18), we proceed along the lines of [52]. In our applications, the Hamiltonian is a function of multiple space dimensions. However, we shall discretise the spatial terms in dimension by dimension fashion. Hence it is sufficient to consider the one-dimensional case.

Let us first consider a simple case where $H(\phi_x) = c\phi_x$, and c is a non-zero constant. Hence the equation 2.18 reduces to the *one dimensional advection equation*

$$\phi_t + c\phi_x = 0, \tag{2.19}$$

with the initial condition

$$\phi(x,0) = f(x). \tag{2.20}$$

The initial value problem 2.19–2.20 has the exact solution

$$\phi(x,t) = f(x-ct). \tag{2.21}$$

In other words, the solution of ϕ at point x and time t is given by the initial data at $x-ct$ [52]. In a geometrical sense, one can interpret this as the solution being constant along the lines with slope c in the x–t plane, as shown in figure 2.1. Hence if $c>0$ then the the information propagates from left to right in the x–t plane and for $c<0$ the information propagates from right to left. In the case of spatially varying c (i.e. $c=c(x)$), we get a set of curves along which the solution $\phi(x,t)$ is constant. These curves are known as *characteristics* and are important in developing appropriate numerical schemes because they produce the *domain of influence* and the *domain of dependence* for a given point in the x–t plane [52].

In order to approximate the equation 2.19 we discretise the x–t plane in the usual manner by introducing $x_i = i\Delta x$ and $t_n = n\Delta t$. We can approximate the time derivative by a *forward Euler* method given by

$$\phi_t \approx \frac{\phi_i^{n+1} - \phi_i^n}{\Delta t}, \tag{2.22}$$

where $\phi_i^n = \phi(x_i, t_n)$.

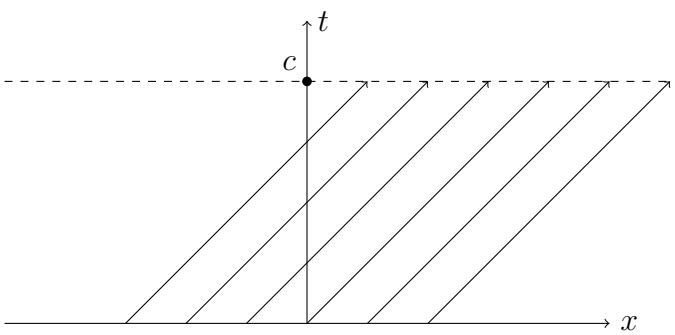

Figure 2.1: The solution $\phi(x,t)$ is constant along the lines with slope c

The spatial derivative at the node (i,n) can be approximated using two nodes in three different manners as

$$(\phi_x^+)_i^n \approx \frac{\phi_{i+1}^n - \phi_i^n}{\Delta x}, \tag{2.23}$$

$$(\phi_x^-)_i^n \approx \frac{\phi_i^n - \phi_{i-1}^n}{\Delta x}, \tag{2.24}$$

$$(\phi_x^0)_i^n \approx \frac{\phi_{i+1}^n - \phi_{i-1}^n}{2\Delta x}. \tag{2.25}$$

Substituting 2.22 and 2.23–2.25 into the equation 2.19 produces the *forward*, *backward* and *centred* schemes given by

$$\phi_i^{n+1} = \phi_i^n - \Delta t c(\phi_x^+)_i^n, \tag{2.26}$$

$$\phi_i^{n+1} = \phi_i^n - \Delta t c(\phi_x^-)_i^n, \tag{2.27}$$

$$\phi_i^{n+1} = \phi_i^n - \Delta t c(\phi_x^0)_i^n, \tag{2.28}$$

respectively.

The scheme 2.26 approximates the solution on node $i, n+1$ using the nodes i,n and $i+1,n$. Hence it assumes that the information for the solution propagates from right to left. Similarly the scheme 2.27 assumes that the information propagates from left to right and scheme 2.28 assumes that the information propagates from both sides [52].

Therefore in the light of our previous discussion on the advection equation, it follows that one should approximate the solution of the equation 2.19 by

$$\phi_i^{n+1} = \phi_i^n - \Delta t c(\phi_x^+)_i^n \text{ if } c < 0 \tag{2.29}$$

and

$$\phi_i^{n+1} = \phi_i^n - \Delta t c(\phi_x^-)_i^n \text{ if } c > 0. \tag{2.30}$$

These numerical schemes produce an approximation to the solution that is first order accurate in both space and time. The next section is devoted to the

discussion on developing higher order upwinding methods.

2.4.2 ENO Schemes

In the upwinding methods, it is essential to approximate the spatial derivatives using the correct set of nodes in the direction where the information is coming from. Hence for the approximation of ϕ_x we choose either nodes to the left (ϕ_x^-) or to the right (ϕ_x^+).

The main principle of essentially non-oscillatory (ENO) approximations for ϕ_x^- or ϕ_x^+, is to choose a set of nodes that gives a smoothest possible polynomial approximation for the derivatives of desired accuracy [34]. Proceeding along the lines of [34], one can obtain such approximations from the divided differences of ϕ. The zeroth divided difference at node i is given by the value of the function.

$$D_i^0\phi = \phi_i.$$

The first divided defences are defined at the midpoints of the grid

$$D^1\phi_{i+1/2} = \frac{D_{i+1}^0\phi - D_i^0\phi}{\Delta x}.$$

The second divided difference are defined as

$$D_i^2\phi = \frac{D^1\phi_{i+1/2} - D^1\phi_{i-1/2}}{2\Delta x}$$

and the third divided differences as

$$D_{i+1/2}^3\phi = \frac{D_{i+1}^2\phi - D_i^2\phi}{3\Delta x},$$

and so on.

We wish to approximate $\phi(x)$ as a polynomial of the form

$$\phi(x) = Q_0(x) + Q_1(x) + Q_2(x) + Q_3(x). \tag{2.31}$$

Here each $Q_i(x)$ is and i-th order polynomial that interpolates $\phi(x)$ across a

selected set of nodes. Starting with a node i, we set Q_0 to he value of ϕ at x_i. Then the derivative at the point x_i is given by

$$\phi_x(x_i) = Q_1^{'}(x_i) + Q_2^{'}(x_i) + Q_3^{'}(x_i), \tag{2.32}$$

as the constant term Q_0 vanishes upon differentiation. In order to find ϕ_i^- we start at node $k = i-1$ and to find ϕ_i^+ with start at $k = i$. We define

$$Q_1(x) = (D^1_{k+1/2}\phi)(x - x_i)$$

so that

$$Q_1^{'}(x_i) = D^1_{k+1/2}\phi.$$

Note that with this definition, the first-order accurate ENO1 scheme is simply the usual upwind differencing. In order to improve the accuracy of the approximation, we include the $Q_2^{'}(x_i)$ and $Q_3^{'}(x_i)$ to obtain second-order ENO2 and third-order ENO3 approximations respectively.

For the next term we have two choices. Either we include the $D^2_k\phi$ or we include $D^2_{k+1}\phi$. We make our decision based on which of these gives smoother polynomial interpolation. The main observation is that smooth data tend to produce small numbers in the divided difference table and quickly varying data tent to produce large numbers in the difference tables [34]. Hence if

$$|D^2_k\phi| \leq |D^2_{k+1}\phi|,$$

we set $c = D^2_k\phi$ and $k^* = k-1$, and if

$$|D^2_k\phi| \geq |D^2_{k+1}\phi|,$$

we set $c = D^2_{k+1}\phi$ and $k^* = k$. Then we can define

$$Q_2(x) = c(x - x_k)(x - x_{k+1}),$$

we gives

$$Q_2^{'}(x_i) = c(2(i-k)-1)\Delta x,$$

giving the second order accurate ENO2 scheme.

Again, for the next term we have two choices, either we include $D^3_{k^*+1/2}\phi$ or $D^3_{k^*+3/2}\phi$. By the same reasoning as above, if

$$|D^3_{k^*+1/2}\phi| \leq D^3_{k^*+3/2}\phi,$$

we set $c^* = D^3_{k^*+1/2}\phi$, and if

$$|D^3_{k^*+1/2}\phi| \geq D^3_{k^*+3/2}\phi,$$

we set $c^* = D^3_{k^*+3/2}\phi$. Then we define

$$Q_3(x) = c^*(x - x_{k^*})(x - x_{k^*-1})(x - x_{k^*-2})$$

such that

$$Q_3^{'}(x_i) = c^*(3(i-k^*)^2 - 6(i-k^*) + 2)(\Delta x)^2.$$

Which produces a third order accurate ENO3 scheme.

2.4.3 WENO Schemes

In the previous section we have derived approximations to the derivatives of the function ϕ. In particular, the ENO3 approximation to ϕ_x^- picks one particular stencil of nodes from the set $\{\phi_{i-3}, \phi_{i-2}, \phi_{i-1}, \phi_i, \phi_{i+1}, \phi_{i+2}\}$ that would produce the smoothest possible polynomial approximation to ϕ_x^-. Similarly, when approximating ϕ_x^+ ENO3 chooses a stencil from the set

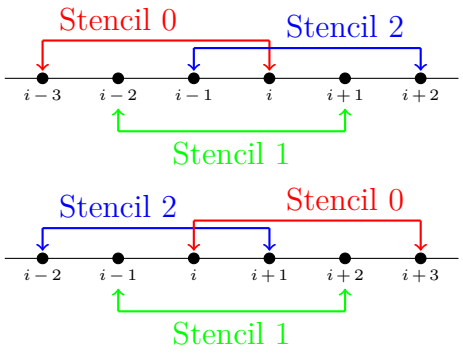

Figure 2.2: Three possibilities of choosing a stencil for ϕ_x^- approximation (above) and ϕ_x^+ approximation (below).

$\{\phi_{i-2}, \phi_{i-1}, \phi_i, \phi_{i+1}, \phi_{i+2}, \phi_{i+3}\}$, as illustrated in figure 2.2.

However, Liu et al. in [27] claimed that picking only one particular stencil from the set of nodes is unnecessary in the regions where the function is smooth and well behaved. Therefore they proposed a method of weighted essentially non-oscillatory (WENO) schemes. The idea behind WENO procedures is to take a convex combination of the three possible ENO3 approximations that can arise from a given set of nodes. The weights in the convex combination are chosen such that if any of the ENO3 approximations interpolate across a discontinuity, it will be given minimal weight. On the other hand, if the function is smooth, all the ENO3 approximations make a significant contribution. Jiang and Shu [22] improved the method by introducing a new method of measuring the smoothness of the polynomial. The resulting WENO scheme is fifth-order accurate instead of the fourth-order accuracy of the method proposed in [27]. To illustrate the of the WENO scheme, we will proceed along the lines of Jiang and Peng [21], who extended the WENO method to the Hamilton-Jacobi framework.

From the left-biased set $\{\phi_{i-3}, \phi_{i-2}, \phi_{i-1}, \phi_i, \phi_{i+1}, \phi_{i+2}\}$ we can produce three different ENO3 approximations for ϕ_x^- given by

$$\phi_{x,i}^{-,0} = \frac{1}{3}\frac{\phi_{i-2}-\phi_{i-3}}{\Delta x} - \frac{7}{6}\frac{\phi_{i-1}-\phi_{i-2}}{\Delta x} + \frac{11}{6}\frac{\phi_i-\phi_{i-1}}{\Delta x}, \tag{2.33}$$

$$\phi_{x,1}^{-,1} = -\frac{1}{6}\frac{\phi_{i-1}-\phi_{i-2}}{\Delta x} + \frac{5}{6}\frac{\phi_i-\phi_{i-1}}{\Delta x} + \frac{1}{3}\frac{\phi_{i+1}-\phi_i}{\Delta x}, \tag{2.34}$$

$$\phi_{x,i}^{-,2} = \frac{1}{3}\frac{\phi_i-\phi_{i-1}}{\Delta x} + \frac{5}{6}\frac{\phi_{i+1}-\phi_i}{\Delta x} - \frac{1}{6}\frac{\phi_{i+2}-\phi_{i+1}}{\Delta x}, \tag{2.35}$$

where $\phi_{x,i}^{-,k}$ is an ENO3 approximation based on the k-th stencil, as shown in figure 2.2.

The WENO approximation take the convex combination of $\phi_{x,i}^{-,k}$ for $k = 0, 1, 2$. Hence WENO approximation to ϕ_x^- at the node i is given by

$$\phi_{x,i}^{-} = \omega_0\phi_{x,i}^{-,0} + \omega_1\phi_{x,i}^{-,1} + \omega_2\phi_{x,i}^{-,2}, \tag{2.36}$$

where $\omega_k \geq 0$ for $k = 0, 1, 2$ and

$$\omega_0 + \omega_1 + \omega_2 = 1. \tag{2.37}$$

One can note that if we set $\omega_0 = 0.1$, $\omega_1 = 0.6$, $\omega_2 = 0.3$, the equation (2.36) becomes

$$\phi^-_{x,i} = \frac{1}{30}\frac{\phi_{i-2} - \phi_{i-3}}{\Delta x} - \frac{13}{60}\frac{\phi_{i-1} - \phi_{i-2}}{\Delta x} + \frac{47}{60}\frac{\phi_i - \phi_{i-1}}{\Delta x} + \frac{9}{20}\frac{\phi_{i+1} - \phi_i}{\Delta x} - \frac{1}{20}\frac{\phi_{i+2} - \phi_{i+1}}{\Delta x}. \tag{2.38}$$

The above equation (2.38) produces on optimal fifth-order approximation on the six point stencil. Therefore, we would like to choose the weights ω_k to be as close as possible to the optimal values in the smooth regions, however, one would prefer a digital values for ω_k in non-smooth regions near discontinuities. We will discuss the choice of ω_k later.

Firstly, let us notice that if we choose

$$\omega_0 = 0.1 + O((\Delta x)^2), \tag{2.39}$$

$$\omega_1 = 0.6 + O((\Delta x)^2), \tag{2.40}$$

$$\omega_2 = 0.3 + O((\Delta x)^2). \tag{2.41}$$

The resulting scheme will still be fifth-order accurate in the smooth regions. To demostrade this, let us rewrite the values for ω_k as

$$\omega_0 = 0.1 + C_0(\Delta x)^2, \tag{2.42}$$

$$\omega_1 = 0.6 + C_1(\Delta x)^2, \tag{2.43}$$

$$\omega_2 = 0.3 + C_2(\Delta x)^2, \tag{2.44}$$

where C_k is $O(1)$. Substituting (2.42-2.44) into the equation (2.36) produces

$$\phi^-_{x,i} = \overbrace{0.1\phi^{-,0}_{x,i} + 0.6\phi^{-,1}_{x,i} + 0.3\phi^{-,2}_{x,i}}^{A} + \underbrace{C_0(\Delta x)^2\phi^{-,0}_{x,i} + C_1(\Delta x)^2\phi^{-,1}_{x,i} + C_2(\Delta x)^2\phi^{-,2}_{x,i}}_{B}. \quad (2.45)$$

The term given by A gives the optimal fifth order approximation. Hence we can write A as the exact value of $\phi^-_{x,i}$ (denoted by $\phi^{-,E}_{x,i}$) plus a fifth-order error term. Therefore

$$A = \phi^{-,E}_{x,i} + O((\Delta x)^5). \quad (2.46)$$

Examining the terms in B, we can note that each of the ENO3 approximations in B gives the exact value $\phi^{-,E}_{x,i}$ plus a $O((\Delta x)^3)$ term. Therefore we have

$$B = C_0(\Delta x)^2\phi^{-,E}_{x,i} + C_1(\Delta x)^2\phi^{-,E}_{x,i} + C_2(\Delta x)^2\phi^{-,E}_{x,i} + O((\Delta x)^5). \quad (2.47)$$

Since $\omega_0 + \omega_1 + \omega_2 = 1$, it follows that $C_0 + C_1 + C_2 = 0$. And hence $B = O((\Delta x)^5)$. Therefore, adding $O((\Delta x)^2)$ term to the optimal fifth order weights still produces fifth order approximation.

Hence, we would like to choose the weights ω_k such that

1. in smooth regions we require: $\omega_0 = 0.1 + O((\Delta x)^2)$, $\omega_1 = 0.6 + O((\Delta x)^2)$ and $\omega_2 = 0.3 + O((\Delta x)^2)$.

2. if the stencil contains a singularity, then the weights adaptively approach the digital values of 1 or 0.

Since all the weights add up to unity, we can set

$$\omega_1 = 1 - \omega_0 - \omega_2.$$

Substituting the above into (2.36), we obtain

$$\phi^{-}_{x,i} = \omega_0 \phi^{-,0}_{x,i} + (1-\omega_0-\omega_2)\phi^{-,1}_{x,i} + \omega_2 \phi^{-,2}_{x,i}. \tag{2.48}$$

Hence

$$\phi^{-}_{x,i} = \frac{1}{2}(\phi^{-,1}_{x,i} + \phi^{-,2}_{x,i}) + \omega_0(\phi^{-,0}_{x,i} - \phi^{-,1}_{x,i}) + \left(\omega_2 - \frac{1}{2}\right)(\phi^{-,2}_{x,i} - \phi^{-,1}_{x,i}). \tag{2.49}$$

Substituting the expression for $\phi^{-,k}_{x,i}$ into the above equation (2.49) one obtains

$$\phi^{-}_{x,i} = \frac{1}{12}\left(-\frac{\phi_{i-1}-\phi_{i-2}}{\Delta x} + 7\frac{\phi_i - \phi_{i-1}}{\Delta x} + 7\frac{\phi_{i+1}-\phi_i}{\Delta x} - \frac{\phi_{i+2}-\phi_{i+1}}{\Delta x}\right) - \Phi^{WENO}(a,b,c,d), \tag{2.50}$$

where

$$\Phi^{WENO}(a,b,c,d) = \frac{1}{3}\omega_0(a-2b+c) + \frac{1}{6}\left(\omega_2 - \frac{1}{2}\right)(b-2c+d), \tag{2.51}$$

and

$$a = \frac{\phi_{i-1} - 2\phi_{i-2} + \phi_{i-3}}{\Delta x}, \tag{2.52}$$

$$b = \frac{\phi_i - 2\phi_{i-1} + \phi_{i-2}}{\Delta x}, \tag{2.53}$$

$$c = \frac{\phi_{i+1} - 2\phi_i + \phi_{i-1}}{\Delta x}, \tag{2.54}$$

$$d = \frac{\phi_{i+2} - 2\phi_{i+1} + \phi_i}{\Delta x}, \tag{2.55}$$

Following the work done in [21], we can define the quantities α_0, α_1 and α_2 as

$$\alpha_0 = \frac{0.1}{(\epsilon + IS_0)^2}, \tag{2.56}$$

$$\alpha_1 = \frac{0.6}{(\epsilon + IS_1)^2}, \tag{2.57}$$

$$\alpha_2 = \frac{0.3}{(\epsilon + IS_2)^2}, \tag{2.58}$$

where IS_k are measures of the smoothness of the stencil k and they are defined as

$$IS_0 = \frac{13}{12}(a-b)^2 + \frac{1}{4}(a-3b)^2, \tag{2.59}$$

$$IS_1 = \frac{13}{12}(b-c)^2 + \frac{1}{4}(b+c)^2, \tag{2.60}$$

$$IS_2 = \frac{13}{12}(c-d)^2 + \frac{1}{4}(3c-d)^2. \tag{2.61}$$

The ϵ term is included in the expressions to prevent from division by zero. In practical applications, $\epsilon = 10^{-6}$. The numerical tests done by Jiang and Shu in [22] suggest that the numerical results are not sensitive to the choice of ϵ, if it lies in the range from 10^{-5} to 10^{-7}.

One can then set the weight values equal to

$$\omega_0 = \frac{\alpha_0}{\alpha_0 + \alpha_1 + \alpha_2}, \tag{2.62}$$

$$\omega_1 = \frac{\alpha_1}{\alpha_0 + \alpha_1 + \alpha_2}, \tag{2.63}$$

$$\omega_2 = \frac{\alpha_2}{\alpha_0 + \alpha_1 + \alpha_2}. \tag{2.64}$$

It is clear that with this definitions the condition

$$\sum_{k=0}^{2} \omega_k = 1 \tag{2.65}$$

is satisfied. Moreover, in smooth regions the smoothness measures IS_k are small in comparison to ϵ. Hence we have

$$\alpha_0 \approx 0.1\epsilon^{-2}, \tag{2.66}$$

$$\alpha_1 \approx 0.6\epsilon^{-2}, \tag{2.67}$$

$$\alpha_2 \approx 0.3\epsilon^{-2}, \tag{2.68}$$

and the method recovers the optimal weights. We can note that if the measures of smoothness are not small enough to be dominated by ϵ, we still recover the optimal values for ω_k as long as IS_k are approximately equal to each other, as we would expect in the regions with small variation [34].

On the other hand, a large variation in the data on a particular stencil leads to a large value of the smoothness measure. Hence the corresponding value of α is small, and the stencil will be given minimal weight. An issue might arise in the WENO method when all IS_k are large. In this case, none of the stencils are particularly useful [34]. However, ENO methods suffer from this particular issue, as well. Fortunately, in practice, these instances are usually local in space and time, and the methods can recover after the situation passes [34].

Following the same line of reasoning as with the left bias approximation $\phi^-_{x,i}$ one can show the right bias approximation is given by

$$\phi^+_{x,i} = \frac{1}{12}\left(-\frac{\phi_{i-1}-\phi_{i-2}}{\Delta x} + 7\frac{\phi_i-\phi_{i-1}}{\Delta x} + 7\frac{\phi_{i+1}-\phi_i}{\Delta x} - \frac{\phi_{i+2}-\phi_{i+1}}{\Delta x}\right) - \Phi^{WENO}(a,b,c,d), \quad (2.69)$$

with

$$a = \frac{\phi_{i+3}-2\phi_{i+2}+\phi_{i+1}}{\Delta x}, \quad (2.70)$$

$$b = \frac{\phi_{i+2}-2\phi_{i+1}+\phi_i}{\Delta x}, \quad (2.71)$$

$$c = \frac{\phi_{i+1}-2\phi_i+\phi_{i-1}}{\Delta x}, \quad (2.72)$$

$$d = \frac{\phi_i-2\phi_{i-1}+\phi_{i-2}}{\Delta x}. \quad (2.73)$$

2.4.4 TVD Runge-Kutta

Our discussion so far has been mainly focused on the numerical treatment of the spatial terms. We have developed an ENO and WENO numerical procedure that allows us to discretise the spatial terms up to fifth-order accuracy.

However, the temporal forward Euler approximation is given in (2.22) is only first-order accurate. From practice, we know that the level set methods are sensitive to spatial truncation errors, and hence the higher-order ENO or WENO schemes are desirable [34]. On the other hand, the temporal errors tend not to produce a significant deterioration of the numerics.

However, there are certain instances when higher temporal accuracy is desired. This section is devoted to the higher-order time discretisations of the level set equations. To achieve this, we shall use the *method of lines* approach. The method of lines approach assumes that the temporal discretisation of the PDE can be treated separately from the spatial one in a semi-discrete manner.

Following the notation from the section 2.4.1, we define the *total variation* as

$$TV(\phi) = \sum_i |\phi_{i+1} - \phi_i|. \tag{2.74}$$

Then the method is said to be *total variation diminishing* (TVD) if

$$TV(\phi^{n+1}) \leq TV(\phi^n). \tag{2.75}$$

We say that the method is *total variation bounded* (TVB) in $0 \leq t \leq T$ if

$$TV(\phi^n) \leq B. \tag{2.76}$$

For some fixed B, where B depends on $TV(\phi^0)$.

The advantage of TVD/TVB schemes is that they prevent from the creation of spurious oscillations as a result of high order temporal accuracy. In [54] Shu and Osher proposed TVD schemes based Runge-Kutta (TVD-RK) discretisation. The simple first-order TVD-RK method is the forward Euler scheme described in section 2.4.1. The higher-order RK method is obtained by taking the convex combinations of Forward Euler steps [34]. Then if the basic forward Euler step coupled with the space discretisation is TVD, the resulting higher-order RK method is also TVD.

An issue arises from the fact that ENO or WENO methods in conjunction with the forward Euler time discretisation are not TVD. However, the numerical evidence suggests such methods are TVB; therefore, the final higher-order method is still TVB [34].

We shall present here a third-order TVD-RK scheme for the level set equation (2.12). The details of the derivation as well as further analysis of the method can be found in [54].

Given a time $t^n = n\Delta t$, the method starts by taking one Euler step

$$\frac{\phi^{n+1} - \phi^n}{\Delta t} + F^n |\nabla \phi^n| = 0. \tag{2.77}$$

this is then follow by a second Euler step

$$\frac{\phi^{n+2} - \phi^{n+1}}{\Delta t} + F^{n+1} |\nabla \phi^{n+1}| = 0. \tag{2.78}$$

Then one takes the averaging step

$$\phi^{n+1/2} = \frac{3}{4}\phi^n + \frac{1}{4}\phi^{n+2}, \tag{2.79}$$

which produces an approximation to ϕ at the half time interval $t^{n+1/2}$. Another Euler step is then taken to give an approximation at $t^{n+3/2}$. Namely

$$\frac{\phi^{n+3/2} - \phi^{n+1/2}}{\Delta t} + F^{n+1/2} |\nabla \phi^{n+1/2}| = 0. \tag{2.80}$$

Finally, a second averaging step is taken the get the solution at time t^n,

$$\phi^{n+1} = \frac{1}{3}\phi^n + \frac{2}{3}\phi^{n+3/2}. \tag{2.81}$$

In our computations, we shall use the ENO2 method coupled with the third-order TVD-RK for solving the level set equation (2.12) and fifth-order WENO method coupled with the third-order TVD-RK for solving the reinitialisation equation (2.15).

2.5 Other Level Set Schemes

Osher and Sethian first introduced the level set method in [35]. Since then, various extensions and adaptations of the classical method have been developed. This section provides an overview of different approaches to various stages of the scheme, along with some recent developments.

2.5.1 Narrow Banding

In the level set method described so far in this chapter, we have solved the level set equation for ϕ on the whole computational domain. This approach is called the *full matrix* approach [52]. However, in practice, we are interested in the zero level set of the function and not the behaviour of ϕ far away from it. Therefore, the full matrix might be considered wasteful.

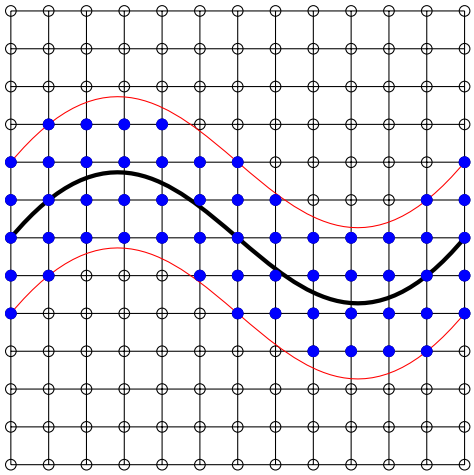

Figure 2.3: The red lines indicate the narrow band around the zero level set (black), point inside (blue) are tagged as "alive"

The idea behind the *narrow band methods* is to perform calculation only in the neighbourhood of the zero level set. Chopp first introduced the method in [5]. The basic outline of the algorithm is described below.

- points inside the narrow band (of user prescribed width) are tagged as "alive"
- "land mines" are constructed to indicate the edge of the narrow band
- points outside the narrow band with large positive (negative) value are initialised as "far away"
- the level set equation is solved until landmine is hit
- the narrow band is rebuilt

- repeat the loop

More details on the typical band size, accuracy and speed can be found in [52, 34, 35]

2.5.2 Stationary Level Set Formulation

Suppose that our speed function F in the level set equation (2.12) is restricted such that $F > 0$ or $F < 0$. In this case, the interface crosses each point in the computational domain only once. One can then define the *first crossing time* for a given point $\mathbf{x}$, as the time that the interface first crosses the point $\mathbf{x}$. In other words, it is the time when $\phi(\mathbf{x}, t)$ changes its sign. Let us denote $T(\mathbf{x})$ as the first crossing time for $\mathbf{x}$. Then from the definition of $T(\mathbf{x})$ we have

$$\Gamma(t) = \{\mathbf{x} | T(\mathbf{x}) = t\}. \tag{2.82}$$

This newly defined level set function $T(\mathbf{x})$ gives rise to the *stationary level set* formulation since the explicit dependence on t has been eliminated. Osher in [33] showed that $T(\mathbf{x})$ satisfies

$$|\nabla T| F = 1. \tag{2.83}$$

The stationary formulation of the level set method plays a crucial role in the fast marching schemes discussed in the next section.

2.5.3 Fast Marching Level Set

The fast marching method is based on the stationary level set formulation. Hence can only be used if the speed function always positive or negative. Then the propagation of the level set function is given by the equation (2.83). Defining the forward and backward difference operators in the x and y directions as

$$D^{+,x}_{i,j} T = \frac{T_{i+1,j} - T_{i,j}}{\Delta x}, \tag{2.84}$$

$$D^{-,x}_{i,j} T = \frac{T_{i,j} - T_{i-1,j}}{\Delta x}, \tag{2.85}$$

$$D^{+;y}_{i,j}T = \frac{T_{i,j+1} - T_{i,j}}{\Delta y}, \tag{2.86}$$

$$D^{-;y}_{i,j}T = \frac{T_{i,j} - T_{i,j-1}}{\Delta y}, \tag{2.87}$$

respectively, one can obtain the approximation to the equation (2.83) given by

$$\max(D^{-;x}_{i,j}T, 0)^2 + \min(D^{+;x}_{i,j}T, 0)^2 + \max(D^{-;y}_{i,j}T, 0)^2 + \min(D^{+;y}_{i,j}T, 0)^2 = F^{-2}_{i,j}. \tag{2.88}$$

The method is based on the observation that the information propagates in one direction only. For $F > 0$ the propagation is from smaller values of T to larger values (opposite is true when $F < 0$). For now, let us assume that the speed function is always positive. Hence we can build the solution outwards from the smallest value of T. The algorithm for the fast marching method is as follows:

- Initialise
  - all the points for which $T = 0$ are put in the set "known"
  - all the neighbouring point to those in "known" are placed in the set "trial" and T is set to $T = \Delta y / F_{i,j}$
  - the rest of the point are placed in the set "far" and we set $T = \inf$ for these points
- Marching
  - Begin loop. Find the point in "trail" with the smallest value of T and move it to "known"
  - put all the neighbouring points to the smallest value point that are in "far" to the set "trial" and remove them from "far"
  - recompute the values of the points in "trial" according to the equation (2.83)
  - repeat the loop

Details on the method and additional analysis can be found in [34] and [52].

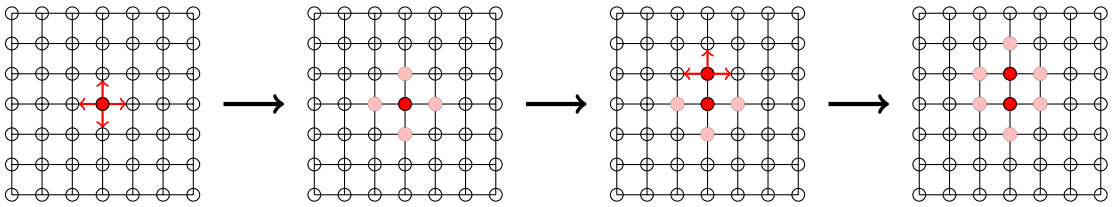

Figure 2.4: Illustration of the fast marching algorithm. A point in 'trial' (pink) with the smallest value is moved to 'known', and all its neighbours moved to 'trial'. Then the values of the 'known' points are updated and process repeats

2.6 Summary

The Level Set method provides a framework for capturing complex interface shapes without the need for parametrisation of these objects. An auxiliary function ϕ is used to describe the position of the moving boundary as its zero level set. Such formulation makes it easy to track interfaces that change topology and can describe a wide array of possible geometries. Usually, the auxiliary function ϕ is taken to be the signed distance function.

The movement of the interface is captured by appropriately advecting the level set function using the level set equation (2.12) with a suitably defined speed function F. Since even after one time step, ϕ ceased to be the signed distance function, it needs to be frequently reinitialised. This is achieved by iterating the equation (2.15) till steady state.

During the numerical approximation process of the equations (2.12) and (2.15) one needs to use the correct upwind schemes for the solutions to be stable.

There are many extensions to the standard level set method such as the narrow band method and the stationary level set formulation.

Chapter 3

Compact Finite Differencing

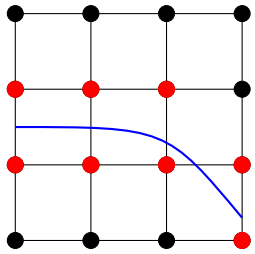

Figure 3.1: The interface (blue) cutting the computational grid creating non-uniform stencils centred around the red points

So far we have discussed the derivation and discretisation of the level set equation. The method for solving the temperature equations has not yet been sufficiently addressed. By the assumption of a quasi-steady state, the problem reduces to solving Laplace equations in both the solid and liquid regions. In the light of the level set formulation, the interface is allowed to move fluidly across the grid. Therefore, one needs to take into account grid points adjacent to the interface where the computational stencil might be non-uniform, as illustrated in figure 3.1. We shall use the method of boundary interpolation to address this issue.

3.1 Boundary Interpolation Method

Suppose that we would like to approximate the Laplace operator on a non-uniform five-point stencil and that the distances from the centre point to its neighbours are known. Let us denote by

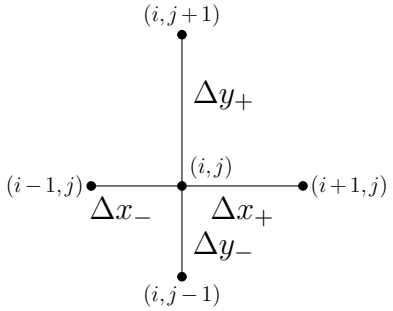

Figure 3.2: Non-uniform stencil

$\Delta x_-, \Delta x_+, \Delta y_-, \Delta y_+$ the distances from the central node (i, j) to its left, right, bottom and top neighbouring nodes respectively (as shown in the figure 3.2).

We would like to find an approximation to the derivative of the function based on the three grid points in both x and y directions. Hence we can write

$$\frac{\partial T}{\partial x} \approx aT_{i-1,j} + bT_{i,j} + cT_{i+1,j}, \tag{3.1}$$

$$\frac{\partial T}{\partial y} \approx cT_{i,j-1} + dT_{i,j} + eT_{i,j+1}. \tag{3.2}$$

Focusing on the x derivative first, one obtains from the Taylor series expansion

$$T_{i-1,j} = T_{i,j} - \Delta x_- \frac{\partial T}{\partial x} + \frac{(\Delta x_-)^2}{2}\frac{\partial^2 T}{\partial x^2} - \frac{(\Delta x_-)^3}{6}\frac{\partial^3 T}{\partial x^3} + O((\Delta x_-)^4), \tag{3.3}$$

$$T_{i+1,j} = T_{i,j} + \Delta x_+ \frac{\partial T}{\partial x} + \frac{(\Delta x_+)^2}{2}\frac{\partial^2 T}{\partial x^2} + \frac{(\Delta x_+)^3}{6}\frac{\partial^3 T}{\partial x^3} + O((\Delta x_+)^4). \tag{3.4}$$

Substituting (3.3-3.4) into equation (3.1) we find

$$\begin{aligned}\frac{\partial T}{\partial x} = (a+b+c)T_{i,j} + (-a\Delta x_- + c\Delta x_+)\frac{\partial T}{\partial x} \\ + (a\frac{(\Delta x_-)^2}{2} + c\frac{(\Delta x_+)^2}{2})\frac{\partial^2 T}{\partial x^2} + (-a\frac{(\Delta x_-)^3}{6} + c\frac{(\Delta x_+)^3}{6})\frac{\partial^3 T}{\partial x^3} \\ + O((\Delta x_-)^4, (\Delta x_+)^4).\end{aligned} \tag{3.5}$$

One should note that it is not possible to eliminate the second and third derivative from the expression (3.5) at the same time. Therefore we require

$$a + b + c = 0, \tag{3.6}$$

$$-a\Delta x_- + c\Delta x_+ = 1, \tag{3.7}$$

$$a\frac{(\Delta x_-)^2}{2} + c\frac{(\Delta x_+)^2}{2} = 0. \tag{3.8}$$

The solution to the system above is

$$a = -\frac{\Delta x_+}{\Delta x_-(\Delta x_+ + \Delta x_-)}, \tag{3.9}$$

$$c = \frac{\Delta x_-}{\Delta x_+(\Delta x_+ + \Delta x_-)}, \tag{3.10}$$

$$b = -a - c, \tag{3.11}$$

and hence

$$\left.\frac{\partial T}{\partial x}\right|_{i,j} = -\frac{\Delta x_+}{\Delta x_-(\Delta x_+ + \Delta x_-)} T_{i-1,j} + \left(\frac{\Delta x_+}{\Delta x_-(\Delta x_+ + \Delta x_-)} - \frac{\Delta x_-}{\Delta x_+(\Delta x_+ + \Delta x_-)}\right) T_{i,j} + \frac{\Delta x_-}{\Delta x_+(\Delta x_+ + \Delta x_-)} T_{i+1,j} + O(\Delta x_-, \Delta x_+). \tag{3.12}$$

Then from symmetry, the y derivative is approximated by

$$\left.\frac{\partial T}{\partial y}\right|_{i,j} = -\frac{\Delta y_+}{\Delta y_-(\Delta y_+ + \Delta y_-)} T_{i,j-1} + \left(\frac{\Delta y_+}{\Delta y_-(\Delta y_+ + \Delta y_-)} - \frac{\Delta y_-}{\Delta y_+(\Delta y_+ + \Delta y_-)}\right) T_{i,j} + \frac{\Delta y_-}{\Delta y_+(\Delta y_+ + \Delta y_-)} T_{i,j+1} + O(\Delta y_-, \Delta y_+). \tag{3.13}$$

Similarly to the discussion above, we can define the approximations to the second derivatives as

$$\frac{\partial^2 T}{\partial x^2} \approx a T_{i-1,j} + b T_{i,j} + c T_{i+1,j}, \tag{3.14}$$

$$\frac{\partial^2 T}{\partial y^2} \approx c T_{i,j-1} + d T_{i,j} + e T_{i,j+1}. \tag{3.15}$$

Following the same Taylor series analysis as for the one for the first derivative we obtain

$$\frac{\partial^2 T}{\partial x^2} = (a+b+c) T_{i,j} + (-a\Delta x_- + c\Delta x_+)\frac{\partial T}{\partial x} + (a\frac{(\Delta x_-)^2}{2} + c\frac{(\Delta x_+)^2}{2})\frac{\partial^2 T}{\partial x^2} + (-a\frac{(\Delta x_-)^3}{6} + c\frac{(\Delta x_+)^3}{6})\frac{\partial^3 T}{\partial x^3} + O((\Delta x_-)^4, (\Delta x_+)^4). \tag{3.16}$$

Similarly one can note that it is not possible to eliminate the first and third derivative from the expression at the same time. Therefore we require

$$a+b+c=0, \tag{3.17}$$

$$-a\Delta x_- + c\Delta x_+ = 0, \tag{3.18}$$

$$a\frac{(\Delta x_-)^2}{2} + c\frac{(\Delta x_+)^2}{2} = 1. \tag{3.19}$$

By solving the system we obtain

$$a = \frac{2}{\Delta x_-(\Delta x_- + \Delta x_+)}, \tag{3.20}$$

$$c = \frac{2}{\Delta x_+(\Delta x_- + \Delta x_+)}, \tag{3.21}$$

$$b = -a - c. \tag{3.22}$$

Hence the approximations to the second derivatives with respect to x and y are given as

$$\begin{aligned}\left.\frac{\partial^2 T}{\partial x^2}\right|_{i,j} = {} & \frac{2}{\Delta x_-(\Delta x_- + \Delta x_+)} T_{i-1,j} + \left(-\frac{2}{\Delta x_- \Delta x_+}\right) T_{i,j} \\ & + \frac{2}{\Delta x_+(\Delta x_- + \Delta x_+)} T_{i+1,j} + \frac{\Delta x_+ - \Delta x_-}{3}\frac{\partial^3 T}{\partial x^3} \\ & + O((\Delta x_-)^2, (\Delta x_+)^2),\end{aligned} \tag{3.23}$$

and

$$\begin{aligned}\left.\frac{\partial^2 T}{\partial y^2}\right|_{i,j} = {} & \frac{2}{\Delta y_-(\Delta y_- + \Delta y_+)} T_{i,j-1} + \left(-\frac{2}{\Delta y_- \Delta y_+}\right) T_{i,j} \\ & + \frac{2}{\Delta y_+(\Delta y_- + \Delta y_+)} T_{i,j+1} + \frac{\Delta y_+ - \Delta y_-}{3}\frac{\partial^3 T}{\partial y^3} \\ & + O((\Delta y_-)^2, (\Delta y_+)^2),\end{aligned} \tag{3.24}$$

respectively. Therefore on the non-uniform grid the Laplacian operator can be

written as

$$\nabla^2 T = \frac{2T_{i,j+1}}{\Delta y_+(\Delta y_+ + \Delta y_-)} + \frac{2T_{i+1,j}}{\Delta x_+(\Delta x_+ + \Delta x_-)} - \left(\frac{2}{\Delta x_+ \Delta x_-} + \frac{2}{\Delta y_+ \Delta y_-}\right) T_{i,j} + \frac{2T_{i,j-1}}{\Delta y_-(\Delta y_+ + \Delta y_-)} + \frac{2T_{i-1,j}}{\Delta x_-(\Delta x_+ + \Delta x_-)} + e_{i,j}, \quad (3.25)$$

where $e_{i,j}$ is the *local truncation error* of the approximation given by

$$e_{i,j} = \frac{\Delta x_+ - \Delta x_-}{3} \frac{\partial^3 T}{\partial x^3}\bigg|_{i,j} + \frac{\Delta y_+ - \Delta y_-}{3} \frac{\partial^3 T}{\partial y^3}\bigg|_{i,j} + O(h^2, k^2), \quad (3.26)$$

and $h = \max(x_+, x_-)$ and $k = \max(y_+, y_-)$. Hence on the nodes adjacent to the interface, the approximation to the temperature values is only first-order accurate. This is highly undesirable since these values are crucial in determining the correct movement of the solidification front. The low accuracy in these regions may give rise to numerical errors that can undermine the overall scheme during the time marching process.

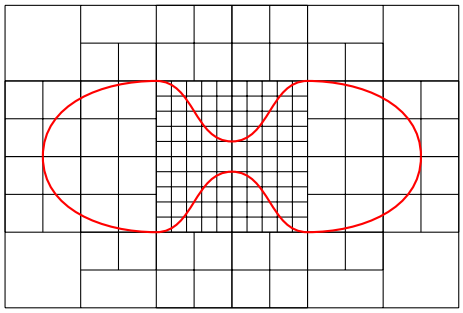

Figure 3.3: Adaptive grid based on the curvature of the interface

The accuracy of the approximation can be improved by extending the computational stencil. Such large stencils are challenging to implement around the edges of the computational domain where little data is available for the computations. Moreover, an issue arises in the regions where the interface exhibits a high curvature. In order to effectively capture the behaviour of the front, one needs to decrease the spacing of the computational grid. As most of the computational grid is, in fact, uniform, to increase efficiency, one might consider the use of an *adaptive grid*. However, this method requires relatively frequent regenerations of the grid based on the shape of the interface. Secondly,

an adaptive grid produces 'T-shaped' nodes that require special treatment during the computation.

Another way of achieving higher order differencing but without the extension of the computational stencils is the *compact finite difference* method. We pursue this possibility here.

3.2 Compact Finite Difference Approximations

The motivation behind the compact schemes is to develop a high order approximation to the governing equation without extending the computational stencil. It is achieved by storing the values of the derivatives of the function on the computational nodes as well as the functional values. This section provides a discussion on developing the compact approximations to the Laplace equation on non-uniform grids. From the previous section we know that the local truncation error of our method is given by

$$e_{i,j} = \frac{\Delta x_+ - \Delta x_-}{3}\left.\frac{\partial^3 T}{\partial x^3}\right|_{i,j} + \frac{\Delta y_+ - \Delta y_-}{3}\left.\frac{\partial^3 T}{\partial y^3}\right|_{i,j} + O(h^2, k^2). \tag{3.27}$$

One can note that on a uniform grid (when $\Delta x_- = \Delta x_+$ and $\Delta y_- = \Delta y_+$), the first two terms in (3.27) vanish and second order accuracy is restored.

Let us define $D^x_{i,j}$ and $D^y_{i,j}$ as the central difference approximations to the first derivatives with respect to x and y, respectively. Then using the results from the previous section, we can write

$$\begin{aligned} D^x_{i,j} = &-\frac{\Delta x_+}{\Delta x_-(\Delta x_+ + \Delta x_-)} T_{i-1,j} \\ &+ \left(\frac{\Delta x_+}{\Delta x_-(\Delta x_+ + \Delta x_-)} - \frac{\Delta x_-}{\Delta x_+(\Delta x_+ + \Delta x_-)}\right) T_{i,j} \\ &+ \frac{\Delta x_-}{\Delta x_+(\Delta x_+ + \Delta x_-)} T_{i+1,j}, \end{aligned} \tag{3.28}$$

$$D^y_{i,j} = -\frac{\Delta y_+}{\Delta y_-(\Delta y_+ + \Delta y_-)} T_{i,j-1} + \left(\frac{\Delta y_+}{\Delta y_-(\Delta y_+ + \Delta y_-)} - \frac{\Delta y_-}{\Delta y_+(\Delta y_+ + \Delta y_-)} \right) T_{i,j} + \frac{\Delta y_-}{\Delta y_+(\Delta y_+ + \Delta y_-)} T_{i,j+1}. \quad (3.29)$$

To reduce the error of the approximation given in (3.25), we can define the approximations to the third derivatives as

$$\left.\frac{\partial^3 T}{\partial x^3}\right|_{i,j} \approx \frac{2}{\Delta x_-(\Delta x_- + \Delta x_+)} D^x_{i-1,j} + \left(-\frac{2}{\Delta x_- \Delta x_+} \right) D^x_{i,j} + \frac{2}{\Delta x_+(\Delta x_- + \Delta x_+)} D^x_{i+1,j}, \quad (3.30)$$

$$\left.\frac{\partial^3 T}{\partial y^3}\right|_{i,j} \approx \frac{2}{\Delta y_-(\Delta y_- + \Delta y_+)} D^y_{i,j-1} + \left(-\frac{2}{\Delta y_- \Delta y_+} \right) D^y_{i,j} + \frac{2}{\Delta y_+(\Delta y_- + \Delta y_+)} D^y_{i,j+1}. \quad (3.31)$$

Substituting (3.30-3.31) into the equation (3.25) we can obtain the compact approximation to the Laplace operator as

$$\begin{aligned} \left.\nabla^2 T\right|_{i,j} \approx\ & A^x_{i,j} \left(T_{i-1,j} + \frac{\Delta x_+ - \Delta x_-}{3} D^x_{i-1,j} \right) \\ & + A^y_{i,j} \left(T_{i,j-1} + \frac{\Delta y_+ - \Delta y_-}{3} D^y_{i,j-1} \right) \\ & + B^x_{i,j} \left(T_{i+1,j} + \frac{\Delta x_+ - \Delta x_-}{3} D^x_{i+1,j} \right) \\ & + B^y_{i,j} \left(T_{i,j+1} + \frac{\Delta y_+ - \Delta y_-}{3} D^y_{i,j+1} \right) \\ & + C^x_{i,j} D^x_{i,j} + C^y_{i,j} D^y_{i,j} - E_{i,j} T_{i,j}. \end{aligned} \quad (3.32)$$

Here

$$A^x_{i,j} = \frac{2}{\Delta x_-(\Delta x_+ + \Delta x_-)}, \quad (3.33)$$

$$B^x_{i,j} = \frac{2}{\Delta x_+(\Delta x_+ + \Delta x_-)}, \tag{3.34}$$

$$C^x_{i,j} = \frac{2(\Delta x_+ + \Delta x_-)}{\Delta x_- \Delta x_+}, \tag{3.35}$$

$$A^y_{i,j} = \frac{2}{\Delta y_-(\Delta y_+ + \Delta y_-)}, \tag{3.36}$$

$$B^y_{i,j} = \frac{2}{\Delta y_+(\Delta y_+ + \Delta y_-)}, \tag{3.37}$$

$$C^y_{i,j} = \frac{2(\Delta y_+ + \Delta y_-)}{\Delta y_- \Delta y_+}, \tag{3.38}$$

$$E_{i,j} = \left(\frac{2}{\Delta x_+ \Delta x_-} + \frac{2}{\Delta y_+ \Delta y_-}\right). \tag{3.39}$$

Therefore, given the initial data, we can solve the Laplace equation iteratively by applying

$$\begin{aligned} T^{l+1}_{i,j} = \Bigg(& \left(T^l_{i-1,j} + \frac{\Delta x_+ - \Delta x_-}{3} D^{x,l}_{i-1,j}\right) \\ & + A^y_{i,j}\left(T^l_{i,j-1} + \frac{\Delta y_+ - \Delta y_-}{3} D^{y,l}_{i,j-1}\right) \\ & + B^x_{i,j}\left(T^l_{i+1,j} + \frac{\Delta x_+ - \Delta x_-}{3} D^{x,l}_{i+1,j}\right) \\ & + B^y_{i,j}\left(T^l_{i,j+1} + \frac{\Delta y_+ - \Delta y_-}{3} D^{y,l}_{i,j+1}\right) \\ & + C^x_{i,j} D^{x,l}_{i,j} + C^y_{i,j} D^{y,l}_{i,j}\Bigg) / E_{i,j}, \end{aligned} \tag{3.40}$$

where $T^l_{i,j}$ is the approximation to the temperature value at the node (i,j) in the l-th iteration. Substituting the expressions for the difference operators in the above equation recovers the second-order non-compact approximation of the Laplace equation based on the nine point stencil. Therefore, by using the derivative values on the nodes, as well as, of the temperature values, we have created a second-order accurate method using a smaller five-point stencil.

3.3 Boundary Conditions

Up to this stage, we have discussed the method for solving the temperature equation in the computational domain. However, the solution is clearly dependent on the boundary conditions imposed at the edges of the computational domain. We would like to develop a procedure for treating different types of boundary condition in the compact framework. In particular, we discuss Dirichlet, Neumann and Robin types of boundary conditions. In the discussion that follows, we will only consider conditions imposed on the left and right boundaries of the domain, i.e. $x = 0$ and $x = L$, ignoring the y dependence.

3.3.1 Dirichlet Boundary Conditions

Given a problem with Dirichlet boundary conditions a difficulty arises in computing the difference operators at the nodes $i = 0$ and $i = m$, where $m = L/\Delta x$. We can no longer use central difference since not enough computational nodes are available. Instead we can consider the following. Suppose we approximate the temperature as

$$T(x) \approx a + bx + cx^2, \tag{3.41}$$

for some constants a, b and c. Then at $x = 0$,

$$\frac{\partial T}{\partial x} \approx b. \tag{3.42}$$

Also we have that

$$T_0 = a, \tag{3.43}$$

$$T_1 = a + b\Delta x_1 + c(\Delta x_1)^2, \tag{3.44}$$

and

$$T_2 = a + b(\Delta x_1 + \Delta x_2) + c(\Delta x_1 + \Delta x_2)^2, \tag{3.45}$$

where Δx_1 and Δx_2 are the distances from nodes $i = 0$ to $i = 1$ and $i = 1$ to $i = 2$, respectively. Hence solving this system for a, b, c produces

$$c = \frac{T_1 - T_0 - b\Delta x_1}{(\Delta x_1)^2}, \tag{3.46}$$

$$b = \frac{\Delta x_1}{h\Delta x_1 - h^2}\left(T_2 - \frac{h^2}{(\Delta x_1)^2}T_1 + \left(\frac{h^2}{(\Delta x_1)^2} - 1\right)T_0\right), \tag{3.47}$$

where $h = \Delta x_1 + \Delta x_2$. By symmetry of the problem a similar expression can be obtained for the approximation of the y-derivative. Let $k = (\Delta y_1 + \Delta y_2)$ then we can set

$$D^x_{0,j} = \frac{\Delta x_1}{h\Delta x_1 - h^2}\left(T_{2,j} - \frac{h^2}{(\Delta x_1)^2}T_{1,j} + \left(\frac{h^2}{(\Delta x_1)^2} - 1\right)T_{0,j}\right), \tag{3.48}$$

$$D^y_{i,0} = \frac{\Delta y_1}{h\Delta y_1 - k^2}\left(T_{i,2} - \frac{k^2}{(\Delta y_1)^2}T_{i,1} + \left(\frac{k^2}{(\Delta y_1)^2} - 1\right)T_{i,0}\right). \tag{3.49}$$

In a similar fashion we can derive that

$$D^x_{m,j} = \frac{\Delta x_1}{h\Delta x_1 - h^2}\left(-T_{2,j} + \frac{h^2}{(\Delta x_1)^2}T_{1,j} - \left(\frac{h^2}{(\Delta x_1)^2} - 1\right)T_{0,j}\right), \tag{3.50}$$

$$D^y_{i,n} = \frac{\Delta y_1}{h\Delta y_1 - k^2}\left(-T_{i,2} + \frac{k^2}{(\Delta y_1)^2}T_{i,1} - \left(\frac{k^2}{(\Delta y_1)^2} - 1\right)T_{i,0}\right), \tag{3.51}$$

where $n = H/\Delta y$.

3.3.2 Neumann Boundary Conditions

If instead the value of the derivative is prescribed at the boundary $\left.\frac{\partial T}{\partial x}\right|_{x=0} = f(y)$ and $\left.\frac{\partial T}{\partial x}\right|_{x=L} = g(y)$, we can set

$$D^x_{0,j} = f_j, \tag{3.52}$$

$$D^x_{m,j} = g_j. \tag{3.53}$$

Moreover, using the standard procedure of introducing of ghost nodes $(-1, j)$ and $(m+1, j)$, from the central difference approximations we can write

$$\frac{T_{1,j} - T_{-1,j}}{2\Delta x} = f_j, \tag{3.54}$$

and

$$\frac{T_{m+1,j} - T_{m-1,j}}{2\Delta x} = g_j. \tag{3.55}$$

Giving

$$T_{-1,j} = T_{1,j} - 2\Delta x f_j, \tag{3.56}$$

and

$$T_{m+1,j} = T_{m-1,j} + 2\Delta x g_j. \tag{3.57}$$

Introducing the ghost nodes requires approximations to $D^x_{-1,j}$ and $D^x_{m+1,j}$. These can be achieved by using the one sided stencils as stated in (3.48) and (3.50). Hence substituting the values for the ghost nodes given in (3.56) and (3.57) we obtain

$$D^x_{-1,j} = \frac{\Delta x_1}{h\Delta x_1 - h^2}\left(\frac{h^2}{(\Delta x_1)^2}(T_{1,j} - T_{0,j}) + 2\Delta x_1 f_j\left(\frac{h^2}{(\Delta x_1)^2} - 1\right)\right), \tag{3.58}$$

$$D^x_{m+1,j} = -\frac{\Delta x_1}{h\Delta x_1 - h^2}\left(\frac{h^2}{(\Delta x_1)^2}(T_{m-1,j} - T_{m,j}) + 2\Delta x_1 g_j\left(\frac{h^2}{(\Delta x_1)^2} - 1\right)\right). \tag{3.59}$$

3.3.3 Robin Boundary Conditions

For our purposes Robin boundary conditions are the most appropriate given the modelling at hand. As far as free-drying procedures are concerned, the conditions on the boundary are best defined in terms of heat fluxes that are themselves dependent on the temperature values themselves. Let us suppose

that we are faced with the following conditions on $x = 0$ and $x = L$

$$\frac{\partial T}{\partial x} - k(T^a - T) = 0, \tag{3.60}$$

where k and T^a are constants. Following the discussion on Neumann type boundary conditions we can set

$$D^x_{0,j} = k(T^a - T_{0,j}), \tag{3.61}$$

$$D^x_{m,j} = k(T^a - T_{m,j}), \tag{3.62}$$

and

$$T_{-1,j} = T_{1,j} - 2\Delta x k(T^a - T_{0,j}), \tag{3.63}$$

$$T_{m+1,j} = T_{m-1,j} + 2\Delta x k(T^a - T_{m,j}). \tag{3.64}$$

Once again substituting these expression into the one sided equations for $D^x_{i,j}$ and $D^x_{i,j}$, we obtain

$$D^x_{-1,j} = \frac{\Delta x_1}{h\Delta x_1 - h^2}\left(\frac{h^2}{(\Delta x_1)^2}T_{1,j} - \frac{h^2}{(\Delta x_1)^2}\left(1 + 2\Delta x_1 k\left(\frac{h^2}{(\Delta x_1)^2} - 1\right)\right)T_{0,j}\right), \tag{3.65}$$

$$D^x_{m+1,j} = -\frac{\Delta x_1}{h\Delta x_1 - h^2}\left(\frac{h^2}{(\Delta x_1)^2}T_{m-1,j} - \frac{h^2}{(\Delta x_1)^2}\left(1 + 2\Delta x_1 k\left(\frac{h^2}{(\Delta x_1)^2} - 1\right)\right)T_{m,j}\right). \tag{3.66}$$

3.4 Summary

We have seen that the motion of the front across the computational grid creates nodes with non-uniform stencils. As a result, the standard five-point stencil is only first-order accurate. Therefore, it is necessary to improve the accuracy of the method. Compact differencing provides a scheme of high order accuracy

whilst not extending the computational stencil. The advantage lies in the fact that the computational grid can stay fixed during the time marching process. Hence there is no need to adaptively regenerate the grid even in regions where the interface exhibits high curvature. However, it is necessary to compute and store the values of the function's derivatives, as well as, of the functional values. This increases the computational cost, but, such effects are offset by achieving higher accuracy using a smaller computational stencil.

Chapter 4

Level Set Method and Solidification

4.1 Introduction

In chapter 2 we have introduced the level set method for solving moving boundary problems. The main advantage of this approach is that it handles interfaces undergoing topological changes very well. Unlike in the front fixing schemes, the solidification front can separate, join or fold over itself without requiring any special adjustments to the code. Therefore, this method enables us to model more complicated solidification scenarios.

Chapter 2 provided a discussion on deriving and solving equations associated with the level set method. The only issue that has not yet been addressed is the method of finding and computing the velocity field F that governs the advection of the interface. The problem of defining the velocity field F is heavily dependent on the particular setting we are modelling. However, frequently the speed of the motion of the interface has a meaningful definition only on the interface itself. Therefore, one needs techniques for extending the definition of F to the rest of the computational domain [52]. Over the years, multiple methods have been developed to tackle the problem.

Mallandi, Sethian and Vermuri in [28] used the level set framework to recover the shapes of objects from various visual 2D and 3D data. In order to extend the velocity field to every point in the narrow band, they assigned the value of F at a given point equal to the value of F at the closest point on the

interface. With this construction, the level sets will remain a constant distance from each other [28]. Moreover, this method can be done quite efficiently by tracing back along the gradients of ϕ [52].

Another approach is to evaluate the speed function of the interface using an expression that has meaning only on the front itself. Such a method was used in [51] when solving the problem of dendritic solidification. The authors transformed the condition on the moving front to the form of a boundary integral which was then evaluated both on and off the interface.

Alternatively, one could assign artificial values of the speed function of the interface by continuously extending them in the proper upwind direction using the advection equation. Such a method was used in [4] and will be applied to our scenario as well.

4.2 Solidification

In chapter 1.4 we have formalised mathematically the dynamics of a solidification/melting problem. This section is focused on stating the Stefan problem in terms of the level set framework. We shall base our formulation on the work done by Chen et al. in [4].

From the discussion in chapter 1.4, the multidimensional Stefan problem is given by

$$\frac{\partial T_i}{\partial t} = \nabla^2 T_i \qquad \mathbf{x} \in D_i, \tag{4.1}$$

$$v_n = -\left[\frac{\partial T}{\partial n}\right] \qquad \mathbf{x} \in \Gamma(t), \tag{4.2}$$

where v_n denotes the normal velocity of the interface, and $\left[\frac{\partial T}{\partial n}\right]$ is the jump in the normal derivatives across the interface given by

$$\left[\frac{\partial T}{\partial n}\right] = k_2 \frac{\partial T_2}{\partial n} - k_1 \frac{\partial T_1}{\partial n}. \tag{4.3}$$

The equation (4.2) can then be rewritten in the form

$$v_n = -[\nabla T] \cdot \mathbf{n}, \tag{4.4}$$

where $[\nabla T]$ represents the jump in the temperature gradient from liquid to solid regions. Then by using the level set function ϕ, one obtains

$$v_n = -[\nabla T] \cdot \frac{\nabla \phi}{|\nabla \phi|}. \tag{4.5}$$

Since the velocity field F must agree with v_n on the interface, we have that

$$\phi_t + v_n |\nabla \phi| = 0, \qquad \mathbf{x} \in \Gamma(t). \tag{4.6}$$

Hence combining equations (4.5) and (4.6) gives

$$\phi_t - [\nabla T] \cdot \nabla \phi = 0, \qquad \mathbf{x} \in \Gamma(t). \tag{4.7}$$

Therefore the task is now to extend the definition of $[\nabla T]$ off the solidification interface. We shall proceed along the lines of [4]. Let us define the quantities

$$u^1 = \left[\frac{\partial T}{\partial x}\right], \tag{4.8}$$

$$u^2 = \left[\frac{\partial T}{\partial y}\right]. \tag{4.9}$$

Then we can continuously extend the values for the jumps in derivatives of T using the following advection equations

$$u^1_t + S(\phi)\phi_x u^1_x = 0, \tag{4.10}$$

$$u^2_t + S(\phi)\phi_y u^2_y = 0. \tag{4.11}$$

Here $S(x)$ denotes again the sign function. The equations (4.10) and (4.11) extend continuously u^1 and u^2 by advecting them in the correct upwind direction. Moreover, these advection equations will not distort the values of the derivative jumps on the interface, since $\phi(\mathbf{x}, t) = 0$ on the solidification front therefore $S(\phi)\phi_x$ and $S(\phi)\phi_y$ will be zero, as well. Moreover, for the points on the opposite side of the solidification front we would like the characteristics

of the advection equations to point in the opposite directions. This is again ensured by the $S(\phi\phi_x)$ and $S(\phi\phi_y)$ terms.

4.3 Numerical Discretisation

In this section, we shall derive the numerical approximations to the equations described in section 4.2. The first task is to compute the jumps in the heat fluxes across the interface. Proceeding along the lines of [4], we can define the values of u^1 and u^2 on the nodes adjacent to the interface as

$$u^1_{i,j} = -S_{i,j}(\phi_x)\frac{(T_{i+2,j} - T_{i+1,j}) - (T_{i-1,j} - T_{i-2,j})}{\Delta x}, \tag{4.12}$$

$$u^2_{i,j} = -S_{i,j}(\phi_y)\frac{(T_{i,j+2} - T_{i,j+1}) - (T_{i,j-1} - T_{i,j-2})}{\Delta y}. \tag{4.13}$$

The sign functions in the above expressions ensure that the jumps are consistently computed from solid to liquid regions and we shall use the standard second order central approximations to the spatial derivatives of ϕ. The task of finding these adjacent nodes is straightforward, since we simply check for the nodes where the level set function ϕ changes sign.

As mentioned previously, we would like to continuously extend the jumps to the whole computational domain. This is achieved by solving the advection equations (4.10 - 4.11). We shall use the first-order upwind method to solve them. The choice of the time step Δt_u is relatively arbitrary and the only requirement is that the time step has to satisfy the CFL condition

$$\frac{\Delta t_u}{h} \leq 1,$$

where $h = \min(\Delta x, \Delta y)$. Thus we can write

$$u^{1,n+1}_{i,j} = u^{1,n}_{i,j} - \frac{\Delta t_u}{\Delta x}(u^{1,n}_{i,j} - u^{1,n}_{i-1,j}), \text{ if } S(\phi\phi_x) > 0 \tag{4.14}$$

and

$$u^{1,n+1}_{i,j} = u^{1,n}_{i,j} + \frac{\Delta t_u}{\Delta x}(u^{1,n}_{i+1,j} - u^{1,n}_{i,j}), \text{ if } S(\phi\phi_x) < 0. \tag{4.15}$$

Setting the CFL condition to 0.5, the above gives

$$u_{i,j}^{1,n+1} = u_{i,j}^{1,n} - 0.5(u_{i,j}^{1,n} - u_{i-1,j}^{1,n}), \text{ if } S(\phi\phi_x) > 0, \tag{4.16}$$

and

$$u_{i,j}^{1,n+1} = u_{i,j}^{1,n} + 0.5(u_{i+1,j}^{1,n} - u_{i,j}^{1,n}), \text{ if } S(\phi\phi_x) < 0. \tag{4.17}$$

Having extended the jumps in heat fluxes, we need to construct the velocity field F that will control the movement of the interface. Since at the interface F should correspond to v_n, we set

$$F_{i,j} = u_{i,j}^1 \left(\frac{\phi_x}{|\nabla\phi|}\right)_{i,j} + u_{i,j}^2 \left(\frac{\phi_y}{|\nabla\phi|}\right)_{i,j}. \tag{4.18}$$

Then

$$F_{i,j}|\nabla\phi| = u_{i,j}^1(\phi_x)_{i,j} + u_{i,j}^2(\phi_y)_{i,j}. \tag{4.19}$$

The spatial derivatives are approximated using the second order ENO2 scheme. Therefore substituting the above into the level set equation (2.12) we obtain

$$\phi_t = -(u_{i,j}^1(\phi_x)_{i,j} + u_{i,j}^2(\phi_y)_{i,j}). \tag{4.20}$$

Hence there is no need to explicitly compute $F_{i,j}$ or $|\nabla\phi|$ in this setting. However, in the framework of crystal growth or dendritic solidification one need to take into account the curvature of the interface and hence the computation of $|\nabla\phi|$ is required. The temporal derivative in (4.20) is approximated using the third order TVD Runge-Kutta method described in section 2.4.4.

Finally, it remains to show how to compute the distances $\Delta x_+, \Delta x_-, \Delta y_+, \Delta y_-$ of a computational node to the interface, as used in chapter 3. For illustration, we shall focus on finding $\Delta x_+, \Delta x_-$ as the distances in the y direction can be computed similarly. The key to finding these lies in the fact that level-set function ϕ is a signed distance function. Therefore, if we approximate the interface near a node as a straight line, the values of $|\phi|$ correspond to the

lengths of one of the legs of two similar right-angled trianges, as illustrated in figure 4.1. Then using $\Delta x_+ + \Delta x_- = \Delta x$, one obtains

$$\Delta x_+ = \frac{\Delta x |\phi_{i,j}|}{|\phi_{i,j}| + |\phi_{i+1,j}|},$$

and

$$\Delta x_- = \frac{\Delta x |\phi_{i+1,j}|}{|\phi_{i+1,j}| + |\phi_{i,j}|}.$$

It is important to stress that such coputation work precisely because ϕ is chosen to store the distances of any computational node to the interface, and this procedure would not work if defferent choice for ϕ would be selected such as the temperature field.

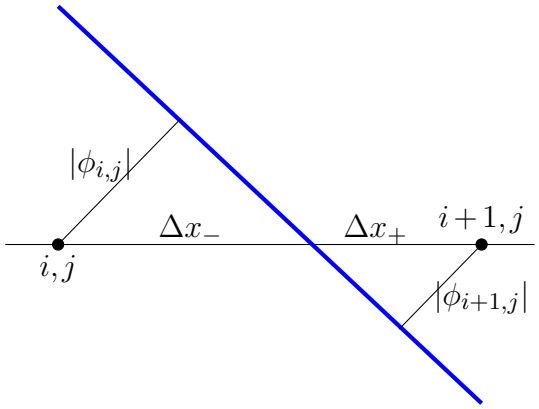

Figure 4.1: Computation of Δx_+ and Δx_-. The blue line correnspponds to the interface position.

4.4 Summary

We shall conclude this chapter with a short outline of the algorithm used.

1. Initialise the temperature field $T(\mathbf{x}, t)$ and the level set function $\phi(\mathbf{x}, t)$ as a signed distance function from the solidification front.

2. Compute the jumps in the temperature gradients u^1 and u^2 for the point adjacent to the interface.

3. Extend the jumps by solving the advection equations (4.10-4.11) and compute $F|\nabla\phi|$ using (4.19).

4. Update ϕ by solving the level set equation (2.12) for one time step, and set ϕ_0 to be equal to ϕ, which is no longer a signed distance function.

5. Reinitialise ϕ to a signed distance function by iterating the reinitialisation equation (2.15) untill steady state is reached (usually 3 or 4 iterations are sufficient to meet the convergence criterion)

6. Update the temperature by solving the Laplace equations in both solid and liquid phases using the compact finite difference method where the computational grid is non-uniform.

7. Repeat the steps 2-6 for the next time step until the desired time t is reached.

Chapter 5

Single Vial Model Discussion

This chapter is devoted to applying the level set method to various models for freeze-drying of a single vial and related inward solidification scenarios.

5.1 Freezing of a Semi-infinite Slab

We shall first look at the one-dimensional freezing problem. Assume that the semi-infinite region $x \in [0, \infty]$ is initially occupied by liquid at fusion temperature $T = 1$. At $t > 0$ the temperature at the boundary at $x = 0$ is then suddenly dropped and subsequently maintained at temperature $T = 0$. As before, we shall assume that the Stefan number β is large and therefore we solve the following system.

$$\frac{d^2T}{dx^2} = 0, \text{ for } x \in [0, f] \tag{5.1}$$

subject to

$$T(0) = 0, \tag{5.2}$$

$$\left.\frac{dT}{dx}\right|_{x=f} = \dot{f} \tag{5.3}$$

and

$$T(f) = 1. \tag{5.4}$$

The system described above has a relatively simple solution. From (5.1), (5.2) and (5.4) we have that $T = x/f$. Then using (5.3) one gets

$$f = (2t)^{1/2}, \tag{5.5}$$

$$T = \frac{y}{(2t)^{1/2}}. \tag{5.6}$$

As before we shall use a small time delay to start the numerical computations. In this case t_1 has been chosen to correspond to $f = 0.3$. The results are shown in figure 5.1. We can see that the computations agree well with the analytical solution.

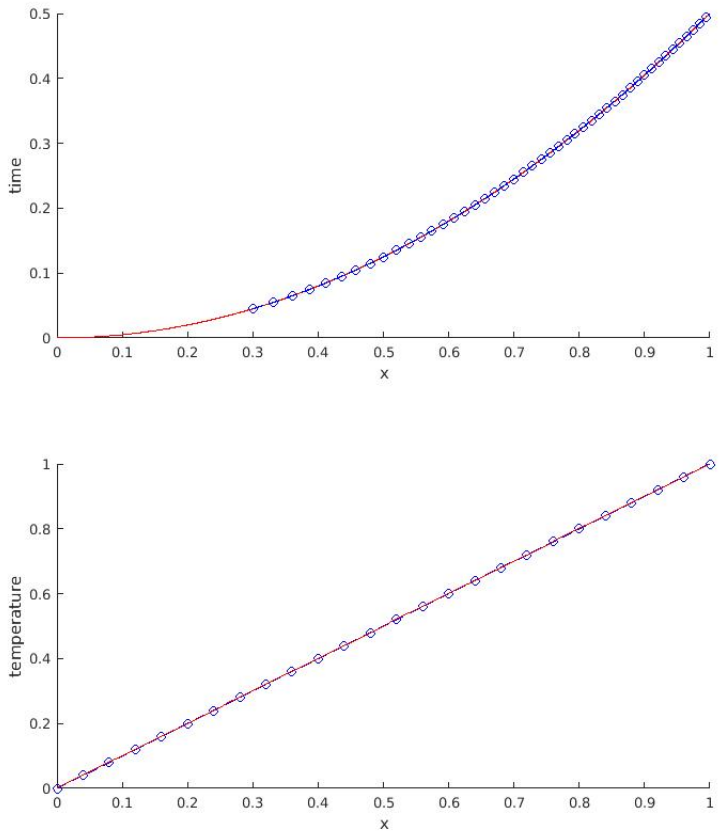

Figure 5.1: Comparison of the analytical (red solid line) solution for the one dimensional problem against the numerics (blue circles). The system was simulated till time $t = 0.5$ with $\Delta x = 0.01$ and $\Delta t = 0.001$. The top graph shows the position of the interface against time and the bottom the final temperature distribution.

The table 5.1 below shows the convergence of the proposed method under the maxim error norm. The results indeed confirm the method converges with order of at least two.

Δx	Maximum absolute error	Order
0.2	3.1×10^{-3}	
0.1	3.916×10^{-4}	2.9876
0.05	6.748×10^{-5}	2.5368
0.02	1.044×10^{-5}	2.0365

Table 5.1: The results of the comparison of the numerical and analytical solution.

5.2 Cylinder Problem

To test the accuracy of the numerical level set method for a two-dimensional setting, let us consider an inward solidification of a cylinder with radius $R = 1$. Let the inside of the cylinder be at the fusion temperature $T = 1$. At time $t > 0$ the temperature on the surface of the cylinder is dropped and subsequently maintained at $T = 0$. Let F denote the frozen thickness. The full description of the problem is presented in figure 5.2.

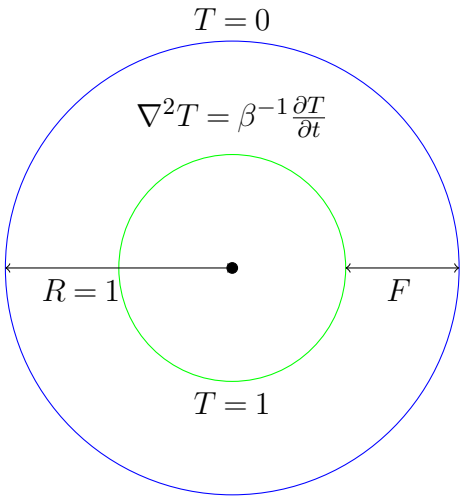

Figure 5.2: Illustration of the inward solidification of the cylinder

5.2.1 Analytical Solution

The heat equation in cylindrical coordinates (assuming radial dependence only) is given by

$$\frac{\partial^2 T}{\partial r^2} + r^{-1}\frac{\partial T}{\partial r} = \beta^{-1}\frac{\partial T}{\partial t},$$

subject to:

$$T(1,\theta) = 0,$$

$$T(1-F,\theta) = 1,$$

$$\left.\frac{\partial T}{\partial r}\right|_{r=1-F} = -\frac{dF}{dt}.$$

Assuming $\beta >> 1$ we can expand T and t in the power series of $1/\beta$.

$$T = T_0 + \beta^{-1}T_1 + O(\beta^{-2}),$$

$$t(F) = t_0 + \beta^{-1}t_1 + O(\beta^{-2}).$$

Hence up to the leading order, we have

$$\frac{\partial^2 T_0}{\partial r^2} + r^{-1}\frac{\partial T_0}{\partial r} = 0,$$

where

$$T_0(1,\theta) = 0,$$

$$T_0(1-F,\theta) = 1,$$

$$\left.\frac{\partial T_0}{\partial r}\right|_{r=1-F} = -\frac{dF}{dt}.$$

This problem has an analytical solution given by

$$T_0 = \frac{\ln(r)}{\ln(1-F)},$$

and

$$t_0(F) = \frac{1}{4}\Big[(1-F)^2(\ln(1-F)^2 - 1) + 1\Big].$$

Hence the full solidification time (at $F = 1$) is at $t_0 = 1/4$.

In computations, the time delay has been chosen to correspond to $F = 0.1$. The comparison of the simulations against the analytical solution is depicted in figure 5.3. The numerics are plotted at times corresponding to the frozen thickness of $0.2, 0.4, 0.6$ and 0.8 for various grid spacings. Again we see a good agreement with the analytical values for sufficiently small refined grids.

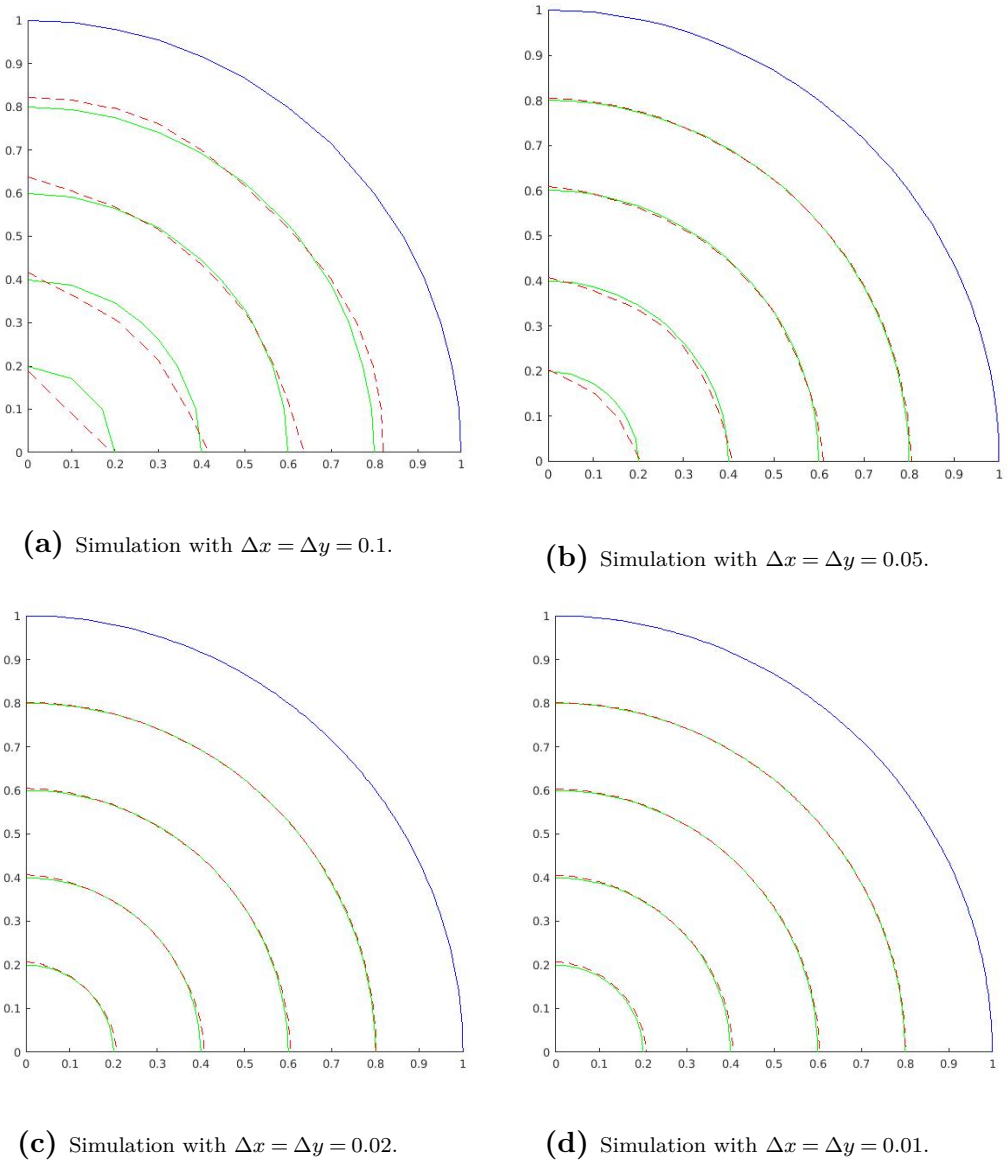

(a) Simulation with $\Delta x = \Delta y = 0.1$.

(b) Simulation with $\Delta x = \Delta y = 0.05$.

(c) Simulation with $\Delta x = \Delta y = 0.02$.

(d) Simulation with $\Delta x = \Delta y = 0.01$.

Figure 5.3: Simulations of the cylinder freezing problem for various grid sizes. The blue line depicts the boundary of the cylinder. Simulated values are show with dotted red lines. Green solid lines represent the analytical solution for given time. For all the simulations, the time step has been chosen as 0.001. The numerical solution agrees with the analytical one well for grid sizes of $\Delta x = \Delta y = 0.01$ and 0.02.

5.3 Single Vial Model

We shall now present a single vial model. Generally, heat transfer can occur via conduction, convection or radiation. Ganguly et al. [14] quantified the contributions experimentally from different means of heat transfer during pharmaceutical freeze-drying processes. The study shows that the heat exchange between the bottom of the vial and the freeze-drying shelf occurs mainly through conduction between the contact points of the vial with the shelf. The sides of the vial interact with its surroundings mainly through radiative heat transfer between the vial and the insides of the freeze-drying chamber. Although under certain conditions, such as atmospheric pressure inside the chamber conduction between the sides of the vial and the surrounding air can play a role, as well.

Therefore, we will compare different combinations of the flux and Dirichlet boundary conditions imposed at the sides of the vial. As before, we use the small-time solution to start the time marching process.

The whole model is summarised in figure 5.4. One of the main assumptions used in this particular scenario is that the Stefan number β is large. Therefore, we use a quasi-steady-state approximation for the governing equation.

Convective and radiative heat fluxes are given by

$$\frac{\partial T}{\partial n} = k(T^a - T(\mathbf{x},t)) \text{ for } \mathbf{x} \in \partial D, t > 0 \tag{5.7}$$

and

$$\frac{\partial T}{\partial n} = \hat{k}((T^a)^4 - (T(\mathbf{x},t))^4) \text{ for } \mathbf{x} \in \partial D, t > 0 \tag{5.8}$$

respectively. Here T^a denotes the surrounding ambient temperature which in our setting is considered to be constant. The values of k and $\hat{k}$ are the heat transfer coefficients and are usually determined experimentally.

In practice, often the convective heat flux coexists with its radiative coun-

terpart. Since

$$(T^a)^4 - T^4 = ((T^a)^2 + T^2)(T^a + T)(T^a - T), \tag{5.9}$$

we can write radiative the heat flux in terms of the convective one with the heat transfer coefficient depending on the ambient and surface temperatures as

$$\frac{\partial T}{\partial n} = k(T^a, T, t)(T^a - T(\mathbf{x}, t)) \text{ for } \mathbf{x} \in \partial D, t > 0. \tag{5.10}$$

The heat transfer coefficient, in general, depends on the material, geometry and the velocity properties of the heat transfer fluid, as well as, the emissivity of the participating media gaps etc. The model with flux boundary conditions is proposed as described in figure 5.4.

The following sections are focused on computing small-time asymptotic solutions with Dirichlet and Robin boundary conditions. These analytical solutions will then be used to start the numerical computations.

5.3.1 Small Time Solution with Dirichlet Boundary Condition

We shall now examine the asymptotic behaviour of the function f for $t << 1$. We expect a thin solidified layer near $y = 0$ along $0 << x << 1$ with small adjustment regions near the corners. The function f can be viewed as a measure of the frozen thickness and since we would expect f to be relatively flat for small times, we can approximate the moving boundary condition by

$$\left.\frac{\partial T}{\partial y}\right|_{y=f(x,t)} = \frac{\partial f}{\partial t}. \tag{5.11}$$

Since $y << 1$ we can let $y = t^\alpha Y$, where $Y \sim 1$ and α is a constant to be determined. Moreover, because $y = f$ at the solidification interface one obtains

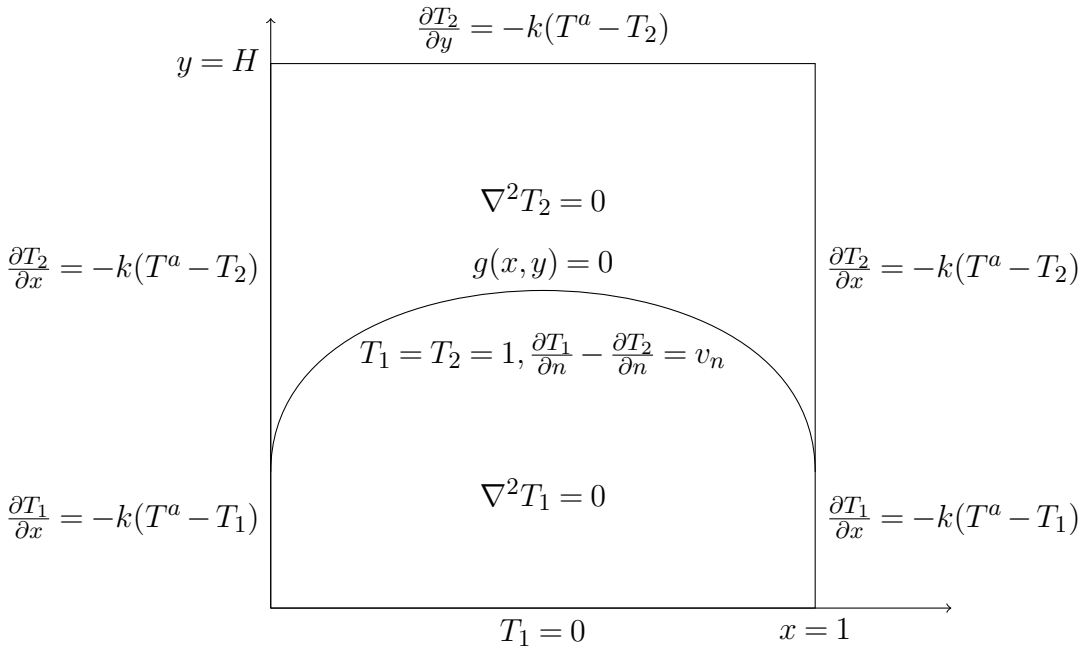

Figure 5.4: Mathematical Formulation of the Heat Flux Model. The Dirichlet boundary condition at $y = 0$ comes from the assumption of perfect contact of the vial with the shelf. The rest of the boundary conditions have been replaced by prescribed convective fluxes. The subscripts 1,2 denote the frozen and liquid regions respectively.

that $f = t^\alpha Y$. Therefore, by the chain rule,

$$\frac{\partial T}{\partial y} = t^{-\alpha} \frac{\partial T}{\partial Y} \tag{5.12}$$

and

$$\frac{\partial f}{\partial t} = \alpha t^{\alpha - 1} Y. \tag{5.13}$$

Substituting these expressions into the boundary condition (5.11), requires

$$-\alpha = \alpha - 1, \tag{5.14}$$

Hence $\alpha = 1/2$.

Then for $x \sim 1$ and $t << 1$ we can expand f and T in power series in t. Hence let

$$f = t^{1/2} f_0 + ..., \tag{5.15}$$

and

$$T = T_0(x,Y) + t^{1/2}T_1(x,Y) + ... \tag{5.16}$$

Substituting 5.16 into the Laplace equation, we find that up to the leading order,

$$\frac{\partial T_0}{\partial Y} = 0. \tag{5.17}$$

Hence

$$T_0(x,Y) = C_1(x)Y + C_2(x). \tag{5.18}$$

Since $T(x,0) = 0$, we have that $C_2(x) = 0$. From 5.15 we know that the moving interface occurs at $Y = f_0$. Since $T = 1$ at the interface we have that $C_1(x) = f_0^{-1}$. Substituting these results into the condition on the boundary 5.11, we then get that $f_0 = 2^{1/2}$ and hence up to the leading order,

$$f = (2t)^{1/2}, \text{ and} \tag{5.19}$$

$$T = \frac{y}{(2t)^{1/2}}. \tag{5.20}$$

5.3.2 Small Time Solution with Robin Boundary Condition

Just as we did for the case of a Dirichlet boundary condition, we shall now investigate the small-time behaviour of a system with a Robin boundary condition. By symmetry of the problem, we shall consider only the left boundary at $x = 0$.

Just as before, for $t << 1$ we expect a small solidified layer to occur in the region where $0 << y << 1$ and $x << 1$. Therefore we can again introduce a scaling $x = t^{\alpha}X$, where X is $O(1)$. We shall assume that the interface is flat and the temperature is independent of y. Since at the interface $T = 1$, we can write the temperature as

$$T = T_0(X) + t^{\beta}T_1(X) + ... \tag{5.21}$$

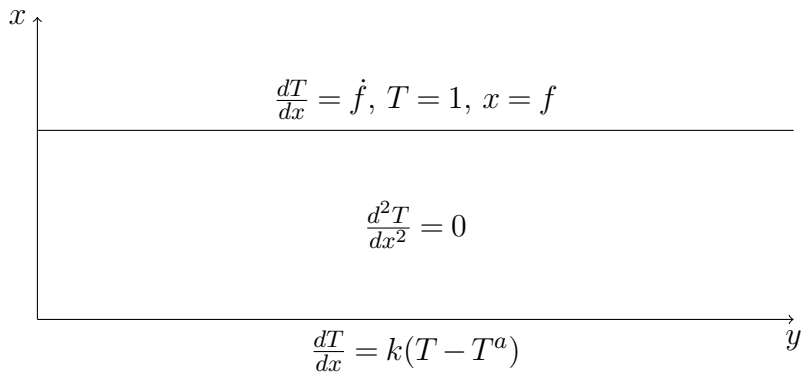

Figure 5.5: Illustration of freezing at small times with Robin boundary condition at $x = 0$.

and the interface as

$$f(t) = t^{\alpha} f_0(X) + ... \tag{5.22}$$

Hence we looking the solution of the equation

$$\frac{d^2T_0}{dX^2} + t^{\beta}\frac{d^2T_1}{dX^2} + .. = 0. \tag{5.23}$$

Subject to

$$T_0(f_0) + t^{\beta}T_1(f_0) + ... = 1, \tag{5.24}$$

$$\left.\frac{dT_0}{dX}\right|_{X=f_0} + t^{\beta}\left.\frac{dT_1}{dX}\right|_{X=f_0} + ... = \alpha t^{2\alpha-1} f_0, \tag{5.25}$$

and

$$\left.\frac{dT_0}{dX}\right|_{X=0} + t^{\beta}\left.\frac{dT_1}{dX}\right|_{X=0} + ... = k\left(t^{\alpha}(T_0(0) - T^a) - t^{\beta-\alpha}T_1(0) + ...\right). \tag{5.26}$$

In order to balance the equation (5.25) we require

$$\beta = 2\alpha - 1. \tag{5.27}$$

Similarly to balance the equation (5.26) we need

$$\beta = \alpha. \tag{5.28}$$

Hence $\beta = \alpha = 1$.

At $O(1)$ the system (5.23-5.26) gives

$$\frac{d^2T_0}{dX^2} = 0, \tag{5.29}$$

$$T_0(f_0) = 1, \tag{5.30}$$

$$\left.\frac{dT_0}{dX}\right|_{X=0} = \left.\frac{dT_0}{dX}\right|_{X=f_0} = 0. \tag{5.31}$$

This has a simple solution $T_0 = 1$.

At $O(t)$ the system (5.23-5.26) becomes

$$\frac{d^2T_1}{dX^2} = 0, \tag{5.32}$$

$$T_1(f_0) = 0, \tag{5.33}$$

$$\left.\frac{dT_1}{dX}\right|_{X=f_0} = f_0, \tag{5.34}$$

and

$$\left.\frac{dT_1}{dX}\right|_{X=0} = k(1-T^a). \tag{5.35}$$

Therefore the solution at order t is

$$T_1(X) = f_0X - f_0^2, \tag{5.36}$$

where

$$f_0 = k(1-T^a). \tag{5.37}$$

Hence the small time solution for Robin boundary condition is given by

$$T(x,t) = 1 + \left(kx(1-T^a) - tk^2(1-T^a)^2\right) \tag{5.38}$$

and

$$f(t) = tk(1-T^a). \tag{5.39}$$

5.3.3 Single Vial Model Results

The results of the single vial model are summarised in figures 5.6, 5.7 and 5.8. In figure 5.6 depicts the numerical simulation with the ambient temperature $T^a = 0$ and the heat transfer coefficient $k = 1$. The Dirichlet boundary condition $T = 0$ is imposed on the top and bottom of the vials. The computations are done using uniform grid $\Delta x = \Delta y = 0.01$ with time step $\Delta t = 0.001$. The procedure has started using the small time solutions at $t = 0.005$ and marched till $t = 0.1$. The figure 5.7 shows simulation done with the same set of parameters as in 5.6 but with the heat transfer coefficient set to $k = 5$.

Because of the boundary conditions imposed, the solidification progresses along all four edges of the vial. In both cases of $k = 1$ and $k = 5$, the rate of progression of the interface along the vertical direction is faster than along the horizontal one. Initially, the temperature distribution stays relatively flat long the x direction, as the contributions of the additional cooling from the sides of the vial did yet penetrated deep enough into the vial. This starts to change around $t = 0.06$ in the case of $k = 1$ and around $t = 0.02$ in the case of $k = 5$ when we see a gradual change of the shape of the interface from rectangular and become more ellipsoid.

The additional heat transfer for $k = 5$ causes the product to completely solidify by $t = 0.1$. However, in the case of $k = 1$, there is still a thin unsolidified layer in the middle of the vial. The figure 5.7 also demonstrates of the proposed method the moment the product fully freezes. Because of the steady-state assumption, when the interface disappears the temperature immediately jumps to a constant value of $T = 0$. Hence there is no gradual cooling of the product.

The figure 5.8 displays a model with $k = 10$ and insulation condition applied on the top. This condition seems more appropriate in the setting of freeze-drying as the vials are sealed with a rubber stopper that is a good thermal insulator. The results show that the interface progresses with almost equal speed along the vertical and horizontal direction. However, because of the absence of cooling from the top, even with a relatively large cooling of the

sides of the vials there is still a significant area of the liquid product at the top-centre of the vial at time $t = 0.1$.

5.4 Volume Change

In the process of developing a mathematical model of freezing, we have made several assumptions. For instance, the latent heat is assumed to be constant, the interface is of infinitesimal thickness, we are neglecting the effects of curvature and surface tension, and the phase temperature is considered to be constant. Most of these simplifications are quite reasonable and consistent with each other.

In particular, we have been neglecting the density change between liquid and solid regions. Such a description was necessary to avoid the movement of the material. Because of the small volume each vial (around 20ml), and relatively small fill volume of the product (around 5ml), neglecting the change of volume during freezing stage does not introduce significant errors, and it is often ignored. However, in many solidification procedures (such as industrial metal casting processes) the study of density change effects is of great importance for determining the final solidified shape of the material and its defects due to porosity.

The purpose of the chapter is to devise a level set formulation of the solidification problem, including the effects of density change.

There are multiple studies in the literature concerning with the density change effects in Stefan type problems. Tao [60] investigated the solidification problems with density jump at the interface in a semi-infinite medium. It was shown that these formulations could be converted into classical Stefan problem with constant densities using an appropriate change of coordinates. Tarzia [62] developed an exact solution for Stefan problems with convective boundary conditions. A simple model of approximate determination of the final solidified shapes during a phase change process with a change of density was developed in [25] based on overall mass conservation. A phase-field deriva-

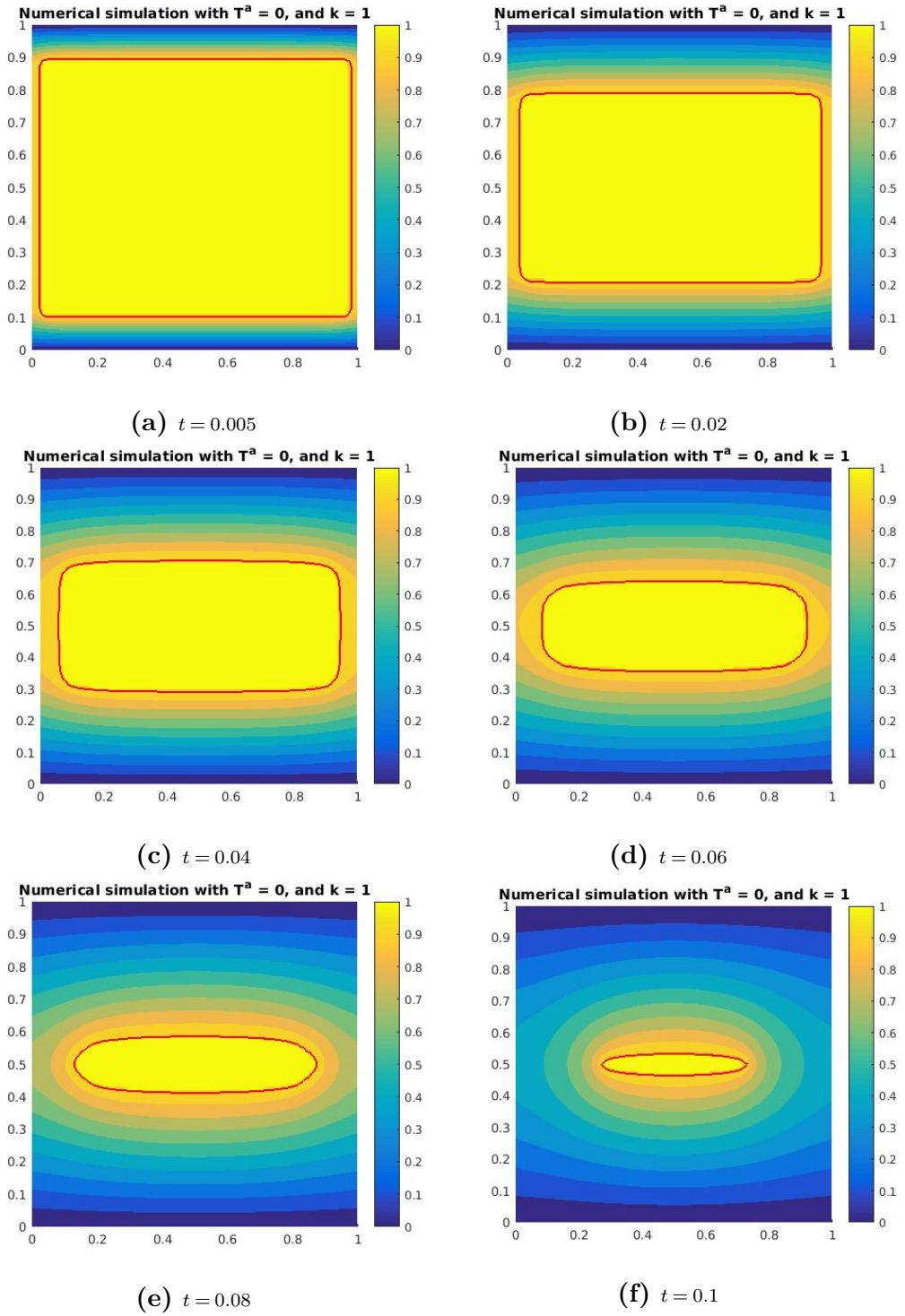

(a) $t = 0.005$ **(b)** $t = 0.02$

(c) $t = 0.04$ **(d)** $t = 0.06$

(e) $t = 0.08$ **(f)** $t = 0.1$

Figure 5.6: Progression of the interface (red) and the temperature profiles. Dirichlet boundary conditions $T = 0$ imposed on the top and bottom of the vial and flux conditions on the sides with $k = 1$. Simulated with $\Delta x = \Delta y = 0.01$ and $\Delta t = 0.001$.

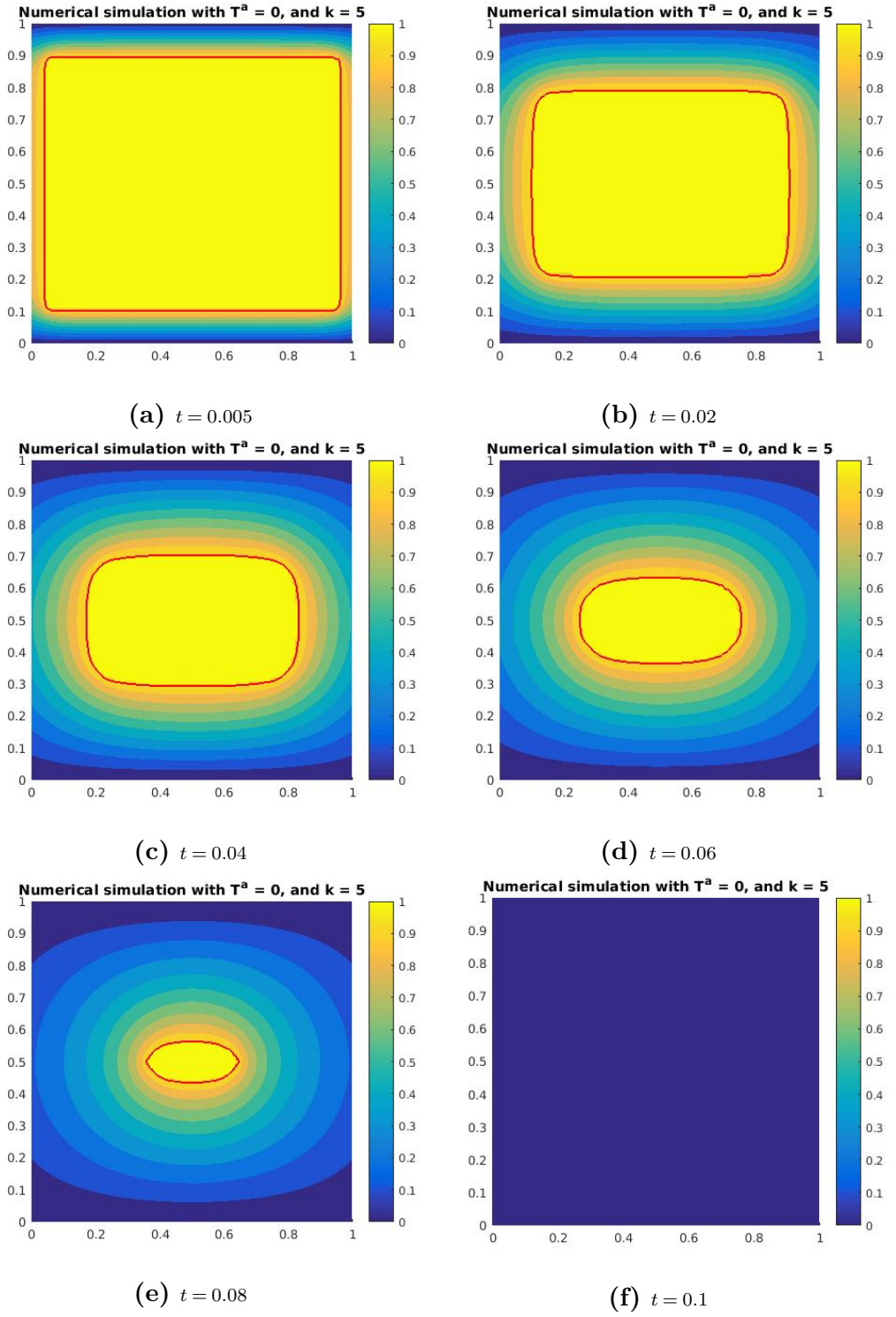

(a) $t = 0.005$ **(b)** $t = 0.02$

(c) $t = 0.04$ **(d)** $t = 0.06$

(e) $t = 0.08$ **(f)** $t = 0.1$

Figure 5.7: Progression of the interface (red) and the temperature profiles. Dirichlet boundary conditions $T = 0$ imposed on the top and bottom of the vial and convective flux conditions on the sides with $k = 5$. Simulated with $\Delta x = \Delta y = 0.01$ and $\Delta t = 0.001$.

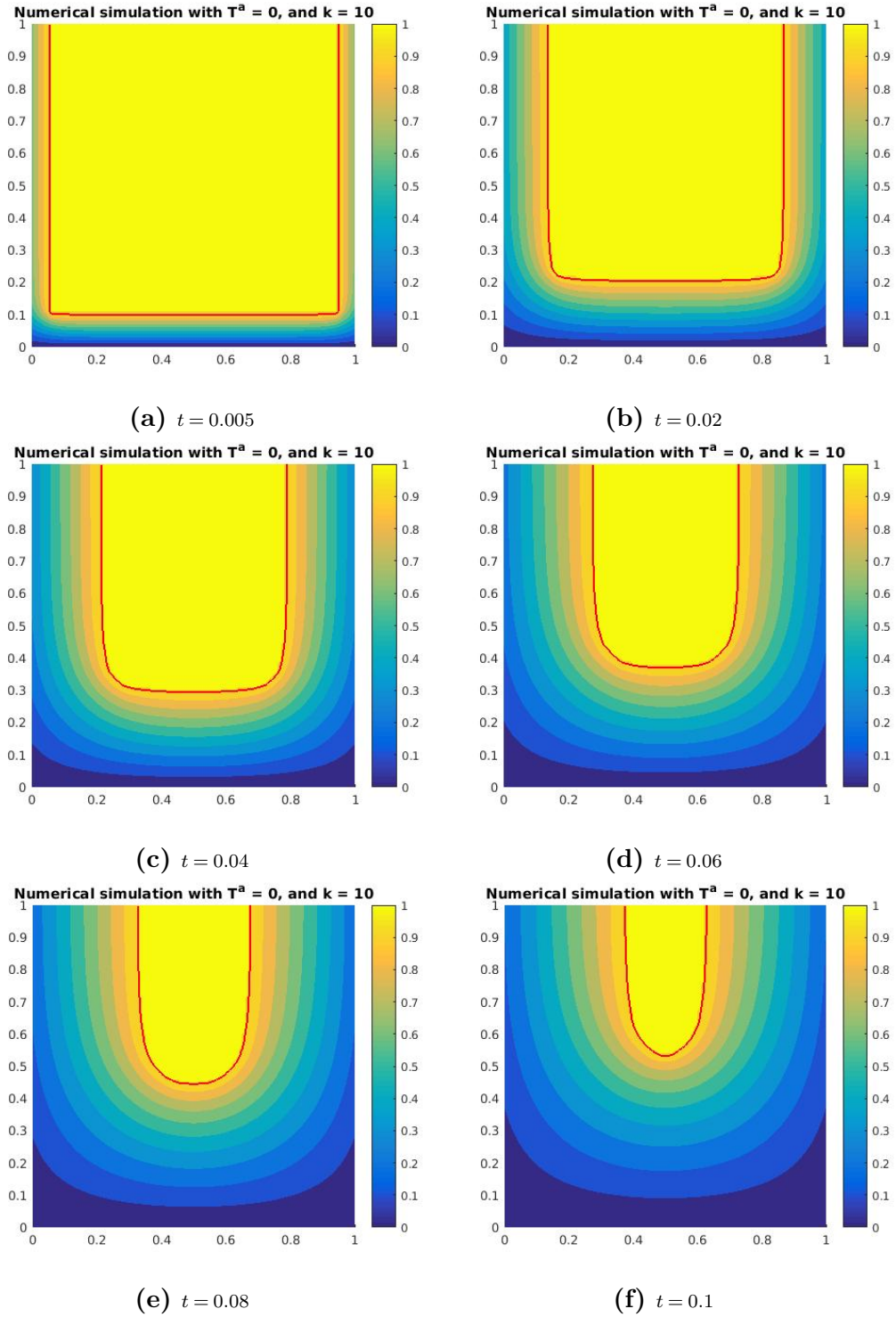

(a) $t = 0.005$ **(b)** $t = 0.02$

(c) $t = 0.04$ **(d)** $t = 0.06$

(e) $t = 0.08$ **(f)** $t = 0.1$

Figure 5.8: Progression of the interface (red) and the temperature profiles. Dirichlet boundary condition $T = 0$ imposed on the bottom of the vial and convective flux conditions on the sides with $k = 10$. Vial is assumed to be insulated from the top by a rubber stopper. Simulated with $\Delta x = \Delta y = 0.01$ and $\Delta t = 0.001$.

tion was introduced in [56]. There are multiple other studies concerning this issue for instance [18, 29, 6, 41].

5.4.1 Mathematical Model with Density Change

We shall now develop a mathematical model of solidification procedure with density change. We shall assume that the densities in the liquid and solid regions (denoted by ρ_2 and ρ_1 respectively) are different but constant. Therefore we shall have a sudden jump in density across the solidification front. Given the small length scale of the problem and our steady-state assumption, we shall ignore the effects of natural convection in the liquid caused by the density change.

Therefore the model has two free boundaries. One between the solid and liquid region and the other representing the current water level in the vial. We shall assume that the second free boundary in planar and located at $y = h(t)$. The Stefan condition with density change has the form

$$k_2 \frac{\partial T_2}{\partial n} - k_1 \frac{\partial T_1}{\partial n} = -\rho_1 H v_n. \tag{5.40}$$

Since the top of the freeze-drying vial consists of rubber stopper that has low thermal conductivity we assume that the system is insulated from the top. Hence

$$\left. \frac{\partial T}{\partial y} \right|_{y=h(t)} = 0. \tag{5.41}$$

The second boundary condition at $y = h(t)$ is derived from the conservation of mass.

Let the total mass of the system by m. Then by mass conservation, we have

$$\frac{dm}{dt} = 0. \tag{5.42}$$

We can write $m = m_1 + m_2$, where m_1, m_2 are the masses of the solid and

liquid regions respectively. Since we assume constant densities, we can write

$$m_1 = V_1\rho_1,$$

$$m_2 = V_2\rho_2,$$

where V_1 and V_2 are the corresponding volumes of the solid and liquid regions, the mass conservation equation then gives

$$\rho_1\frac{dV_1}{dt} + \rho_2\frac{dV_2}{dt} = 0.$$

Let V be the total volume of the solid and liquid regions combined. Then the above equation can be rewritten as

$$\frac{dV}{dt} = \frac{\rho_2 - \rho_1}{\rho_2}\frac{dV_1}{dt}. \tag{5.43}$$

Since the vial is of unit length and we have assumed the water level to be flat, the total volume is given by

$$V(t) = h(t). \tag{5.44}$$

Let $H(\phi)$ be the *Heaviside function* defined as

$$H(\phi) = \begin{cases} 0 & \text{if } \phi \leq 0 \\ 1 & \text{if } \phi > 0 \end{cases}$$

Then the volume of the solid region, defined by $\phi(\mathbf{x}) < 0$, is given by

$$V_1 = \int_D (1 - H(\phi(\mathbf{x})))d\mathbf{x}, \tag{5.45}$$

where D is the whole computational domain.

The integral in (5.45) is approximated as

$$I = \sum_j \sum_i (1 - H_{i,j}) \Delta x \Delta y, \tag{5.46}$$

and the time derivatives are approximated by forward Euler scheme. Hence the value of h at time t_{n+1} is given by

$$h^{n+1} = h_n + \frac{\rho_2 - \rho_1}{\rho_2} \left(I^{n+1} - I^n \right). \tag{5.47}$$

5.4.2 Volume Change Model Results

We shall present here results based on simulation with the initial liquid level $h = 0.5$ and the ambient temperature $T^a = 0$ and the heat transfer coefficient $k = 0.5$. The simulation was run until time $t = 0.1$. The density ratio $\frac{\rho_1}{\rho_2} = 1.087$ is chosen to reflect the scenario for freezing of water. We imposed the Dirichlet boundary condition at the bottom of the vial, and heat flux conditions at the sides of the vial. We once again use the small-time solution at time $t = 0.005$ to start the time marching process. The results are summarised in figure 5.9.

Because of the relatively small amount of cooling from the vial sides, the temperature distributions remains relatively flat along the x direction throughout the time marching process. The primary source of cooling comes from the shelf, and hence the interface progresses from the bottom up with relatively small lateral movement. The blue lines in figure 5.9 reference the current position of the liquid level. The water level gradually rises from the initial position of 0.5 to a level of 0.6 at time $t = 0.1$. At the final time, one can note that the solidification interface actually crosses the liquid level near the side of the vial.

We would like to stress that there is one crucial aspect that is not correctly handled in the current implementation of the volume changes scheme. We are only solving the heat equation in the region where $y \leq h(t)$, when the solidification front reaches the water, the frozen product is not allowed to cool to the final state when the temperature is constant $T = 0$ across the whole solidified region. Since we have fixed the boundary condition $T = 1$ at the

solidification interface. To mitigate the problem, one would have to change the boundary condition on the interface to, for instance, the insulation condition in the regions where the interface has reached the liquid level.

5.5 Summary

In this chapter, we have presented a level set method coupled with compact finite differencing techniques. We have applied the method to two simple solidification scenarios and compared them to the analytical solution. We have also presented a single vial model with heat flux boundary conditions. The main disadvantage of the current model is that it treats a vial in isolation. In freeze-drying practice, one needs to take into consideration the interactions of multiple vials inside the freeze-drying chamber as well as the interactions between the vials themselves. In the next chapter, we shall focus on modelling the heat transfer on a tray of vials where we take into consideration the interactions of heat exchange between the vials as well as the sides of the freeze-drying chamber.

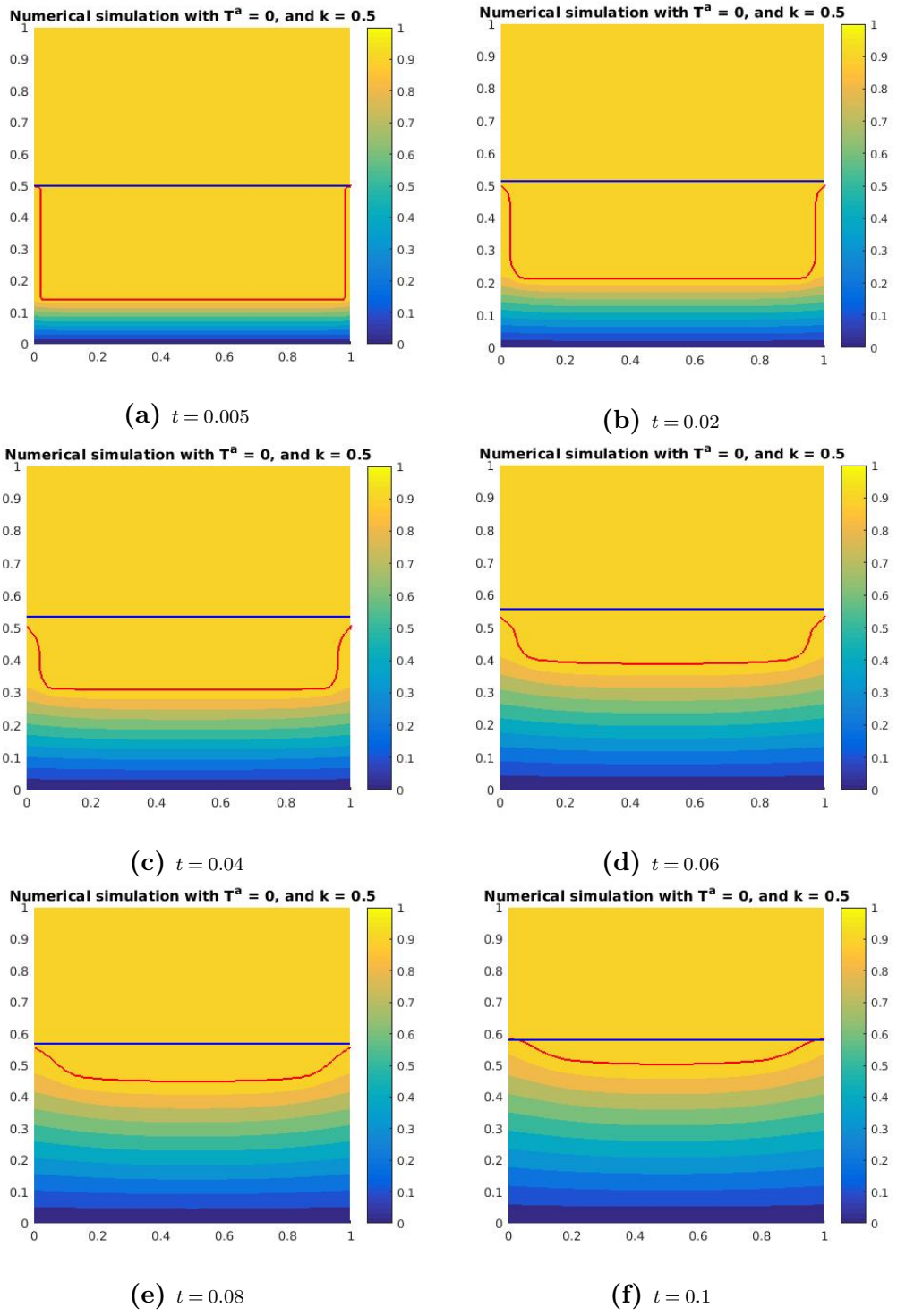

(a) $t = 0.005$ **(b)** $t = 0.02$

(c) $t = 0.04$ **(d)** $t = 0.06$

(e) $t = 0.08$ **(f)** $t = 0.1$

Figure 5.9: Progression of the interface (red) and the temperature profiles and current water level in blue. Dirichlet boundary condition $T = 0$ imposed on the bottom of the vial and convective flux conditions on the sides with $k = 5$. Vial is assumed to be insulated from the top by a rubber stopper. Simulated with $\Delta x = \Delta y = 0.01$ and $\Delta t = 0.001$.

Chapter 6

Heat transfer modelling of a tray of vials

6.1 Introduction

Our discussion so far has been focused on modelling the freezing process of an inside a single vial. However, there is evidence that in large scale freeze-drying applications, the heat transfer depends on the position of the vial [43]. The vials that are in the centre of the tray can be considered to be thermally insulated along their edges. For such vials simple spatially one-dimensional models, such as the one developed by Velardi and Barressi in [66], have been shown to be appropriate. On the other hand, the vials that are placed along the edges of the tray experience extra heat transfer contributions from the edges of the freeze-drying chamber and the rails running along the tray.

This atypical heat transfer is often referred to as *the edge vial effect*. It is clear that when building a model for these vials, it is no longer viable to assume axisymmetric scenario as with the centre vials. Several authors observed this effect experimentally and described the relative contributions of each mode of heat transfer [43, 49, 44].

The purpose of this chapter is to extend our single vial models developed earlier in order to describe the behaviour of a full tray of vials. In particular, we are interested in how far can the edge vial effect penetrated into the tray.

In our model, we assume that the dominant mode of heat transfer between the vials is via radiation. From studies done by Ganguly, Nail, and Alexeenko in [14] we know that especially at low pressures radiation plays a vital role as a heat transfer mechanism inside the freeze-drying chamber. However, neglecting convection and conduction will definitely result in underestimation of the edge effect. Secondly, we shall assume a very simplified geometry of the individual vials. The vials are modelled as cuboids that are placed in a square arrangement, which is different from the real cylindrical vials since usually the latter is in a hexagonal arrangement. This particular simplification allows for more straightforward implementation of the boundary conditions at the sides of the vials. In particular, the computation of the view factors is simpler for two parallel planes, and one does not need to consider any shadowing effects of the adjacent vials. Moreover, the computation of the derivatives normal to the surfaces of the vials is straightforward, as well.

We shall treat the heat transfer inside the vial and in-between the vials separately in a two-stage model. In the first stage, take the surface temperatures of the vials and use a radiation model described in section (6.4) to obtain net heat fluxes leaving the surface of each vial. These are then used in the second stage as boundary conditions for the computations inside each of the vials. To capture the dynamics of the interactions between the vials more accurately, we shall no longer use the assumption of a quasi-steady state. The main reason for switching to the non-steady setting was the anticipation that the radiative heat transfer between the vials would work on a smaller time scale to that of the progression of the interface. However, the numerical simulations will show that the temperature field does indeed settle relatively quickly into steady-state even with the vial interactions. Hence the quasi-steady-state approximation used previously would have been sufficient.

This chapter is structured as follows. In section 6.2, we present a new compact finite difference method for approximating the spatial derivatives in the governing equation. We will not use the compact scheme developed earlier

in chapter 3. The old compact scheme was developed for solving the models with quasi-steady-steady approximation and would be cumbersome to apply in the setting of non-steady problems. Therefore we develop this new compact scheme better suited for parabolic PDE problems. Section 6.3 provides a brief introduction to ADI methods for solving diffusion equations and its implementation within our compact scheme. The model of heat transfer between the vials in discussed in section 6.4, and the final two-stage model is presented in the final section 6.5

6.2 Heat transfer inside the vial

Let us assume that the contents of the three-dimensional vials are initially at the fusion temperature. Hence within each vial, we need to solve the heat conduction equation

$$\rho_s c_s \frac{\partial T}{\partial t} = k_s \nabla^2 T, \tag{6.1}$$

subject to the following initial and boundary conditions

$$T(x,y,z,0) = T_{in}(x,y,z), \tag{6.2}$$

$$-k_{side} \left.\frac{\partial T}{\partial x}\right|_{x=0} = q^{(1)}(y,z), \tag{6.3}$$

$$k_{side} \left.\frac{\partial T}{\partial x}\right|_{x=L} = q^{(2)}(y,z), \tag{6.4}$$

$$-k_{side} \left.\frac{\partial T}{\partial y}\right|_{y=0} = q^{(3)}(x,z), \tag{6.5}$$

$$k_{side} \left.\frac{\partial T}{\partial y}\right|_{y=L} = q^{(4)}(x,z), \tag{6.6}$$

$$k_{sh} \left.\frac{\partial T}{\partial z}\right|_{z=0} = T - T_{sh}, \tag{6.7}$$

$$\left.\frac{\partial T}{\partial z}\right|_{z=L} = 0. \tag{6.8}$$

Here T represents the absolute temperature, $\nabla^2 T$ is the three-dimensional laplacian

$$\nabla^2 T \equiv \frac{\partial^2 T}{\partial x^2} + \frac{\partial^2 T}{\partial y^2} + \frac{\partial^2 T}{\partial y^2},$$

and k_{sh}, k_{side} are the conductive and radiative heat transfer coefficients, respectively. The quantities ρ_s, c_s, k_s are the density, heat capacity and thermal conductivity of the solid region, respectively. The quantities $q^{(i)}$ are radiative heat fluxes caused by the heat exchange of the vial with its neighbouring vials (in the case of centre vials) and the wall of the freeze-drying chamber (in the case of edge and corner vials). Often, in practice, the vials are sealed on the top by a rubber stopper that is a relatively good thermal insulator. Therefore we shall assume that the vial is insulated from the top.

Let us denote the solid-liquid interface by $\Gamma(t)$. We shall assume that the solidification occurs at a fixed temperature of T_m,

$$T(x,y,z,t) = T_m \text{ on } \Gamma(t). \tag{6.9}$$

The system is closed by the classical Stefan condition on the interface,

$$\rho_s H_s V_n = k_s \frac{\partial T}{\partial n}, \tag{6.10}$$

where H_s is the latent heat of fusion, V_n is the velocity of the interface in the normal direction and $\frac{\partial T}{\partial n}$ is the normal derivative of the temperature.

It is useful now to introduce the following non-dimensional quantities

$$\hat{x} = \frac{x}{L}, \hat{y} = \frac{y}{L}, \hat{z} = \frac{z}{L}, \tau = \frac{k_s t}{\rho_s c_s L^2},$$

$$\theta = \frac{T - T_{sh}}{T_{in} - T_{sh}}.$$

The system (6.1-6.10) then simplifies to solving

$$\frac{\partial \theta}{\partial \tau} = \nabla^2 \theta \qquad \hat{x}, \hat{y}, \hat{y} \in [0,1], \tag{6.11}$$

subject to

$$\theta(\hat{x},\hat{y},\hat{z},0) = 1, \tag{6.12}$$

$$-\frac{\partial\theta}{\partial\hat{x}}\bigg|_{\hat{x}=0} = \hat{q}^{(1)}, \tag{6.13}$$

$$\frac{\partial\theta}{\partial\hat{x}}\bigg|_{\hat{x}=1} = \hat{q}^{(2)}, \tag{6.14}$$

$$-\frac{\partial\theta}{\partial\hat{y}}\bigg|_{\hat{y}=0} = \hat{q}^{(3)}, \tag{6.15}$$

$$\frac{\partial\theta}{\partial\hat{y}}\bigg|_{\hat{y}=1} = \hat{q}^{(4)}, \tag{6.16}$$

$$\frac{\partial\theta}{\partial\hat{z}}\bigg|_{\hat{z}=0} = \mathrm{Bi}\theta, \tag{6.17}$$

$$\frac{\partial\theta}{\partial\hat{z}}\bigg|_{\hat{z}=1} = 0. \tag{6.18}$$

Here

$$\mathrm{Bi} = \frac{L}{k_{self}},$$

$$\hat{q}^{(i)} = \frac{Lq^{(i)}}{k_{side}(T_{in} - T_{sh})}.$$

Since we are assuming the vials are initially at the fusion temperature, we have

$$T_{in} = T_m.$$

Hence the two conditions at the moving interface Γ become

$$\theta = 1 \tag{6.19}$$

and

$$v_n = \beta^{-1}\frac{\partial\theta}{\partial n}, \tag{6.20}$$

where β is the Stefan number given by

$$\beta^{-1} = \frac{c_s(T_{in} - T_{sh})}{H_s}, \tag{6.21}$$

and v_n is the non-dimensional velocity of the interface in the direction normal to the interface, related to V_n by

$$v_n = \frac{L\rho_s c_s}{k_s} V_n. \tag{6.22}$$

6.2.1 Solving the field equation

Here we present a compact finite difference scheme for solving the system (6.1–6.10).

The solidification front is allowed to cross the computational grid freely. Therefore, one needs to take into account grid points adjacent to the interface where the computational stencil might be non-uniform. In order to maintain the accuracy of the method, standard finite difference approaches would require grid refinements and/or extensions of the computational stencil [64, 65]. To avoid these issues, we shall develop a compact finite difference scheme. This scheme will provide a high order method of approximating the derivative terms using the standard three-point stencil. However, the drawback of the method lies in the fact that the approximations to the spatial derivative terms cannot be computed explicitly, and a system of equations needs to be solved at each time step.

The work presented here builds upon the compact scheme developed by Zhao et al in [69] and [70]. Their work here is extended to non-uniform grids in multiple space dimensions. Secondly, we have applied what we believe is different, more efficient time marching procedure to that in [70].

As we are planning on discretising the spatial terms in dimension by dimension fashion, for now, it is sufficient to consider the one-dimensional case. Let us suppose that we have a grid of N unequally spaced points, each denoted by x_i. Throughout the analysis that follows we shall use Θ_i to represent the numerical approximation of $\theta_i = \theta(x_i, t)$.

6.2.2 Interior nodes

We shall first focus on the interior nodes. We aim to find a higher order approximation to the first and second-order derivatives using only a three-point stencil. As a starting point, we consider the following scheme,

$$a_i\theta_{xx,i+1}+b_i\theta_{xx,i}+c_i\theta_{xx,i-1}= \frac{2\theta_{i+1}}{\Delta x_{+,i}(\Delta x_{+,i}+\Delta x_{-,i})}-\frac{2\theta_i}{\Delta x_{+,i}\Delta x_{-,i}}+\frac{2\theta_{i-1}}{\Delta x_{-,i}(\Delta x_{+,i}+\Delta x_{-,i})}, \quad (6.23)$$

where $\Delta x_{+,i}$ and $\Delta x_{-,i}$ are the distances from the node i to nodes $i+1$ and $i-1$ respectively, and a_i, b_i and c_i are constants to be determined.

Expanding all the relevant quantities about x_i we obtain

$$\begin{aligned}(a_i+b_i+c_i)\theta_{xx,i}+(a_i\Delta x_{+,i}-c_i\Delta x_{-,i})\theta_{xxx,i}+ \\ \left(\frac{a_i\Delta x_{+,i}^2}{2}+\frac{c_i\Delta x_{-,i}^2}{2}\right)\theta_{xxxx,i}+O(l)= \\ \theta_{xx,i}+\frac{\Delta x_{+,i}-\Delta x_{-,i}}{3}\theta_{xxx,i}+ \\ \left(\frac{\Delta x_{+,i}^2-\Delta x_{+,i}\Delta x_{-,i}+\Delta x_{-,i}^2}{12}\right)\theta_{xxxx,i}+O(l). \quad (6.24)\end{aligned}$$

Here $l=\max(\Delta x_{+,i}^3,\Delta x_{-,i}^3)$. Hence we require the following:

$$a_i+b_i+c_i=1, \quad (6.25)$$

$$a_i\Delta x_{+,i}-c_i\Delta x_{-,i}=\frac{\Delta x_{+,i}-\Delta x_{-,i}}{3}, \quad (6.26)$$

$$\frac{a_i\Delta x_{+,i}}{2}+\frac{c_i\Delta x_{-,i}}{2}=\frac{\Delta x_{+,i}^2-\Delta x_{+,i}\Delta x_{-,i}+\Delta x_{-,i}^2}{12}. \quad (6.27)$$

Solving the above system we obtain

$$a_i=\frac{\Delta x_{+,i}^2+\Delta x_{+,i}\Delta x_{-,i}-\Delta x_{-,i}^2}{6\Delta x_{+,i}(\Delta x_{+,i}+\Delta x_{-,i})}, \quad (6.28)$$

$$b_i=\frac{\Delta x_{+,i}^2+3\Delta x_{+,i}\Delta x_{-,i}+\Delta x_{-,i}^2}{6\Delta x_{+,i}\Delta x_{-,i}}, \quad (6.29)$$

$$c_i = \frac{\Delta x_{-,i}^2 + \Delta x_{+,i}\Delta x_{-,i} - \Delta x_{+,i}^2}{6\Delta x_{-,i}(\Delta x_{+,i} + \Delta x_{-,i})}. \tag{6.30}$$

Hence we have produced a compact scheme that is third order in the interior of the domain. Next, we shall move the discussion towards the boundary nodes. Here, it is essential to make the distinction between the nodes that are adjacent to the solidification interface, where we have Dirichlet boundary conditions, and those at the edge of the computational domain with Neumann or Robin conditions.

6.2.3 Boundary nodes: Dirichlet condition

We shall start the discussion on boundary nodes by considering the nodes adjacent to the interface. At the solidification front, we require $\theta = 1$. Let x_k be the node located at the solidification front. The following compact scheme is used:

$$b_k\theta_k + a_k\Delta x^2\theta_{xx,k+1} + c_k h^2\theta_{xx,k+2} = e_k\theta_{k+1} + f_k\theta_{k+2}, \tag{6.31}$$

where Δx and h are the distances between x_k and x_{k+1} and between x_k and x_{k+2} respectively, and a_k, b_k, c_k, e_k and f_k are constants to be determined. As before, we expand all the quantities above around x_k. Hence we obtain

$$\begin{aligned} b_k\theta_k + (a_k\Delta x^2 + c_k h^2)\theta_{xx,k} + \left(a_k\Delta x^3 + c_k h^3\right)\theta_{xxx,k} + O(h^4) = \\ (e_k + f_k)\theta_k + (e_k\Delta x + f_k h)\theta_{x,k} + \left(\frac{e_k\Delta x^2}{2} + \frac{f_k h^2}{2}\right)\theta_{xx,k} + \\ \left(\frac{e_k\Delta x^3}{6} + \frac{f_k h^3}{6}\right)\theta_{xxx,k} + O(h^4). \end{aligned} \tag{6.32}$$

Using $\theta_k = 1$ one obtains

$$b = e + f, \tag{6.33}$$

$$0 = e\Delta x + fh, \tag{6.34}$$

$$a\Delta x^2 + ch^2 = \frac{e\Delta x^2}{2} + \frac{fh^2}{2}, \tag{6.35}$$

$$a\Delta x^3 + ch^3 = \frac{e\Delta x^3}{6} + \frac{fh^3}{6}. \tag{6.36}$$

Since the above system consists of 5 unknowns but only four equations, we shall set $f = 1$, which then gives

$$a_k = \frac{2h^2 - \Delta x h}{6\Delta x^2}, \tag{6.37}$$

$$b_k = \frac{\Delta x - h}{\Delta x}, \tag{6.38}$$

$$c_k = \frac{h - 2\Delta x}{6h}, \tag{6.39}$$

$$e_k = -\frac{h}{\Delta x}. \tag{6.40}$$

The compact scheme derived above is second order accurate. One should note that high accuracy around the points adjacent to the interface is highly desirable as these values are crucial for advecting the interface correctly.

6.2.4 Boundary nodes: Neumann/Robin condition

Let us now consider boundary conditions with prescribed values of the derivatives. We shall assume that at the node x_0, we must satisfy the condition $\theta_{x,0} = Q$. Here Q can be a function of x as well as θ. Similarly to the Dirichlet case, we shall consider the following compact scheme:

$$b\theta_{x,0} + a\theta_{xx,0} + c\theta_{xx,1} = e\theta_0 + f\theta_1. \tag{6.41}$$

Expanding and then equating the corresponding terms, one obtains:

$$a = \frac{\Delta x^2}{3}, \tag{6.42}$$

$$b = \Delta x, \tag{6.43}$$

$$c = \frac{\Delta x^2}{6}, \tag{6.44}$$

$$e = -1, \tag{6.45}$$

$$f = 1. \tag{6.46}$$

This concludes the computations of the approximations of the spatial derivatives in the governing equation. Now we shall focus our attention on implementing the time marching procedure within the context of the compact scheme.

6.3 Time stepping

In this chapter so far, we have focused our discussion on the treatment of the spatial derivatives. In this section, we will derive a time-efficient method of implementing the compact methods developed in section 6.2. The Crank-Nicolson algorithm is a popular choice for solving one-dimensional parabolic equations. However, a naive generalisation of Crank-Nicolson to two or three spatial dimensions produces a matrix equation that is block-tridiagonal rather than tridiagonal as in the one-dimensional case. Inverting such a matrix is quite computationally inefficient. Therefore, *time-splitting* methods such as *locally one-dimensional* (LOD) methods and *alternating direction implicit* (ADI) methods are generally prefered.

The main idea behind these approaches is to split the original multidimensional equation into a series of simpler one-dimensional problems. In particular, the implementation of LOD techniques consists of first splitting the differential equation into a series of one-dimensional equations and then discretisation of the resulting system. For our purposes, however, we shall limit the discussion solely to the ADI method. An interested reader can find the details of LOD techniques and their implementation in the publications by Yanenko [19] or Mitchell and Griffiths [30].

In contrast to the LOD methods ADI techniques require first the the discretisation of the differential equation, followed by factorising the appropriate terms and then splitting the system into smaller one-dimensional problems. These techniques provide an efficient way of separating large multidimensional problems into one-dimensional tridiagonal systems. Peaceman and Rachford first developed the ADI methods in [37] with the detailed aspects of the meth-

ods described by Douglas in [11]. A particular drawback of the method developed by Rachford and Douglas in [37] and [11] is that although the method is unconditionally stable in two dimensions, its natural extension to three dimensions produces a technique that is only conditionally stable. The reason for this is that this method produces a set of one-dimensional systems that are on their own only conditionally stable. However, the error increase from an explicit term is balanced by the corresponding implicit term in the next one-dimensional system. Hence provided that the number of one-dimensional steps is even, the overall scheme is unconditionally stable; however, in the case of three-dimensional problems, the overall methods is only conditionally stable. Further details and analysis can be found in [20, 63]. To overcome this difficulty, new, improved ADI methods were later developed for three-dimensional diffusion equations by Douglas and Rachford [10], and later by Brian [2] and Douglas [8]. Gao and Wang presented a general extension of the Peaceman and Rachford ADI methods to n-dimensional problems in [15].

In recent years, there has been growing interest in applying ADI methods to fractional differential equations. A three-point combined compact ADI scheme has been applied in [16] to two-dimensional time-fractional advection-diffusion equations. Wang et al. [68] used a combination of split-step and ADI methods in solving the fractional Schrödinger equation in two dimensions.

6.3.1 Basic derivation of ADI scheme

We shall start our discussion with a derivation of a simple ADI scheme. We use the two-dimensional diffusion equation as an illustrative example of the method, since the generalisation to higher-dimensional problems is straightforward.

Let us consider the following initial boundary value problem:

$$u_t = u_{xx} + u_{yy} + f(x,y,t), \qquad 0 < x < 1, 0 < y < Y, t > 0; \tag{6.47}$$

$$u(x,y,t=0) = u_0(x,y), \qquad 0 < x < 1, 0 < y < Y; \tag{6.48}$$

$$u(0,y,t) = g_0(y,t), u(1,y,t) = g_1(y,t), \qquad 0 < y < Y, t > 0; \tag{6.49}$$

$$u(x,0,t) = g_2(x,t), u(x,Y,t) = g_3(x,t), \qquad 0 < x < 1, t > 0; \tag{6.50}$$

Let δ_x^2 and δ_y^2 be be the usual second order difference operators,

$$\delta_x^2 U_{i,j}^n = \frac{U_{i+1,j}^n - 2U_{i,j}^n + U_{i-1,j}^n}{\Delta x^2}, \tag{6.51}$$

$$\delta_y^2 U_{i,j}^n = \frac{U_{i,j+1}^n - 2U_{i,j}^n + U_{i,j-1}^n}{\Delta y^2}. \tag{6.52}$$

Then, following a naive generalisation of the Crank-Nicolson scheme, we can discretise the equation (6.47) as,

$$U_{i,j}^{n+1} = U_{i,j} + \frac{\Delta t}{2}\left(\delta_x^2 + \delta_y^2\right)\left(U_{i,j}^n + U_{i,j}^{n+1}\right) + \Delta t f_{i,j}^{n+1/2}. \tag{6.53}$$

Here $U_{i,j}^n = u(i\Delta x, j\Delta y, n\Delta t)$. Or, equivalently, we can rewrite the equation above as,

$$\left(1 - \frac{\Delta t}{2}\delta_x^2 - \frac{\Delta t}{2}\delta_y^2\right) U_{i,j}^{n+1} = \left(1 + \frac{\Delta t}{2}\delta_x^2 + \frac{\Delta t}{2}\delta_y^2\right) U_{i,j}^n + \Delta t f_{i,j}^{n+1/2}. \tag{6.54}$$

The scheme above is second-order accurate in time. Hence adding a term in the equation of the order $O(\Delta t^2)$, will not change the overall accuracy of the scheme. Following this reasoning, we add the terms $\frac{\Delta t^2}{4}\delta_x^2\delta_y^2 U_{i,j}^{n+1}$ and $\frac{\Delta t^2}{4}\delta_x^2\delta_y^2 U_{i,j}^n$ to the left-hand side and right-hand side of the equation respectively, giving us,

$$\left(1 - \frac{\Delta t}{2}\delta_x^2 - \frac{\Delta t}{2}\delta_y^2 + \frac{\Delta t^2}{4}\delta_x^2\delta_y^2\right) U_{i,j}^{n+1} = \left(1 + \frac{\Delta t}{2}\delta_x^2 + \frac{\Delta t}{2}\delta_y^2 + \frac{\Delta t^2}{4}\delta_x^2\delta_y^2\right) U_{i,j}^n + \Delta t f_{i,j}^{n+1/2}. \tag{6.55}$$

Finally, these extra terms allow us to factor the operators on both sides of the equation. Thus

$$\left(1-\frac{\Delta t}{2}\delta_x^2\right)\left(1-\frac{\Delta t}{2}\delta_y^2\right)U_{i,j}^{n+1} = \left(1+\frac{\Delta t}{2}\delta_x^2\right)\left(1+\frac{\Delta t}{2}\delta_y^2\right)U_{i,j}^{n}+\Delta t f_{i,j}^{n+1/2}. \quad (6.56)$$

Here, it is important to stress that although the central difference operators δ_x^2 and δ_y^2 commute, this might not be the case in general. Therefore, we have preserved their order in equation (6.56).

Douglas and Gunn in [9] proposed to solve the equation 6.56 in a two step procedure as follows

$$\left(1-\frac{\Delta t}{2}\delta_x^2\right)U_{i,j}^{n+1/2} = \left(1+\frac{\Delta t}{2}\delta_x^2+\Delta t\delta_x^2\right)U_{i,j}^{n}, \quad (6.57)$$

$$\left(1-\frac{\Delta t}{2}\delta_y^2\right)U_{i,j}^{n+1} = U_{i,j}^{n+1/2}-\frac{\Delta t}{2}\delta_y^2 U_{i,j}^{n}. \quad (6.58)$$

One can easily verify that the system above is equivalent to (6.56) by multiplying the equation (6.58) by $\left(1-\frac{\Delta t}{2}\delta_x^2\right)$ and substituting in the right-hand side of the equation (6.57). However, unlike in the original equation, the system (6.57)–(6.58) has unknowns appearing either in the x or in the y direction. Hence finding the solution will involve inverting two tridiagonal matrices as opposed to a single block tridiagonal matrix of the original problem.

The generalisation of the Douglas Gunn method to three spatial dimensions is straight-forward. The resulting equations have the form:

$$\left(1-\frac{\Delta t}{2}\delta_x^2\right)U_{i,j}^{n+1/3} = \left(1+\frac{\Delta t}{2}\delta_x^2+\Delta t\delta_y^2+\Delta t\delta_z^2\right)U_{i,j}^{n}, \quad (6.59)$$

$$\left(1-\frac{\Delta t}{2}\delta_y^2\right)U_{i,j}^{n+2/3} = U_{i,j}^{n+1/3}-\frac{\Delta t}{2}\delta_y^2 U_{i,j}^{n}, \quad (6.60)$$

$$\left(1-\frac{\Delta t}{2}\delta_z^2\right)U_{i,j}^{n+1} = U_{i,j}^{n+2/3}-\frac{\Delta t}{2}\delta_z^2 U_{i,j}^{n}. \quad (6.61)$$

This then concludes our discussion on the basic principles and the derivation of the ADI scheme, and now we shall focus on applying the scheme (6.59–6.61) in the context of the compact method developed in the sections 6.2.1 to 6.2.4.

6.3.2 Compact ADI Scheme

The last remaining problem in the task of solving the temperature the equation is to piece together the ADI methods introduced in the previous section and the compact method developed earlier in this chapter. Our main idea here is to redefine the second-order difference operators δ_x^2, δ_y^2 and δ_z^2.

All of the above difference operators have similar derivations, the only difference between them being in the boundary conditions applied at the various ends of the computational domain. We begin the discussion with the δ_x^2 operator. The vial problem, as stated in the introductory section 6.2, has Neumann boundary conditions $\frac{\partial\theta}{\partial\hat{x}} = \hat{q}$ applied at the edges of the vial. However, a particular slice along the x direction can also intersect with the solidification interface, in which case the Dirichlet boundary condition $\theta = 1$ should be applied there. Hence, generally speaking, we could encounter slices with two Neumann, Neumann and Dirichlet or two Dirichlet conditions imposed on the ends of a particular slice. As an example, we shall consider a case with a Neumann condition on the left boundary and a Dirichlet condition on the right boundary, as the other cases can be derived similarly.

Suppose we have a slice of the computational domain (along the x direction) located at $y = j\Delta y$ and $z = k\Delta z$. Here the total length of the slice is $m+1$. We are interested in computing the approximations to the second derivatives with respect to x along the slice. According to the procedure devised in the sections 6.2.1 to 6.2.4, we can find these approximations by solving

the system

$$a_{i,j,k}\theta_{xx,i+1,j,k} + b_{i,j,k}\theta_{xx,i,j,k} + c_{i,j,k}\theta_{xx,i-1,j,k} = \frac{2\theta_{i+1,j,k}}{\Delta x_{+,i,j,k}(\Delta x_{+,i,j,k} + \Delta x_{-,i,j,k})} - \frac{2\theta_{i,j,k}}{\Delta x_{+,i,j,k}\Delta x_{-,i,j,k}} + \frac{2\theta_{i-1,j,k}}{\Delta x_{-,i,j,k}(\Delta x_{+,i,j,k} + \Delta x_{-,i,j,k})}, \quad (6.62)$$

for $i = 1$ to $i = m-1$. Here

$$a_{i,j,k} = \frac{\Delta x_{+,i,j,k}^2 + \Delta x_{+,i,j,k}\Delta x_{-,i,j,k} - \Delta x_{-,i,j,k}^2}{6\Delta x_{+,i,j,k}(\Delta x_{+,i,j,k} + \Delta x_{-,i,j,k})}, \quad (6.63)$$

$$b_{i,j,k} = \frac{\Delta x_{+,i,j,k}^2 + 3\Delta x_{+,i,j,k}\Delta x_{-,i,j,k} + \Delta x_{-,i,j,k}^2}{6\Delta x_{+,i,j,k}\Delta x_{-,i,j,k}}, \quad (6.64)$$

$$c_{i,j,k} = \frac{\Delta x_{-,i,j,k}^2 + \Delta x_{+,i,j,k}\Delta x_{-,i,j,k} - \Delta x_{+,i,j,k}^2}{6\Delta x_{-,i,j,k}(\Delta x_{+,i,j,k} + \Delta x_{-,i,j,k})}. \quad (6.65)$$

In the case of the boundary node at $i = 0$, the approximations to the second derivative can be calculated by solving

$$b_{j,k}\theta_{x,0,j,k} + c_{j,k}\theta_{xx,0,j,k} + a_{j,k}\theta_{xx,1,j,k} = e_{j,k}\theta_{0,j,k} + f_{j,k}\theta_{1,j,k}, \quad (6.66)$$

with

$$a_{j,k} = \frac{\Delta x_{0,j,k}x^2}{6}, \quad (6.67)$$

$$b_{j,k} = \Delta x_{0,j,k}, \quad (6.68)$$

$$c_{j,k} = \frac{\Delta x_{0,j,k}x^2}{3}, \quad (6.69)$$

$$e_{j,k} = -1, \quad (6.70)$$

$$f_{j,k} = 1. \quad (6.71)$$

Then using the condition $\theta_{x,0,j,k} = q_{j,k}$, we obtain

$$a_{0,j,k}\theta_{xx,0,j,k} + c_{0,j,k}\theta_{xx,1,j,k} = e_{0,j,k}\theta_{0,j,k} + f_{0,j,k}\theta_{1,j,k} - b_{0,j,k}q_{j,k}. \tag{6.72}$$

Lastly, in the case $i = m$ we can proceed in the same way as for $i = 0$, but we use the condition $\theta_{m,j,k} = 1$ instead.

The whole procedure can be compactly written in a matrix form as

$$\mathbf{A}_{j,k}\mathbf{\Theta}_{xx,j,k} = \mathbf{B}_{j,k}\mathbf{\Theta}_{j,k} + \mathbf{b}_{j,k}. \tag{6.73}$$

Here $\mathbf{\Theta}_{xx,j,k}$ and $\mathbf{\Theta}_{j,k}$ are $(m+1)\times 1$ vectors defined as

$$\mathbf{\Theta}_{xx,j,k} = \begin{bmatrix} \theta_{xx,0,j,k} \\ \theta_{xx,1,j,k} \\ \vdots \\ \theta_{xx,m-1,j,k} \\ \theta_{xx,m,j,k} \end{bmatrix}, \ \mathbf{\Theta}_{j,k} = \begin{bmatrix} \theta_{0,j,k} \\ \theta_{1,j,k} \\ \vdots \\ \theta_{m-1,j,k} \\ \theta_{m,j,k} \end{bmatrix}. \tag{6.74}$$

Similarly, $\mathbf{A}_{j,k}$ and $\mathbf{B}_{j,k}$ are $(m+1)\times(m+1)$ matrices given by

$$\mathbf{A}_{j,k} = \begin{bmatrix} a_{0,j,k} & c_{0,j,k} & 0 & \dots & 0 \\ \vdots & & \ddots & & \vdots \\ \dots & a_{i,j,k} & b_{i,j,k} & c_{i,j,k} & \dots \\ 0 & \dots & 0 & a_{m+1,j,k} & c_{m+1,j,k} \end{bmatrix}, \tag{6.75}$$

$$\mathbf{B}_{j,k} = \begin{bmatrix} f_{0,j,k} & e_{0,j,k} & 0 & \dots & 0 \\ \vdots & & \ddots & & \vdots \\ \dots & o_{i,j,k} & p_{i,j,k} & r_{i,j,k} & \dots \\ 0 & \dots & 0 & e_{m+1,j,k} & f_{m+1,j,k} \end{bmatrix}. \tag{6.76}$$

Here

$$o_{i,j,k} = \frac{2}{\Delta x_{-,i}(\Delta x_{+,i} + \Delta x_{-,i})}, \tag{6.77}$$

$$p_{i,j,k} = -\frac{2}{\Delta x_{+,i}\Delta x_{-,i}}, \tag{6.78}$$

$$r_{i,j,k} = \frac{2}{\Delta x_{+,i}(\Delta x_{+,i} + \Delta x_{-,i})}. \tag{6.79}$$

Therefore, we can define the new compact second derivative difference operator δ_x^2 as

$$\delta_x^2 \Theta_{j,k} \equiv \mathbf{A}_{j,k}^{-1}\left(\mathbf{B}_{j,k}\mathbf{\Theta}_{j,k} + \mathbf{b}_{j,k}\right). \tag{6.80}$$

The rest of the operators are defined similarly. This concludes the discussion on the inside-vials transfer, and so next we turn our attention to the heat transfer between the vials.

6.4 Heat transfer between the vials

This section of the chapter discusses the second layer of the two-stage model. Here we shall develop a model for tracking the heat transfer between the vials placed on a tray inside a freeze-drying chamber. In this model, we assume that the dominant method of heat transfer between the vials is via radiation [14]. We shall model the vials as rectangular cuboids. The separation between the vials on a tray is relatively small (few mm), hence we shall assume that a vial exchanges heat directly with its nearest neighbours only. Hence in the case of a vial places in the centre of the tray, we assume heat exchange with its four neighbours and in the case of vials place at the edge or corner of the tray we assume heat exchange with its neighbouring three or two vials and the sides of the freeze-drying chamber.

We will first set up the basic model for a radiative heat transfer between grey diffuse emitters, and secondly, we modify it to our particular freeze-drying application.

6.4.1 Radiation heat transfer

We start the discussion by reviewing the basic principles of radiation heat transfer. The following derivations proceed along the lines of [31].

We shall model the surfaces of the vials as grey, diffuse emitters, absorbers and reflectors. Let ϵ, α and ρ be the surface emissivity, absorptivity, and reflectivity, respectively. Under the conditions stated above, we have

$$\epsilon = \alpha = 1 - \rho. \tag{6.81}$$

We can define *surface radiosity* J as

$$J(\mathbf{x}) = \epsilon(\mathbf{x})E_b(\mathbf{x}) + \rho(\mathbf{x})G(\mathbf{x}). \tag{6.82}$$

Here E_b is the total emissive power of a black body given by

$$E_b(\mathbf{x}) = \sigma T(\mathbf{x})^4, \tag{6.83}$$

where σ is the *Stefan-Boltzmann constant*. The quantity $G(\mathbf{x})$ is the *irradiation* and represents the total heat flux falling onto the surface at location $\mathbf{x}$. Hence J gives the total heat flux leaving the surface at location $\mathbf{x}$. We then can define the net heat flux leaving the surface q as

$$q(\mathbf{x}) = J(\mathbf{x}) - G(\mathbf{x}) = \epsilon(\mathbf{x})E_b(\mathbf{x}) - \alpha(\mathbf{x})G(\mathbf{x}). \tag{6.84}$$

Let us consider an enclosure with total surface area A. Let the view factor $dF_{dA'-dA}$ be the fraction of radiation leaving differential area dA' that is directly intercepted by dA. Therefore we can write

$$G(\mathbf{x})dA = \int_A J(\mathbf{x})dF_{dA'-dA}dA' + G_0(\mathbf{x})dA. \tag{6.85}$$

Here $G_0(\mathbf{x})$ is the radiation arriving at dA from external sources. Using the

reciprocity relation

$$dA' dF_{dA'-dA} = dA dF_{dA-dA'}, \tag{6.86}$$

we can then write

$$G(\mathbf{x}) = \int_A J(\mathbf{x}) dF_{dA-dA'} + G_0(\mathbf{x}). \tag{6.87}$$

Substitution of the above equation (6.87) into (6.84) gives

$$q(\mathbf{x}) = \epsilon(\mathbf{x}) E_b(\mathbf{x}) - \alpha(\mathbf{x}) \left(\int_A J(\mathbf{x}) dF_{dA-dA'} + G_0(\mathbf{x}) \right). \tag{6.88}$$

Eliminating irradiation from equation (6.84) and solving for J we obtain

$$J(\mathbf{x}) = \frac{\epsilon(\mathbf{x})}{\alpha(\mathbf{x})} E_b(\mathbf{x}) + q(\mathbf{x}) \left(1 - \frac{1}{\alpha(\mathbf{x})} \right). \tag{6.89}$$

Substituting the above equation into (6.88) and noting that $\epsilon = \alpha$ we obtain an integral equation relating the surface temperature and heat flux:

$$\frac{q(\mathbf{x})}{\epsilon(\mathbf{x})} - \int_A \left(\frac{1}{\epsilon(\mathbf{x})} - 1 \right) q(\mathbf{x}) dF_{dA-dA'} + G_0(\mathbf{x}) = E_b(\mathbf{x}) - \int_A E_b(\mathbf{x}) dF_{dA-dA'}. \tag{6.90}$$

Therefore, provided that the surface temperature and emissivity are known, we can compute the corresponding heat fluxes by solving equation (6.90). We shall do this by splitting the surfaces into N small segments over which we assume then the radiosity, the temperature and the emissivity are all constant. This allows us to write (6.90) as

$$\frac{q_i}{\epsilon_i} - \sum_{j=1}^{N} \left(\frac{1}{\epsilon_j} - 1 \right) q_j F_{i-j} + G_{0,i} = E_{b,i} - \sum_{j=1}^{N} E_{b,j} F_{i-j}. \tag{6.91}$$

In the next section, we will set up the second layer of the two-stage model. We shall develop the framework presented in this section in the context of a freeze-drying chamber.

6.4.2 Solving the heat flux equation

Having established the basic radiation model, we turn our attention to the particular application in the freeze-drying context. We will consider a simplified scenario. We shall model the vials on the tray as 16 cuboids arranged in a square. We model the sides of the free-drying chamber as infinitely long enclosures around the vials. The purpose of this model is to capture the radiative heat transfer between the vial walls and between the vial walls and the freeze-drying chamber. Furthermore, we assume that the sides of the free-drying chamber and the tray on which the vials are located are at the same temperature. A complete top view of the setup is illustrated in figure 6.1. However, due to the symmetry of the problem, it suffices to model only a quarter of the tray.

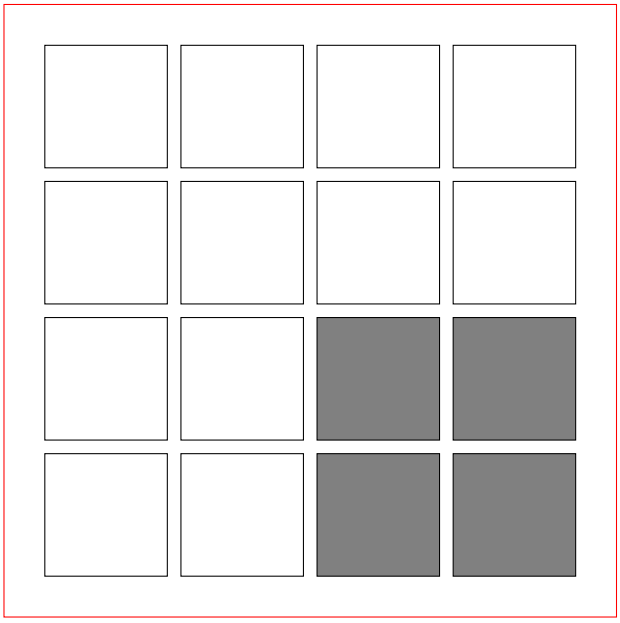

Figure 6.1: A top overview of the vial tray. The red square denotes the sides of the freeze-drying chamber. The smaller white squares are the vials. The shaded squares are the vials used in computations, due to the symmetry of the set-up.

The rest of this section is devoted to calculating the surface radiosities between two neighbouring vials. We will denote the two vials as vial 1 and vial 2. We will neglect any interaction between a vial and the vial diagonally opposite. We justify this by noting that the view factors for a surface segment

decay relatively quickly as we move away from the segment that is located directly opposite. For a usual separation between the vials (around 5mm) and depending on the grid spacing used, the view factor between two directly opposite corner segments is around 0.7 whereas the view factors between a corner segment and the nearest segment on the diagonally opposite vial are the range of 10^{-3} to 10^{-5}. Further, we shall assume that the surface temperatures and the emissivities of the two vials are known. Because of the convex shape of the vials, any element on vial 1 can only be influenced by radiative heat transfer from vial 2 and vice versa. Let $q(x)^{(1)}$ and $q(x)^{(2)}$ denote the radiosities on the neighbouring surfaces on vial 1 and 2, respectively. We discretise the surfaces in the usual manner into $n \times m$ grid, where $q_{i,j} = q(i\Delta x, j\Delta y)$. Furthermore, we assume that the emissivities ϵ_i in the equation (6.91) are constant across all elements.

Let $\mathbf{q}^{(k)}$, $\mathbf{E}_b^{(k)}$ be $nm \times 1$ vectors defined as

$$\mathbf{q}^{(k)} = \begin{bmatrix} q_{0,0}^{(k)} \\ \vdots \\ q_{n,0}^{(k)} \\ q_{0,1}^{(k)} \\ \vdots \\ q_{n,1}^{(k)} \\ \vdots \\ q_{i,j}^{(k)} \\ \vdots \\ q_{n,m}^{(k)} \end{bmatrix}, , \mathbf{E}_b^{(k)} = \begin{bmatrix} E_{b,0,0}^{(k)} \\ \vdots \\ E_{b,n,0}^{(k)} \\ E_{b,0,1}^{(k)} \\ \vdots \\ E_{b,n,1}^{(k)} \\ \vdots \\ E_{b,i,j}^{(k)} \\ \vdots \\ E_{b,n,m}^{(k)} \end{bmatrix} \text{ and } \mathbf{F}_{i,j} = \begin{bmatrix} F_{ij-00} \\ \vdots \\ F_{ij-n0} \\ F_{ij-10} \\ \vdots \\ F_{ij-n0} \\ \vdots \\ F_{ij-ij} \\ \vdots \\ F_{ij-nm} \end{bmatrix}. \tag{6.92}$$

Here F_{ij-kl} is a view factor from the ij element on one vial to kl element of the other vial. Then we can write the equation (6.91) in a matrix form as

$$\begin{bmatrix} \frac{1}{\epsilon}\mathbf{I}_{nm\times nm} & \frac{\epsilon-1}{\epsilon}\mathbf{F} \\ \frac{\epsilon-1}{\epsilon}\mathbf{F} & \frac{1}{\epsilon}\mathbf{I}_{nm\times nm} \end{bmatrix} \begin{bmatrix} \mathbf{q}^{(1)} \\ \mathbf{q}^{(2)} \end{bmatrix} = \begin{bmatrix} \mathbf{E}_b^{(1)} \\ \mathbf{E}_b^{(2)} \end{bmatrix} - \begin{bmatrix} \mathbf{0} & \mathbf{F} \\ \mathbf{F} & \mathbf{0} \end{bmatrix} \begin{bmatrix} \mathbf{E}_b^{(1)} \\ \mathbf{E}_b^{(2)} \end{bmatrix} - E_{b,side} \begin{bmatrix} \mathbf{F}_s \\ \mathbf{F}_s \end{bmatrix}. \quad (6.93)$$

Here, $\mathbf{I}_{nm\times nm}$ is $nm \times nm$ identity matrix, $\mathbf{F}$ is a matrix of view factors and $\mathbf{F}_s$ is a $nm \times 1$ vector given by

$$\mathbf{F} = \begin{bmatrix} \mathbf{F}_{0,0}^T \\ \vdots \\ \mathbf{F}_{n,0}^T \\ \mathbf{F}_{1,0}^T \\ \vdots \\ \mathbf{F}_{n,0}^T \\ \vdots \\ \mathbf{F}_{i,j}^T \\ \vdots \\ \mathbf{F}_{n,m}^T \end{bmatrix}, \quad (6.94)$$

and $\mathbf{F}_s$ is a $nm \times 1$ vector such that the ith component of $\mathbf{F}_s$ is given by

$$\{\mathbf{F}_s\}_i = 1 - \sum_{j=0}^{nm} \{\mathbf{F}\}_{i,j}. \quad (6.95)$$

Also, $E_{b,side}$ is the background radiation comming from the sides of the freeze-dryer to every element, if modelled as a black body. Lastly, the element view factors F_{ij-kl} are between two rectangles in parallel planes taken from [12].

This concludes the computations of heat transfer between the vials. In the next section, we shall combine it with the single vial model developed in section 6.2.

6.5 Two-stage Model Results

Here we finalise the two-stage model developed in this chapter. Given the initial temperature distribution, we compute the radiosities on the vial surfaces using the equation (6.93). Once the radiosities are known, we use them as the boundary conditions for the single vial model and march the governing equations by one time step to produce new temperature distributions and interface positions. These new values are then fed back into equation (6.93), and the whole process is repeated.

We are interested in examining how the sides of the freeze-drying influence the uniformity of the temperatures inside the vials, and how such an effect might propagate from the edge vials to the centre vials.

We assume that the tray shelf and the sides of the freeze-dryer are kept at a constant temperature of 258K and that the vials are initially at fusion temperature 273.15K. As we did in the case of the models presented in chapter 5, we will also kick-start the numerical modelling using a small time delay. We look at the progression of the process using different values of the heat transfer coefficients k_{side}.

The results are presented in the figures that follow. The blue surface represents the position of the solid-liquid interface. All the simulations are done until the non-dimensional time $\tau = 8$, which corresponds to around 4.8 hours. The time step $\Delta\tau$ is taken to be 0.002, and we use a uniform spatial grid with spacing equal to 0.05. The position of the vials in the figures is analogous to the shaded squares in figure 6.1. The results displayed in subsequent figures are showing the model at times $\tau = 1, 4$ and $\tau = 8$. Additional figures showing the intermediate times can be seen in the appendix A.

We can see that in the case of $k_{side} = 1$ the interface remains relatively flat for all vials up to the time $\tau = 1$. Moreover, the temperature distribution is relatively constant along $x - y$ plane. This is especially the case for the centre vial. There is around 0.5K difference between the minimum temperatures of the centre vial and edge vials and around 1K difference between the centre

and corner vials. By the time $\tau = 4$, the difference in minimum temperature increased to 1.5K and 2K between the centre and edge and centre and corner vials, respectively. Furthermore, we can see that the interface starts to curve along the side of the vials that face the walls of the freeze-drying chamber. This effect is amplified by the time of $\tau = 8$. The difference in the minimum temperature remained roughly the same as at $\tau = 4$. On average about two-thirds of the vials are frozen. In the case of $k_{side} = 1$ the centre vial seemed not to be influenced by the edge vial effect are the temperature distribution stayed more or less one-dimensional.

In the case of $k_{side} = 0.5$, a mild curvature is already present in the interface in the edge and corner vials at $\tau = 1$. The sides of the vials that face the walls of the freeze-drying chamber are 0.5K colder than the sides facing other vials. Moreover, the minimum temperature inside the centre vial is 1.5K higher than the minimum temperature of the corner vial and 1K higher than the edge vials. At the time $\tau = 4$ the situation remains qualitatively the same; however, the temperature difference between the minimum values has increased to 3K for corner and 1.5K for edge vials. At the final time, $\tau = 8$ a section of the interface in the corner vials has reached the top of the vial, and the vast majority of the product has solidified. For the edge, vials the interface has almost reached the top of the vials near the side facing the walls. However, the position of the interface at the sides facing the centre vial is almost identical to the case of $k_{side} = 1$. Examining the temperature and interface position of the centre vial, we can note that they are also identical to the case of $k_{side} = 1$. Hence the value of $k_{side} = 0.5$ is not sufficient for the edge vial effect to influence the centre vial.

We can see that for the value $k_{side} = 0.1$ at time $\tau = 1$ there is already a significant difference in temperatures at the sides facing the walls and temperatures at the sides facing the other vials (3K for edge and 4.5K for corner vial). We can also note that the minimum temperature in the centre vial is 3K, 4K higher than the minimum temperature inside the edge and corner vials, respec-

tively. By the time $\tau = 4$ the interface in the edge vials has already reached the top of the vials. Moreover, the corner vial is almost completely solidified with the interface progressing towards the centre vial. At the time $\tau = 8$ all vials apart from the centre one are completely frozen, and most of the corner vial has reached the shelf temperature of 258K. The minimum temperature inside the edge and corner vials is 5K and 7K lower than the minimum temperature inside the centre vial, respectively. We can see that the interface in the centre vial is no longer flat but in curved as the colder edge vials influenced it. We can also note that the sides of the edge vials facing the corner vial are also at lower temperatures to the sides opposite.

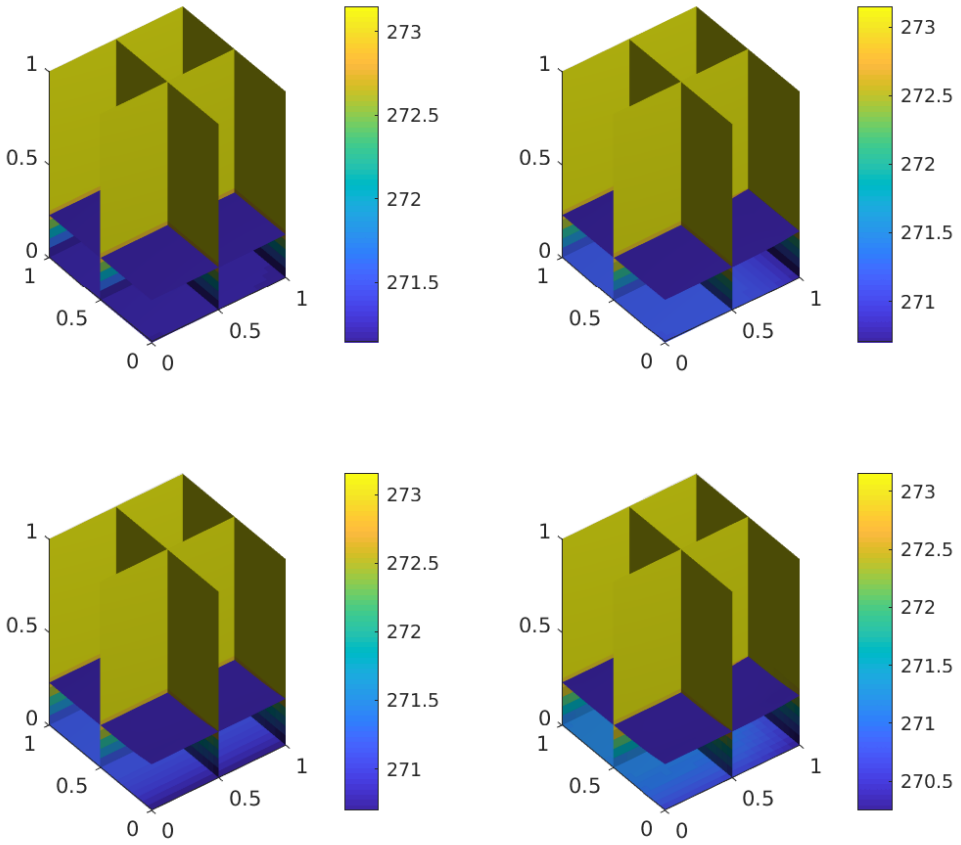

Figure 6.2: $k_{shelf} = 0.76, k_{side} = 1, \tau = 1$

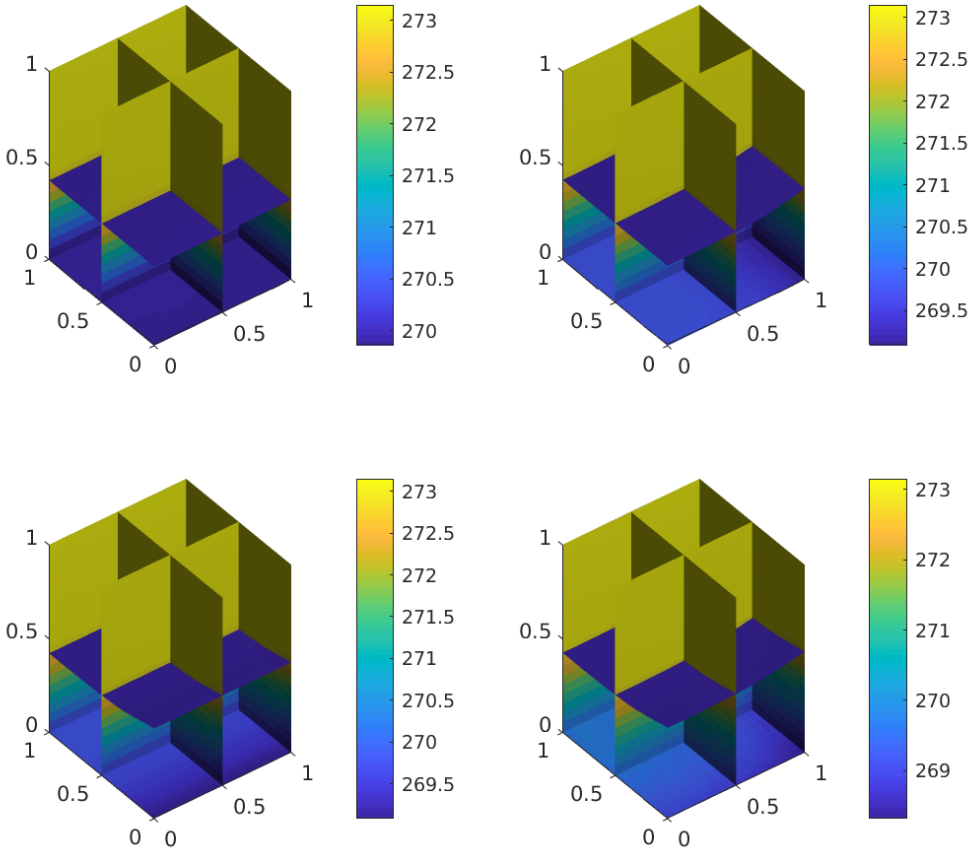

Figure 6.3: $k_{shelf} = 0.76, k_{side} = 1, \tau = 4$

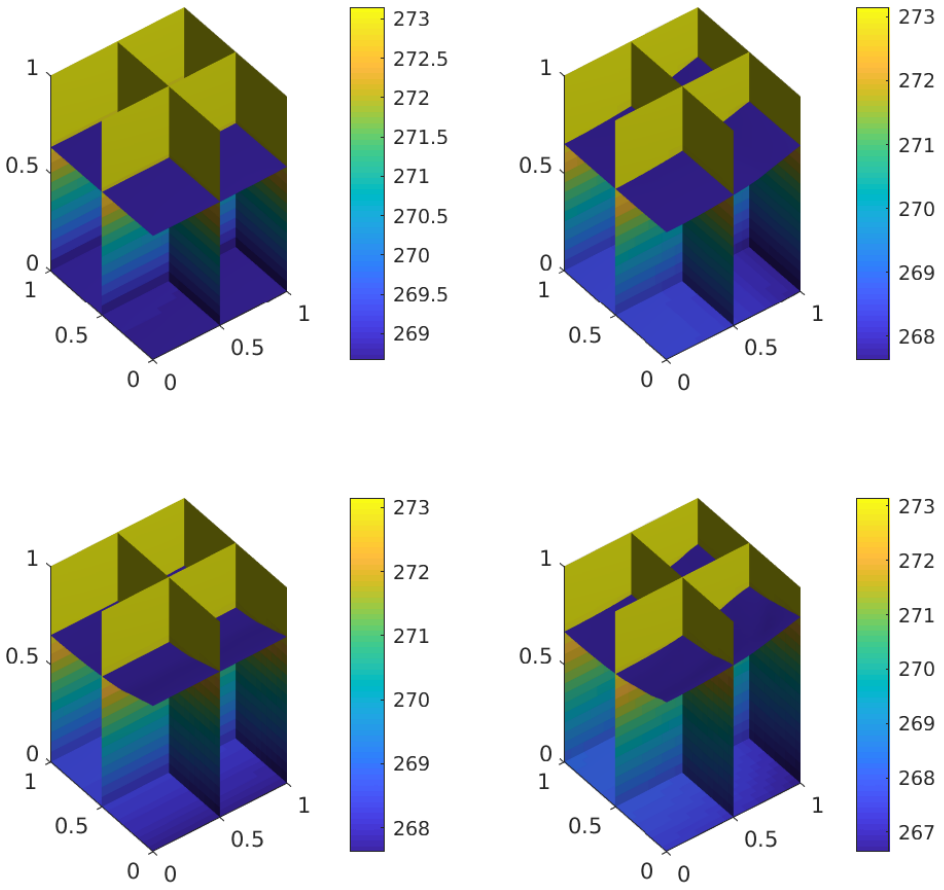

Figure 6.4: $k_{shelf} = 0.76, k_{side} = 1, \tau = 8$

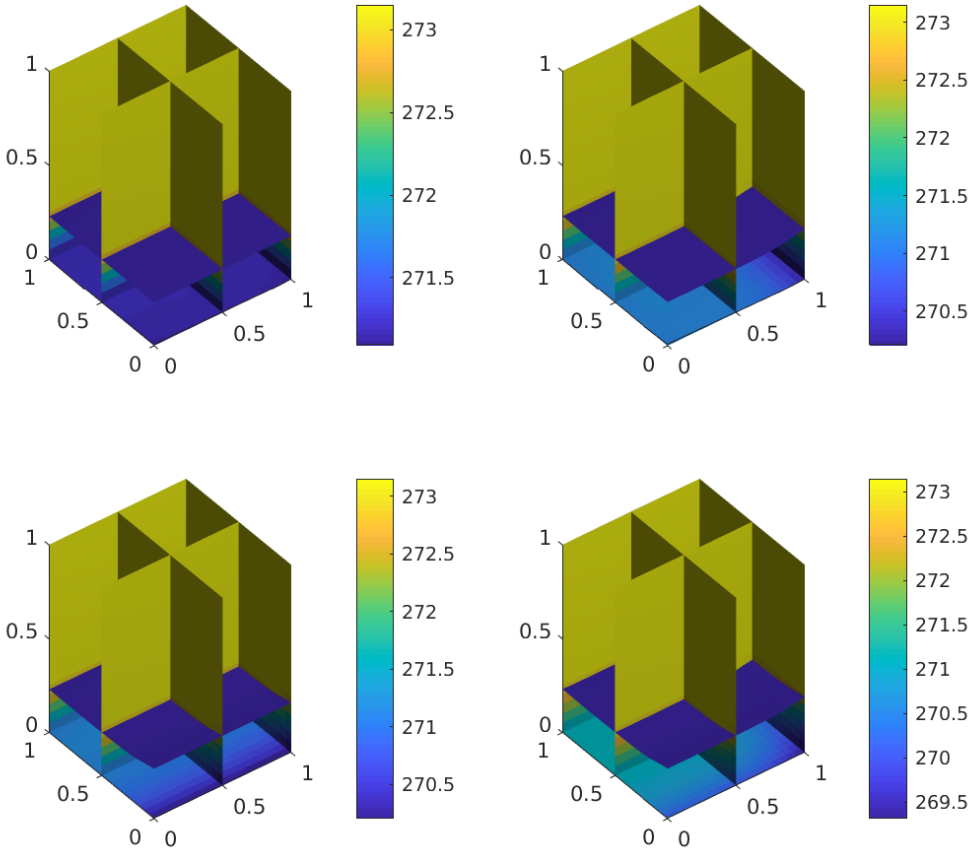

Figure 6.5: $k_{shelf} = 0.76, k_{side} = 0.5, \tau = 1$

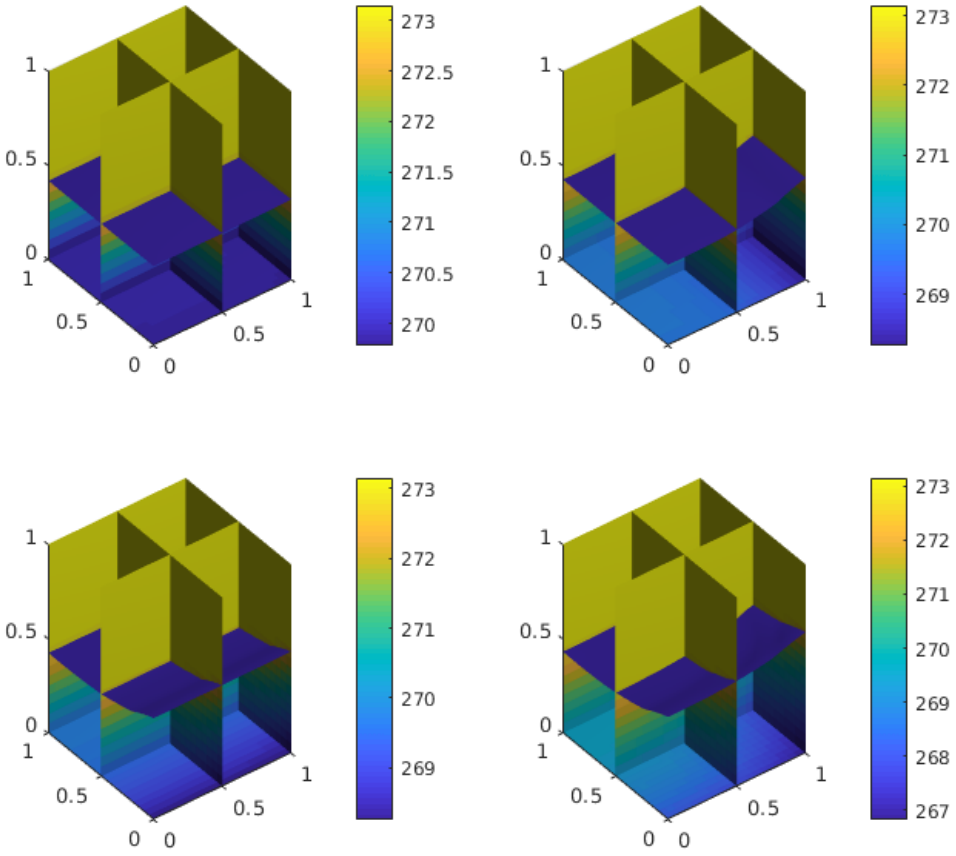

Figure 6.6: $k_{shelf} = 0.76, k_{side} = 0.5, \tau = 4$

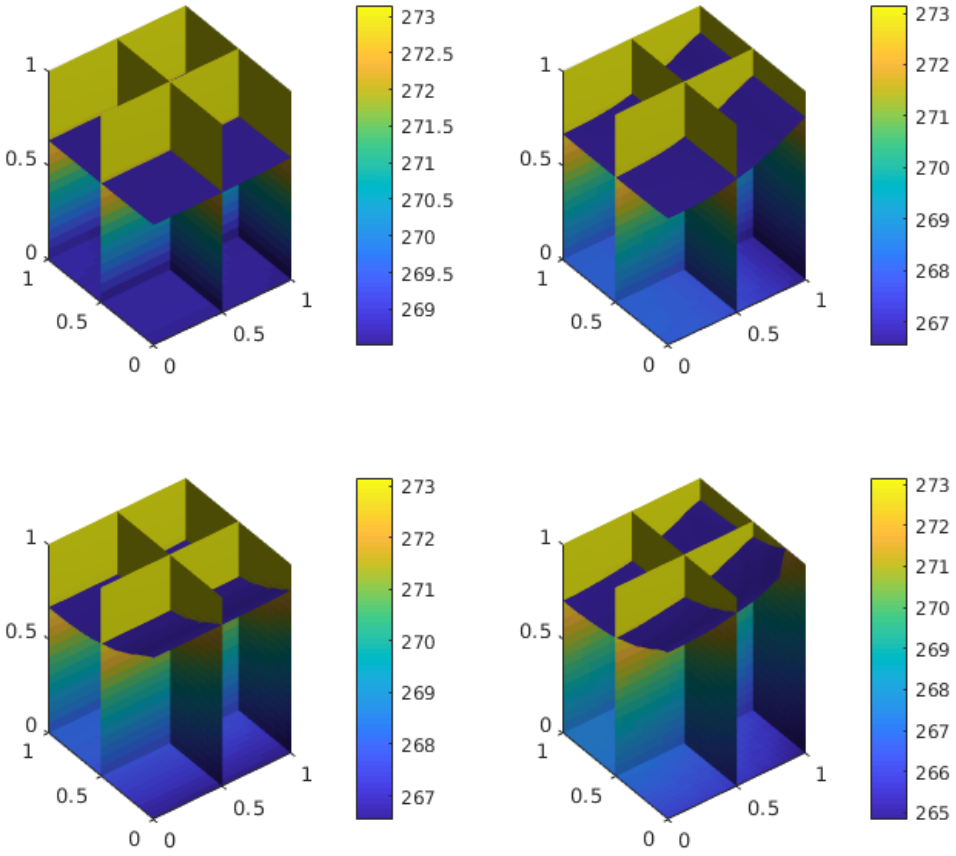

Figure 6.7: $k_{shelf} = 0.76, k_{side} = 0.5, \tau = 8$

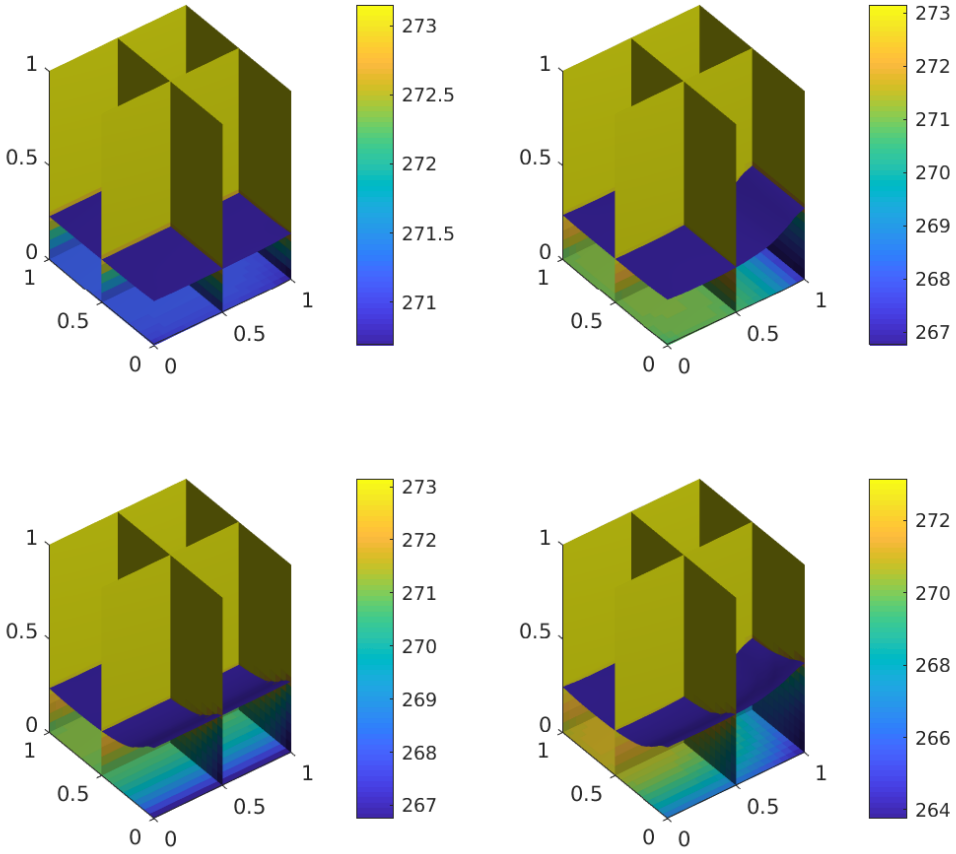

Figure 6.8: $k_{shelf} = 0.76, k_{side} = 0.1, \tau = 1$

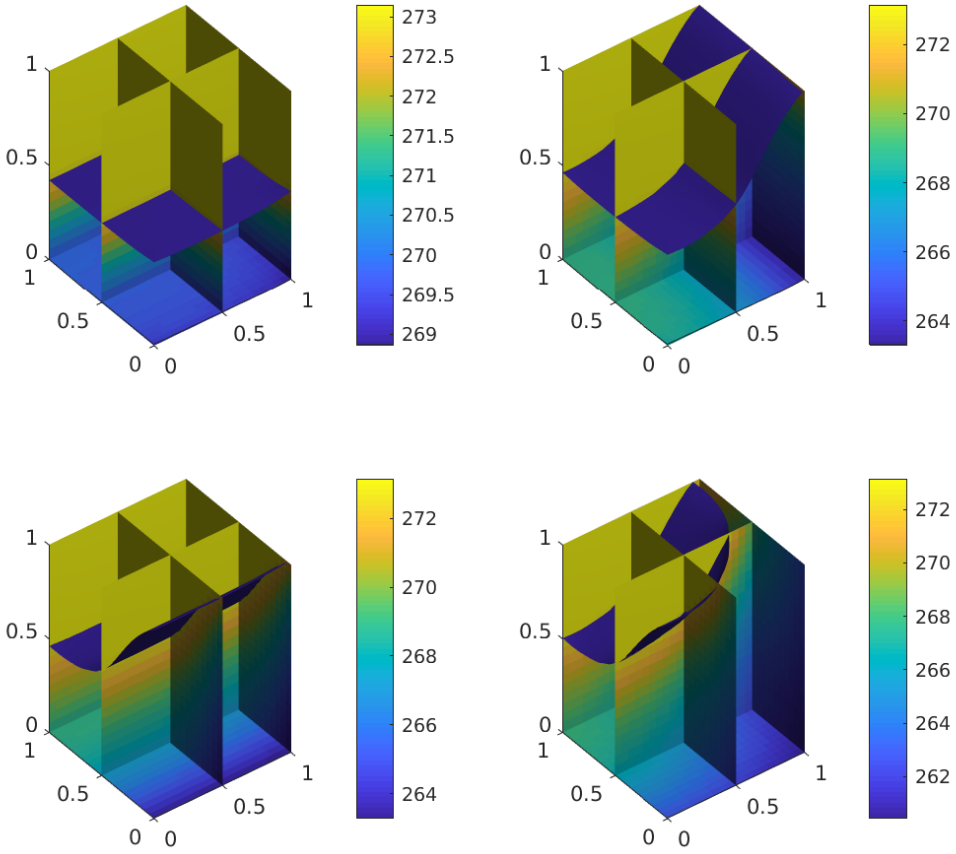

Figure 6.9: $k_{shelf} = 0.76, k_{side} = 0.1, \tau = 4$

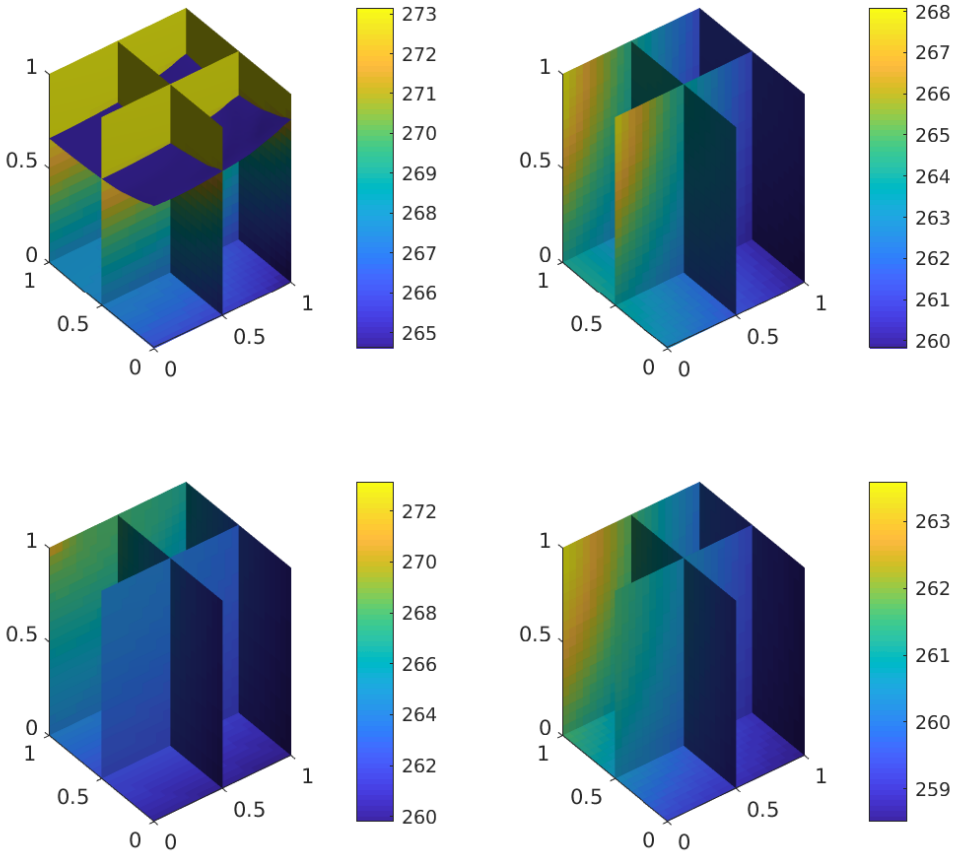

Figure 6.10: $k_{shelf} = 0.76, k_{side} = 0.1, \tau = 8$

6.6 Summary

From the outputs of the model, it is clear that when $k_{side} \geq 1$ the model predicts relatively homogeneous samples and the edge effect is negligible. However, we see that for values of $k_{side} = 0.1$ or $k_{side} = 0.5$ there is a noticeable contribution of the walls of the freeze-dryer onto the temperature distributions in the vials. Moreover, in the case of $k_{side} = 0.1$, the effect penetrated through the edge vials into the neighbouring centre vial.

The rate of freezing influences the size of ice crystals formed during the freezing stage. In general, we would like to produce relatively large ice crystals which during the drying stage would result in larger pore sizes and hence lower mass transfer resistance [24]. However, the presence of the edge vial effect could result in the formation of smaller ice crystals in the vials located at the edge of the freeze-drying tray. These vials could experience longer drying times and attain a higher temperature during the drying stage.

It is important to notice that this effect is very likely also present during the drying stages of the process. Because of the heat applied during these stages, the extra contributions of heat transfer to the vials might increase the temperature of the product over a critical value. This could permanently damage the product, for instance, by the temperature reaching a glass transition value when the product losses its porous structure and collapses [38, 1]. Therefore, understanding the extent to which vials are influenced by the edge effect is important.

The heat transfer coefficient k_{side} can be adjusted by laboratory or industrial design. In theory, a shielding could be implemented to mitigate the effect.

Chapter 7

Chemical Model of Freezing

7.1 Introduction

Here we present a model of solidification that is based on the principles from combustion theory. The idea is to formulate the freezing process mathematically as a chemical reaction whose fuel is the liquid water and the product is solidified ice. It is important to stress that solidification is purely a physical process and the chemistry mentioned above is assumed only in a mathematical sense.

7.2 Chemical reactions

This section provides a short introduction to the basic principles behind the kinetics of chemical reactions, which is the starting point of the proposed model.

Suppose a chemical reaction takes fuel F and turns it into a certain amount of product P and heat. Let ω denote the rate of the chemical reaction. It is reasonable to assume that ω is temperature-dependent. This dependence can be expressed in the form of an *Arrhenius equation* as

$$\omega = A \exp\left(-\frac{E_a}{RT}\right). \tag{7.1}$$

Here, A is the pre-exponential factor, E_a is the activation energy of the reaction

and is assumed to be constant, R is the universal gas constant and T is the absolute temperature.

Let Y denote the mass fraction of the fuel present. Then, assuming that the density of the fuel is independent of temperature, the evolution of Y and T is given by

$$\frac{\partial Y}{\partial t} = -Y\omega, \tag{7.2}$$

$$\frac{\partial T}{\partial t} = D\nabla^2 T + Y\frac{q\omega}{c_p}, \tag{7.3}$$

where D is the thermal diffusivity, c_p is the specific heat capacity and q a constant representing the heat generated per unit of mass of fuel consumed. We shall now reformulate the problem in terms of solidification processes.

7.3 The model

In the present model, we consider solidification to be a reaction whose rate satisfies the Arrhenius law. However, we assume that instead of the absolute temperature, the rate depends purely on the amount of supercooling ΔT_s of the system. Moreover, we take the pre-exponential factor A to be linearly dependent on ΔT_s. This additional dependence is added to the model to ensure the correct behaviour of the temperature field. In particular, it will later prevent the non-dimensional temperature from escaping into negative values, which tended to happen without this additional term. Hence

$$\omega = A\Delta T_s \exp\left(-\frac{E_a}{\Delta T_s}\right). \tag{7.4}$$

Here E_a is again some analogue of the activation energy of the reaction.

Let f be the mass fraction of ice. Hence the fuel mass fraction is given by $Y = 1 - f$. Production of ice releases latent heat, H. Therefore, f will appear as a source term in the temperature equation:

$$\frac{\partial T}{\partial t} = D\nabla^2 T + \frac{H}{c_p}\frac{\partial f}{\partial t}. \tag{7.5}$$

This equation is consistent with equation 7.3 for $q = H$ and

$$Y\omega = \frac{\partial f}{\partial t}.$$

Using the modified Arrhenius law we get

$$\frac{\partial f}{\partial t} = A\Delta T_s(1-f)\exp\left(-\frac{E_a}{\Delta T_s}\right). \tag{7.6}$$

Let us consider a semi-infinite strip of water occupying the region $x \in [0,\infty)$. Furthermore let us assume that the water is initially at fusion temperature, T_{in}. From time $t > 0$ the liquid is being cooled from the boundary at $x = 0$, with rate proportional to $T - T_{sh}$, where T_{sh} is a parameter of the model. The problem can be expressed in non-dimensional form as

$$\begin{aligned} \frac{\partial \theta}{\partial \tau} &= \frac{\partial^2 \theta}{\partial x^2} + \beta\frac{\partial f}{\partial \tau}, & (7.7)\\ \frac{\partial f}{\partial \tau} &= \Lambda(1-f)(1-\theta)\exp\left(\frac{\tilde{E}}{\theta - 1}\right), & (7.8) \end{aligned}$$

where $\Delta T = T_{in} - T_{sh}$, $\tilde{E} = E_a/\Delta T$, β is the Stefan number given by

$$\beta = \frac{H}{\Delta T c_p}, \tag{7.9}$$

and Λ is the ratio

$$\Lambda = \frac{\Delta T A}{\tau_{ref}}. \tag{7.10}$$

Here τ_{ref} is a reference time scale taken to be L^2/D, with L being a reference length scale. The initial conditions are $\theta(0,x) = 1$ and $f(0,x) = 0$. The

boundary condition at $x = 0$ becomes

$$\frac{\partial \theta}{\partial x} = \mathrm{Bi}\theta, \tag{7.11}$$

where Bi is the Biot number of the system. Lastly we impose a far field condition $\theta \to 1$ as $x \to \infty$, which closes the system.

7.4 Numerical results

In this section we present numerical solutions for the system (7.7)–(7.11). In order to test the validity of the model proposed in this chapter, we analyse the results against the small time solution of the sharp interface model discussed in chapter 5. The results are compared to the sharp interface model (red line), with the initial position of the interface at $x = 0.1$. The simulations were computed over a range of the parameters $\Lambda, \tilde{E}$ and β. The following plots represent the values of the ice fraction f plotted against the time.

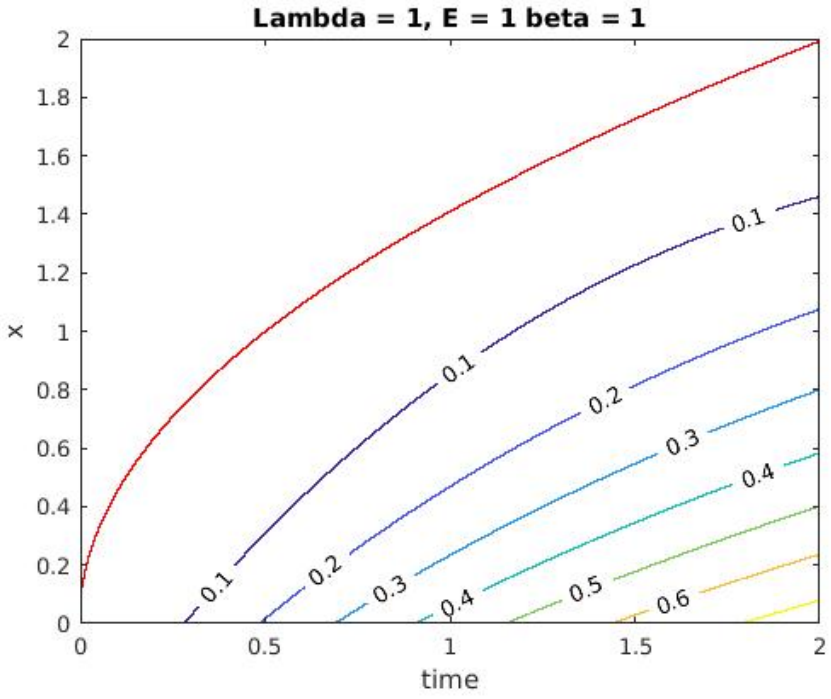

Figure 7.1: Comparison of the small time solution sharp interface and chemical model with $\Lambda = 1, \tilde{E} = 1$ and $\beta = 1$.

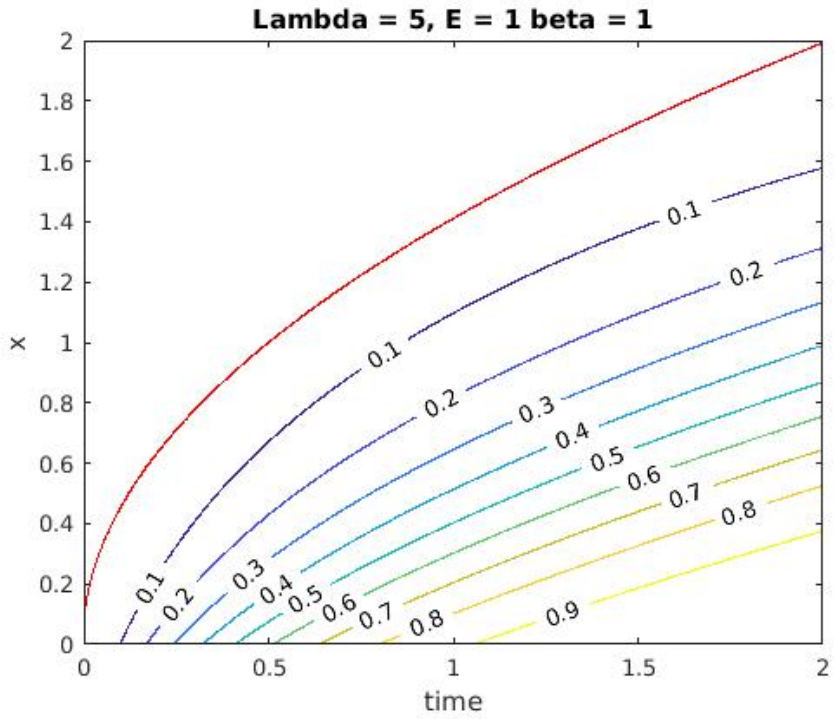

Figure 7.2: Comparison of the small time solution sharp interface and chemical model with $\Lambda = 5, \tilde{E} = 1$ and $\beta = 1$.

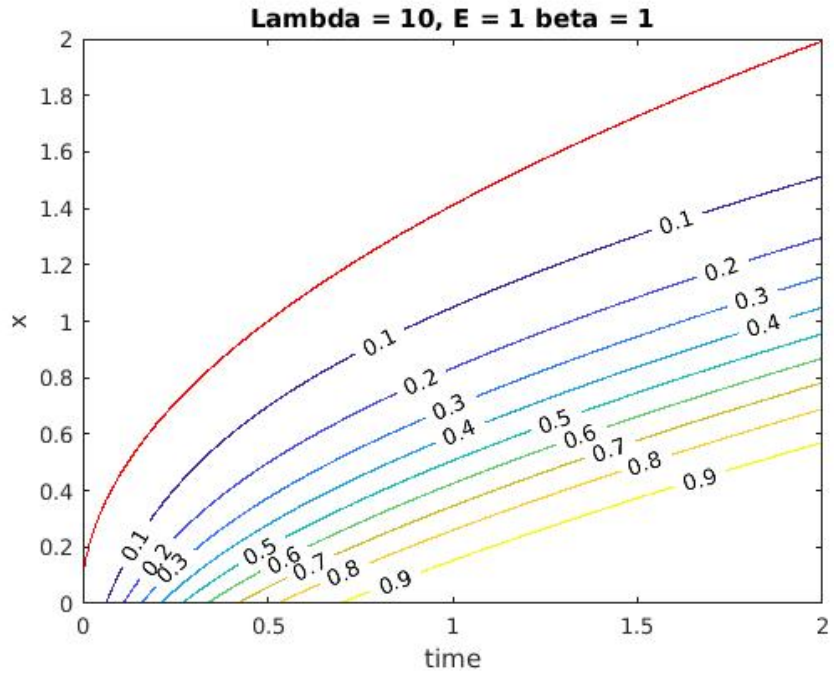

Figure 7.3: Comparison of the small time solution sharp interface and chemical model with $\Lambda = 10, \tilde{E} = 1$ and $\beta = 1$.

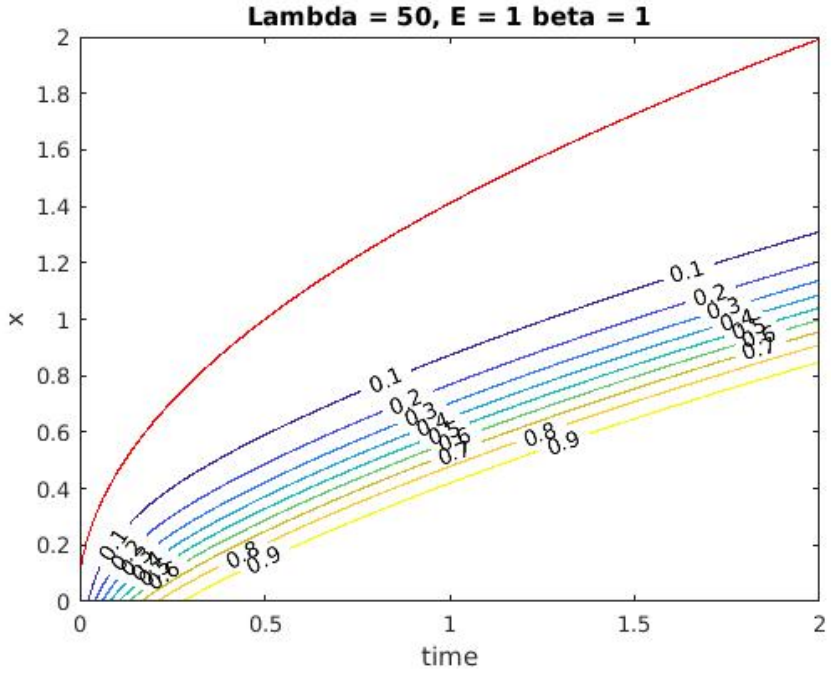

Figure 7.4: Comparison of the small time solution sharp interface and chemical model with $\Lambda = 50, \tilde{E} = 1$ and $\beta = 1$.

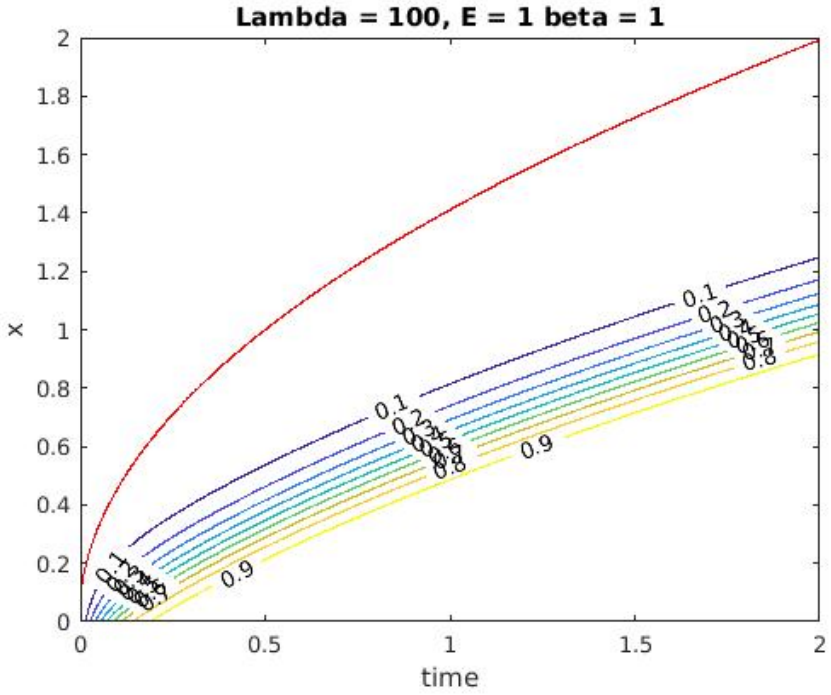

Figure 7.5: Comparison of the small time solution sharp interface and chemical model with $\Lambda = 100, \tilde{E} = 1$ and $\beta = 1$.

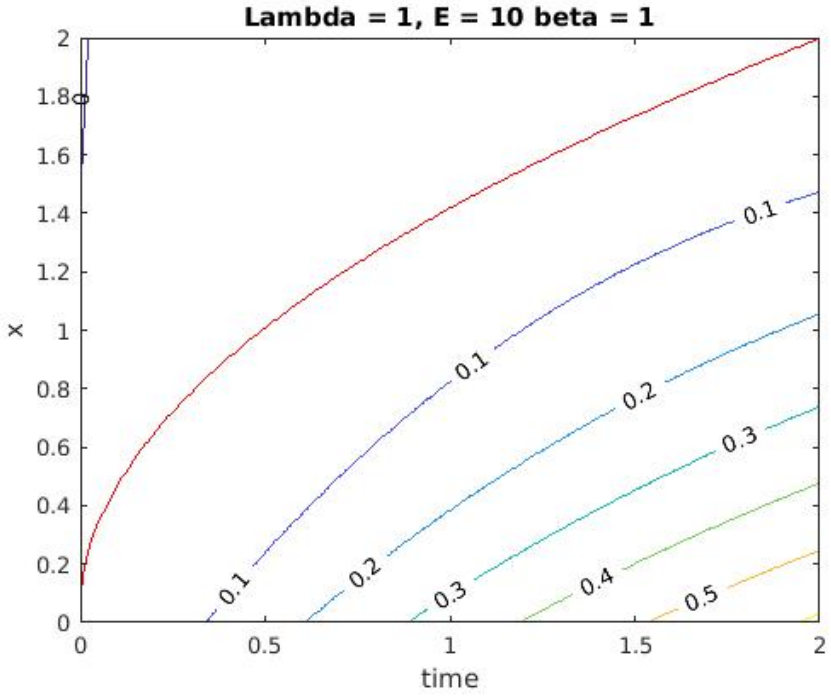

Figure 7.6: Comparison of the small time solution sharp interface and chemical model with $\Lambda = 1, \tilde{E} = 10$ and $\beta = 1$.

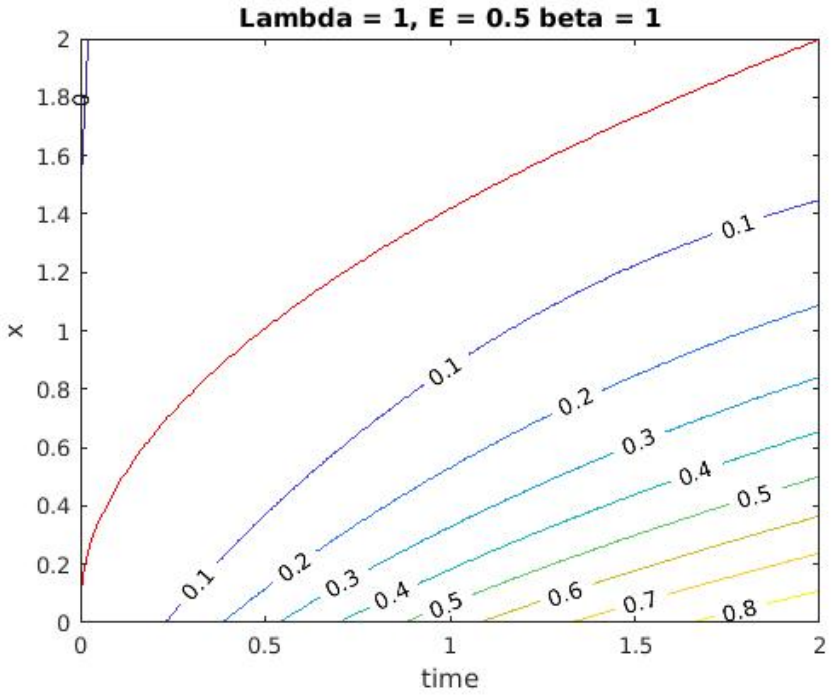

Figure 7.7: Comparison of the small time solution sharp interface and chemical model with $\Lambda = 1, \tilde{E} = 0.5$ and $\beta = 1$.

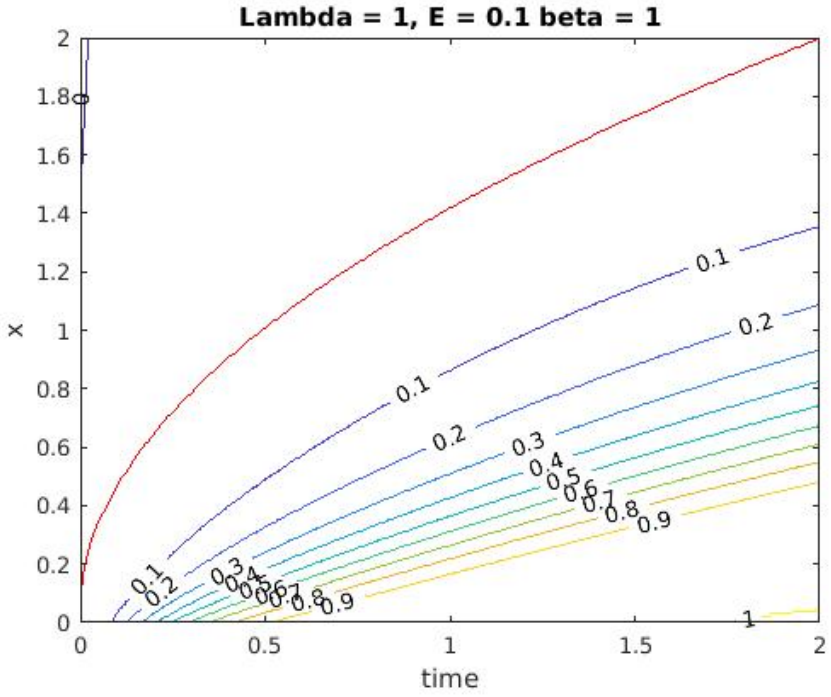

Figure 7.8: Comparison of the small time solution sharp interface and chemical model with $\Lambda = 1, \tilde{E} = 0.1$ and $\beta = 1$.

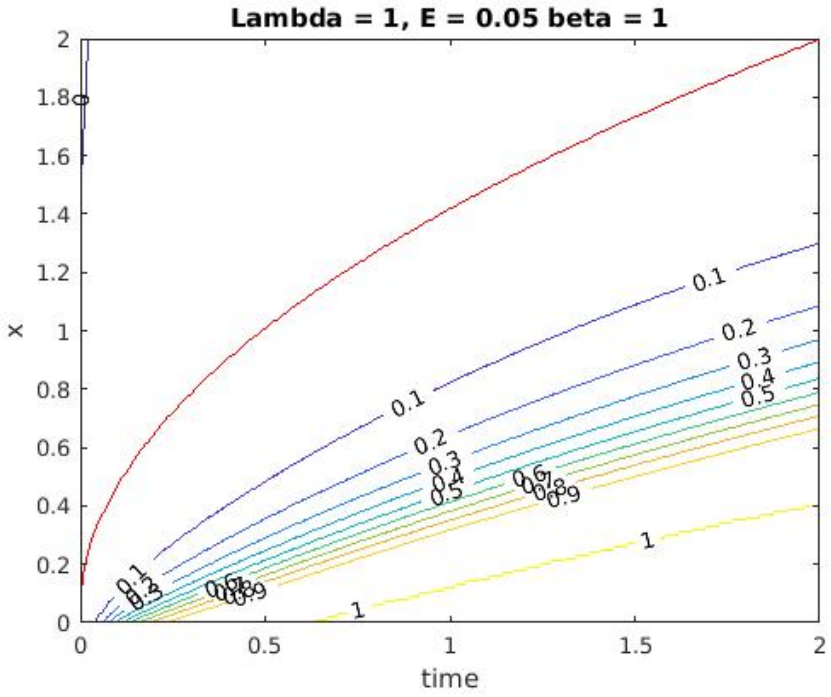

Figure 7.9: Comparison of the small time solution sharp interface and chemical model with $\Lambda = 1, \tilde{E} = 0.05$ and $\beta = 1$.

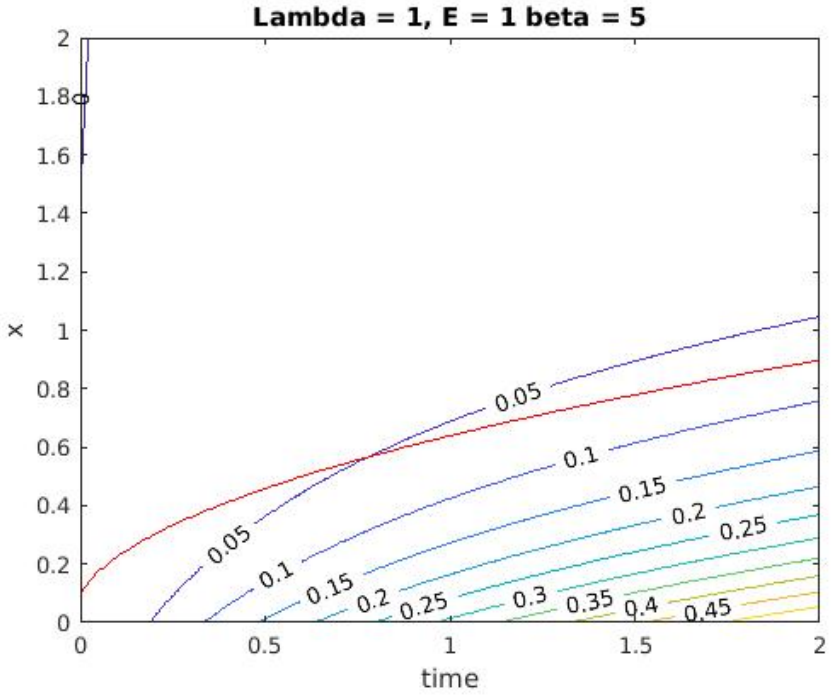

Figure 7.10: Comparison of the small time solution sharp interface and chemical model with $\Lambda = 1, \tilde{E} = 1$ and $\beta = 5$.

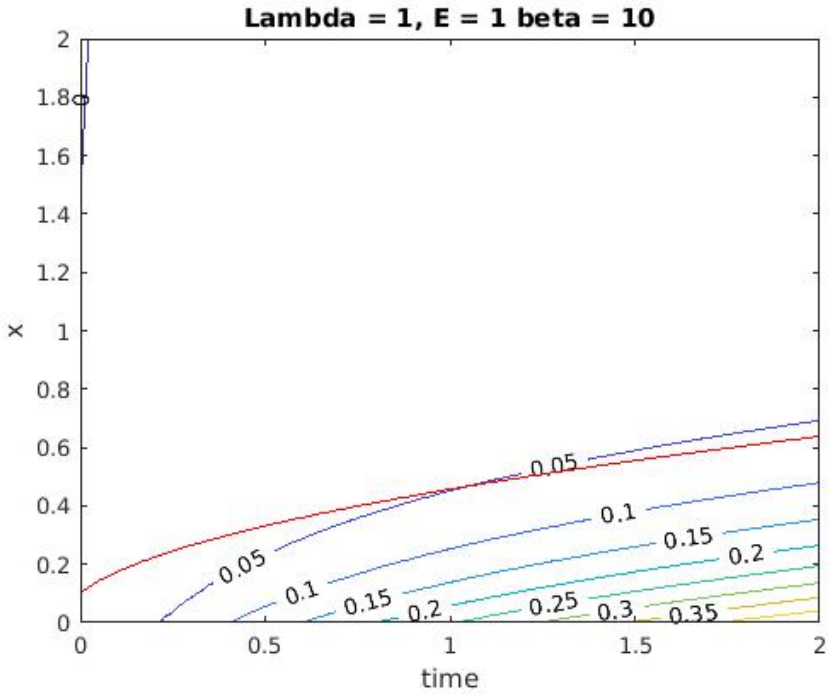

Figure 7.11: Comparison of the small time solution sharp interface and chemical model with $\Lambda = 1, \tilde{E} = 1$ and $\beta = 10$.

The simulations show that increasing Λ and decreasing $\tilde{E}$ both have the effect of increasing the gradients of the ice fraction in the solidifying region, although the $\tilde{E}$ effect is more significant for smaller times. This is natural as $\tilde{E}$ acts as an energy barrier for the ice creation. The parameter β has the usual role of controlling the rate of the ice-liquid interface progression.

7.5 Large β solution

We shall now seek an approximate solution to the system (7.7)-(7.11) for small times, $\tau \ll 1$. In the analysis that follows we assume that the Stefan number of our system, β, is large. By this assumption, we can scale τ as

$$\tau = \beta^{-1}\tilde{\tau}, \tag{7.12}$$

where $\tilde{\tau}$ is strictly $O(1)$. In order to keep the source term in equation (7.7), we need to scale the ice fraction f as

$$f = \beta^{-1}\tilde{f}. \tag{7.13}$$

Here, again, $\tilde{f}$ is an $O(1)$ quantity. Substituting (7.12) and (7.13) into our system (7.7)–(7.8) gives:

$$\beta\frac{\partial\theta}{\partial\tilde{\tau}} = \frac{\partial^2\theta}{\partial x^2} + \beta\frac{\partial\tilde{f}}{\partial\tilde{\tau}}, \tag{7.14}$$

$$\frac{\partial\tilde{f}}{\partial\tilde{\tau}} = \Lambda(1-\beta^{-1}\tilde{f})(1-\theta)\exp\left(\frac{\tilde{E}}{\theta-1}\right). \tag{7.15}$$

Therefore, up to the leading order of β, the diffusion term in (7.14) can be neglected. Similarly in (7.15) we can use the approximation $(1-\beta^{-1}\tilde{f}) \approx 1$. Hence we obtain

$$\frac{\partial\theta}{\partial\tilde{\tau}} = \frac{\partial\tilde{f}}{\partial\tilde{\tau}}, \tag{7.16}$$

$$\frac{\partial\tilde{f}}{\partial\tilde{\tau}} = \Lambda(1-\theta)\exp\left(\frac{\tilde{E}}{\theta-1}\right). \tag{7.17}$$

Since initially, $\theta = 1$, we get that $\theta = 1$ for all $\tilde{\tau}$. However, we would expect a thin boundary layer near $x = 0$, where the diffusion term is significant.

7.5.1 Boundary layer

To investigate the behaviour of the system near $x = 0$, we introduce a new scaled coordinate

$$x = \beta^{-1/2}\tilde{x}, \tag{7.18}$$

with $\tilde{x} = O(1)$. We shall also express the temperature field and the ice fraction in a power series of β as

$$\theta = 1 + \beta^{-1/2}\tilde{\theta}(\tilde{x},\tilde{\tau}) + \beta^{-1}\tilde{\tilde{\theta}}(\tilde{x},\tilde{\tau}) + \ldots \tag{7.19}$$

$$f = \beta^{-3/2}\tilde{\tilde{f}} + \ldots \tag{7.20}$$

Substituting (7.18) and (7.12) into (7.7)-(7.8) we obtain:

$$\frac{\partial\theta}{\partial\tilde{\tau}} = \frac{\partial^2\theta}{\partial\tilde{x}^2} + \beta\frac{\partial f}{\partial\tilde{\tau}}, \tag{7.21}$$

$$\beta\frac{\partial f}{\partial\tilde{\tau}} = \Lambda(1-f)(1-\theta)\exp\left(\frac{\tilde{E}}{\theta-1}\right). \tag{7.22}$$

The boundary condition at $x = 0$ becomes

$$\beta^{1/2}\frac{\partial\theta}{\partial\tilde{x}}\bigg|_{\tilde{x}=0} = \text{Bi}\ \theta(0,\tilde{\tau}). \tag{7.23}$$

Substituting (7.19) and (7.20) into equations (7.21)–(7.22) and collecting the powers of β we get that at the leading order, the system is given by

$$\beta^{-1/2}\frac{\partial\tilde{\theta}}{\partial\tilde{\tau}} = \beta^{-1/2}\frac{\partial^2\tilde{\theta}}{\partial\tilde{x}^2} + \beta^{-1/2}\frac{\partial\tilde{\tilde{f}}}{\partial\tilde{\tau}}, \tag{7.24}$$

$$\beta^{-1/2}\frac{\partial\tilde{\tilde{f}}}{\partial\tilde{\tau}} = -\beta^{-1/2}\Lambda\tilde{\theta}\exp\left(-\frac{\tilde{E}}{\beta^{-1/2}\tilde{\theta}}\right). \tag{7.25}$$

Hence we can reduce the system to a single PDE for $\tilde{\theta}$:

$$\frac{\partial\tilde{\theta}}{\partial\tilde{\tau}} = \frac{\partial^2\tilde{\theta}}{\partial\tilde{x}^2} - \Lambda\tilde{\theta}\exp\left(-\frac{\tilde{E}}{\beta^{-1/2}\tilde{\theta}}\right). \tag{7.26}$$

The exponential term in the above equation could be neglected provided that $\tilde{E}$ is sufficiently small. However, if $\tilde{E} = O(\beta^{-1/2})$, then the term might be significant. For now, let us assume the former and approximate the equation (7.26) as

$$\frac{\partial\tilde{\theta}}{\partial\tilde{\tau}} = \frac{\partial^2\tilde{\theta}}{\partial\tilde{x}^2} - \Lambda\tilde{\theta}, \tag{7.27}$$

subject to

$$\tilde{\theta}(\tilde{x},0) = 0, \tag{7.28}$$

$$\left.\frac{\partial\tilde{\theta}}{\partial\tilde{x}}\right|_{\tilde{x}=0} = \mathrm{Bi}, \tag{7.29}$$

and

$$\tilde{\theta} \to 0 \text{ as } \tilde{x} \to \infty. \tag{7.30}$$

During slow solidification processes, the temperature of the system often reaches a steady-state distribution before the interface progresses. Therefore, we might expect similar behaviour to occur in our system. Hence we should look for steady-state solutions to equation (7.27): this gives

$$\tilde{\theta} = -\frac{\mathrm{Bi}}{\sqrt{\Lambda}}e^{-\sqrt{\Lambda}\tilde{x}}, \tag{7.31}$$

and the ice fraction $\tilde{\tilde{f}}$ is given by

$$\tilde{\tilde{f}} = \tilde{\tau}\sqrt{\Lambda}\mathrm{Bi}e^{-\sqrt{\Lambda}\tilde{x}}. \tag{7.32}$$

The comparisons of the fully numerical and the small-time asymptotical solutions are provided in the next section. The rest of this section is concerned with the transition from the small-time solution to the system where $\tau = O(1)$.

When $\tau = O(1)$ we have that $\tilde{\tau} \to \beta\tau$. Then the equation (7.32) suggests

that in the boundary layer region where $x \sim \beta^{-1/2}$ the ice fraction f is also $O(\beta^{-1/2})$. Therefore, for $\tau \sim 1$ we define

$$\theta = 1 + \beta^{-1/2}\bar{\theta} + \ldots, \tag{7.33}$$

and

$$f = \beta^{-1/2}\bar{f} + \ldots. \tag{7.34}$$

After substituting these into the original system we the equation reduces to

$$0 = \frac{\partial^2 \bar{\theta}}{\partial \tilde{x}^2} + \frac{\partial \bar{f}}{\partial \tau}, \tag{7.35}$$

$$\frac{\partial \bar{f}}{\partial \tau} = -\Lambda \bar{\theta}. \tag{7.36}$$

This is the same steady-state system as in the case of $\tau = O(\beta^{-1/2})$. Hence the ice fraction is still confined to the boundary layer but it is growing in amplitude.

Finally fo larger times, $\tau = \beta^{1/2}\hat{\tau}$, where $\hat{\tau} = O(1)$. Here we expect $f = O(1)$ and expand θ as

$$\theta = 1 + \beta^{-1/2}\hat{\theta} + \ldots \tag{7.37}$$

Hence the system reduces to a set of coupled non-linear equations

$$0 = \frac{\partial^2 \hat{\theta}}{\partial \tilde{x}^2} + \frac{\partial f}{\partial \hat{\tau}}, \tag{7.38}$$

$$\frac{\partial f}{\partial \hat{\tau}} = \Lambda(f-1)\hat{\theta}. \tag{7.39}$$

Subject to

$$\left.\frac{\partial \hat{\theta}}{\partial \tilde{x}}\right|_{\tilde{x}=0} = \mathrm{Bi}, \tag{7.40}$$

$$\left.\hat{\theta}\right|_{\tilde{x}\to 0} = 0, \tag{7.41}$$

and

$$f \sim \hat{\tau}\Lambda^{1/2}\mathrm{Bi}e^{-\Lambda^{1/2}\tilde{x}} \text{ as } \hat{\tau} \to 0_+. \tag{7.42}$$

This last system does not a a closed analytical solution, therefore we change our attention to comparisions of small-time solution to the numerical solution of the full non-linear system.

7.5.2 Comparison

Comparisons between the numerical and small-time asymptotic solutions are given in the following figures.

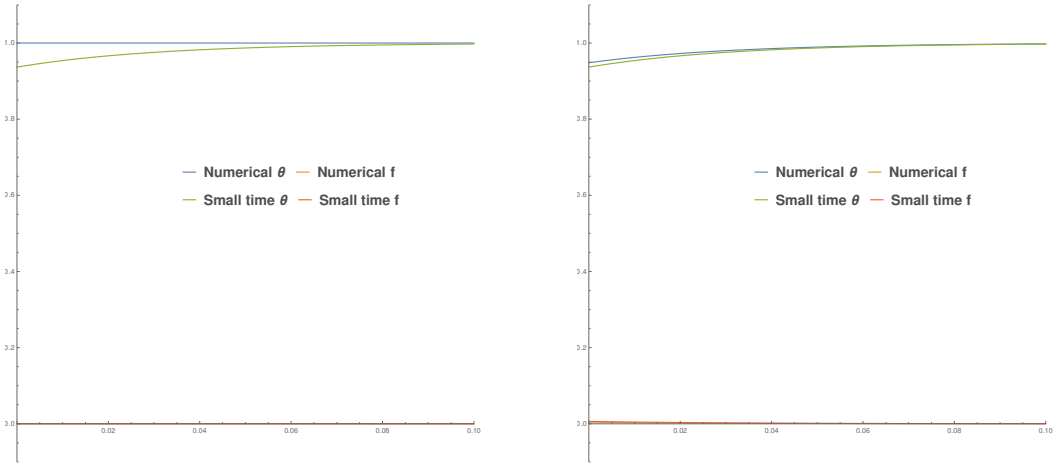

(a) $\tau = 0$ **(b)** $\tau = 0.01$

Figure 7.12: Convergence to steady state solution θ_s.

Figure 7.12 demonstrates that the θ solution indeed converges to a steady-state relatively quickly, whilst the ice fraction remains unchanged.

In figure 7.13 we can see that for a relatively long time the temperature remains in the steady-state and the ice fraction is increasing. During this period there is a reasonable agreement between the small-time approximating and the numerical solutions. However, after $\tau \approx 1$ the temperature becomes unsteady again and the small-time solution starts to break down as shown in figure 7.14.

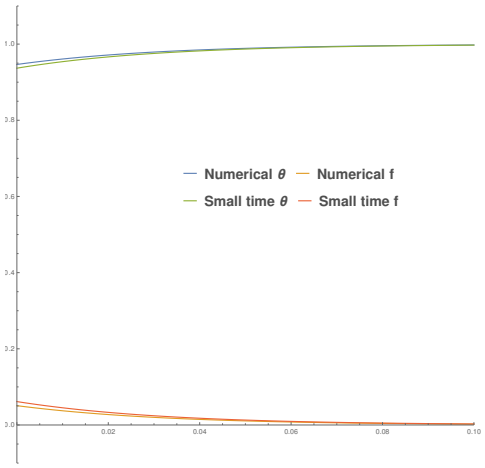

(a) $\tau = 0.1$

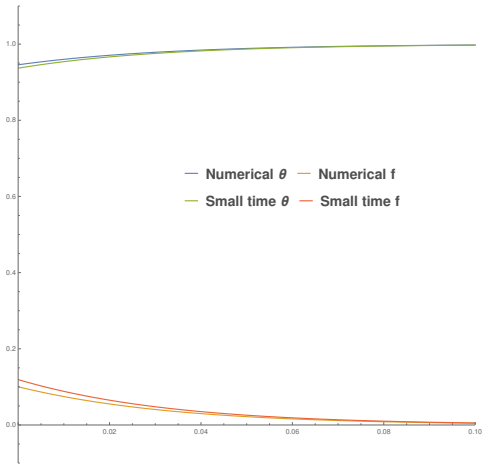

(b) $\tau = 0.2$

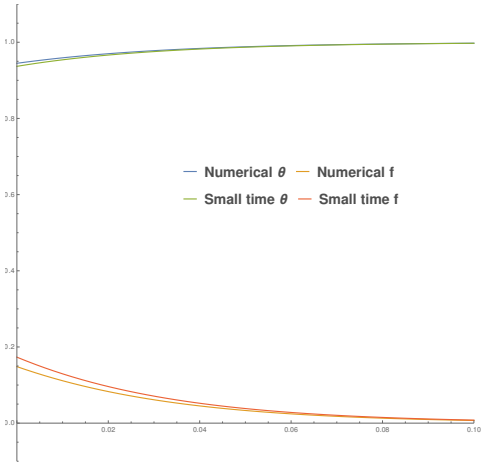

(c) $\tau = 0.3$

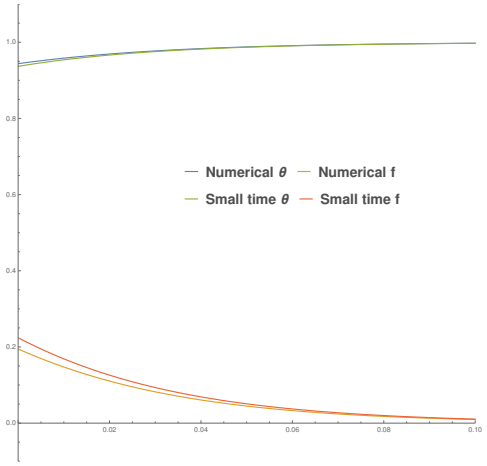

(d) $\tau = 0.4$

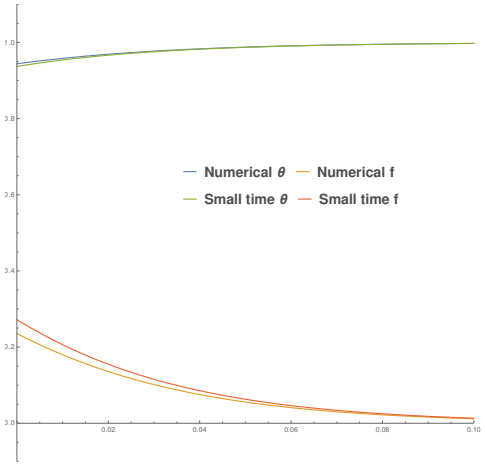

(e) $\tau = 0.5$

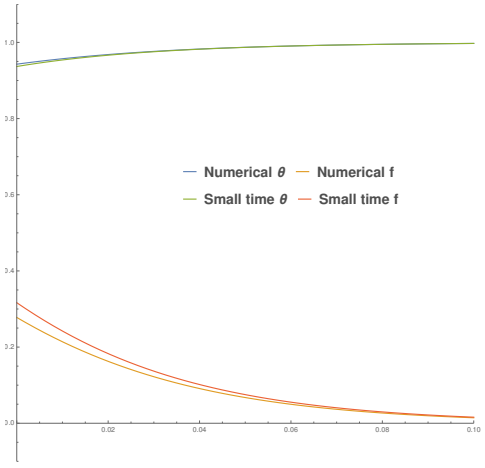

(f) $\tau = 0.6$

Figure 7.13: Progression of the ice fraction, temperature remains unchanged.

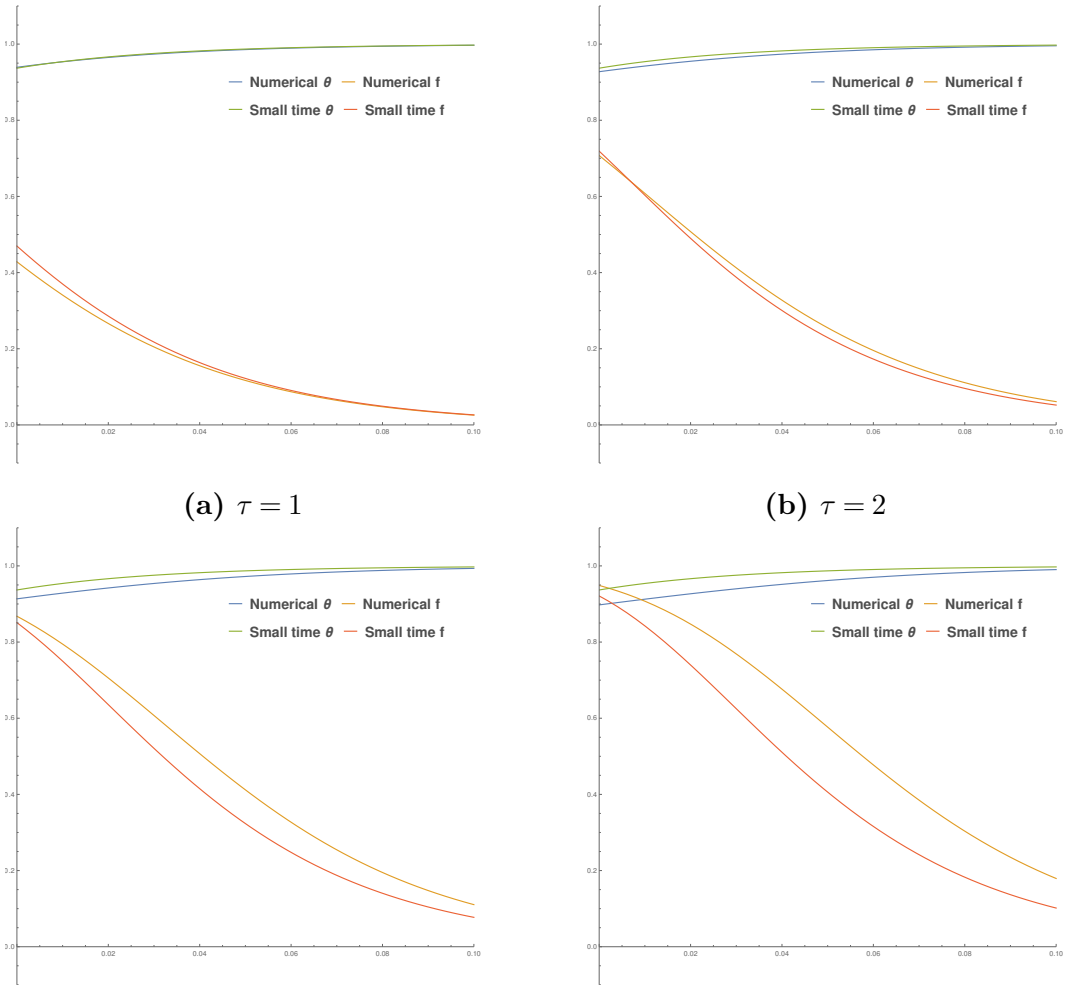

(a) $\tau = 1$ **(b)** $\tau = 2$

(c) $\tau = 3$ **(d)** $\tau = 4$

Figure 7.14: Gradual breaking of the steady-state temperature solution and continuing progression of the ice fraction within the boundary layer.

7.6 Summary

We have presented a new model for solidification scenarios based on modelling freezing as chemical reactions driven by the modified Arrhenius equation.

We have examined the resulting system of PDEs and developed approximate asymptotical solutions valid within a small boundary layer. However, in order to practically implement the current model, one needs to estimate the values of Λ and $\tilde{E}$. One possible approach would involve comparing the chemical model to standard freezing models.

Chapter 8

Discussion and conclusions

We started our discussion with a basic introduction to the principles and methods of freeze-drying. In this work, the first stage of freeze-drying, the freezing stage was modelled as a specific type of free moving boundary problem, the Stefan problem.

Throughout the chapters 2 to 4 we have adopted a level set method coupled with compact finite differencing to solidification scenarios. In chapter 5 we have applied this method to three setting. Firstly, the method we compared to an analytical solution for a simplified problem of freezing of a semi-infinite slab and inward solidification of a cylinder. Then we have developed a simple model of freezing of a single vial, which was further adapted to include the effects of density change.

However, these models have taken the vial in isolation. In order to better understand how the vials inside the freeze-drying chamber can influence each other, we needed to simulate multiple vials at once. This motivated the introduction of a two-stage model in chapter 6.

The two-stage model tried to capture the interaction between the vials during the freeze-drying process. So far, the models used in mathematical modelling of these processes heavily relied on the assumption that the heat transfer inside the vials is radially symmetric. However, we have shown that under certain conditions the "edge effect" caused by the extra heat transfer

contribution from the sides of the freeze-dryer is not only present in the outermost vials but can also penetrate the vials neighbouring them.

However, to fully understand the impact of this on the final product, we would need to simulate all the stages of freeze-drying, rather than just the first one. Also, to better improve the results, we should include different aspects of the freeze-drying chamber into the analysis. These include the metal rail that often surrounds the vials or the glass door of the chamber. Secondly, currently, we are not taking into consideration the heat transfer inside the glass of the vial. It is assumed that this effect can be captured by the heat transfer rate coefficients in the boundary conditions of the setup.

Moreover, the simplistic geometry of the vial that we used throughout this work might not be sufficient to describe the problem accurately. We have also assumed that the vial bottoms are flat and hence they have perfect contact with the shelf they sit on. However, we know that the bottom shape of the vials is often concave, and hence the centre of the vial bottoms can experience lower heat transfer rates compared to the edges.

Finally, we have presented a novel way of looking at solidification scenarios inspired by chemical reactions. We have assumed that the freezing problem could be set up as a chemical reaction driven by a modified Arrhenius equation. We examined the problem asymptotically using the assumption of a large Stefan number parameter. This allowed us to study the system in the boundary layer located in the region of $x = O(\beta^{-1/2})$, where β is a large solidification parameter.

Although this model showed promise, in order to fully implement it, we would also need a procedure of estimating the rest of the parameters. This could be done, for instance, by numerically fitting them so that the whole system would agree with the standard solidification models.

Due to the widespread use and importance, freeze-drying is still an active area of research. In this work, we have demonstrated that some of the modelling assumptions used today might not always be valid, especially for the

vials located near the edge of the freeze-drying chamber. The hope is that better modelling of these vials and understanding of the processes involved would help us to mitigate the resulting heterogeneity of the product and decrease the manufacturing costs as well as the cost related to wastage of the final product.

It is hoped that similar techniques could be applied to the drying stages. This is despite the extra features and complications due to the need to accurately capture the coupled heat and mass transfer as well as modelling escape of water vapour through the dried product.

Appendix A

Two-stage Model Additional Figures

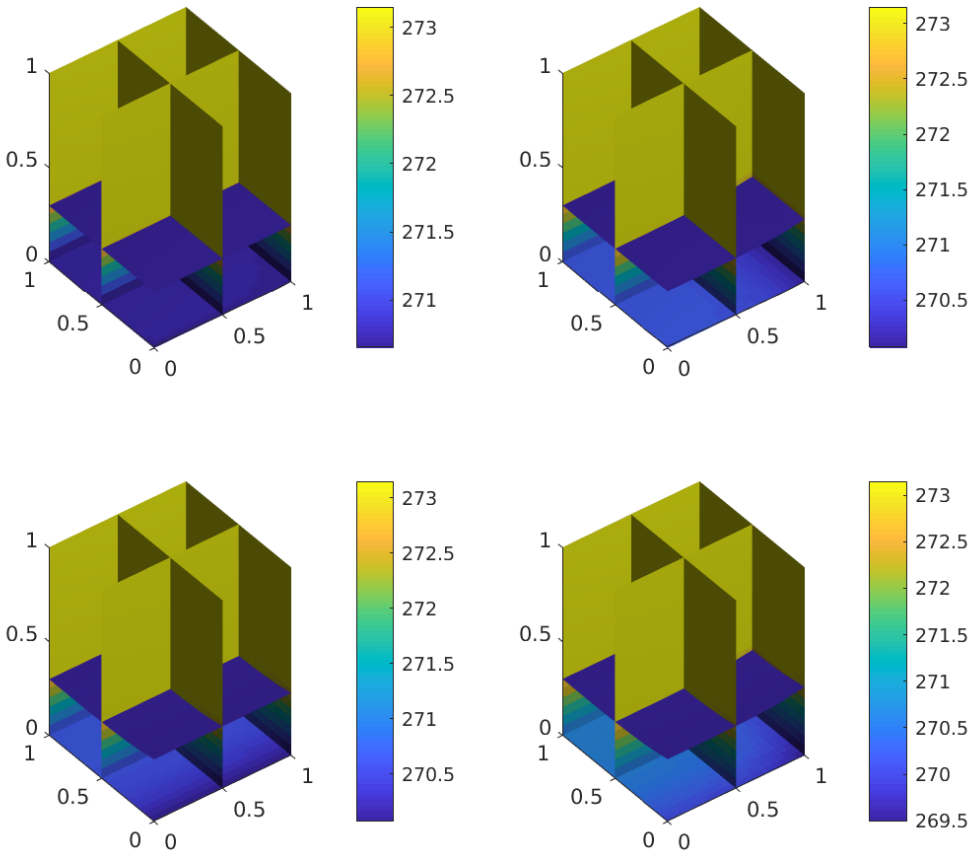

Figure A.1: $k_{shelf} = 0.76, k_{side} = 1, \tau = 2$

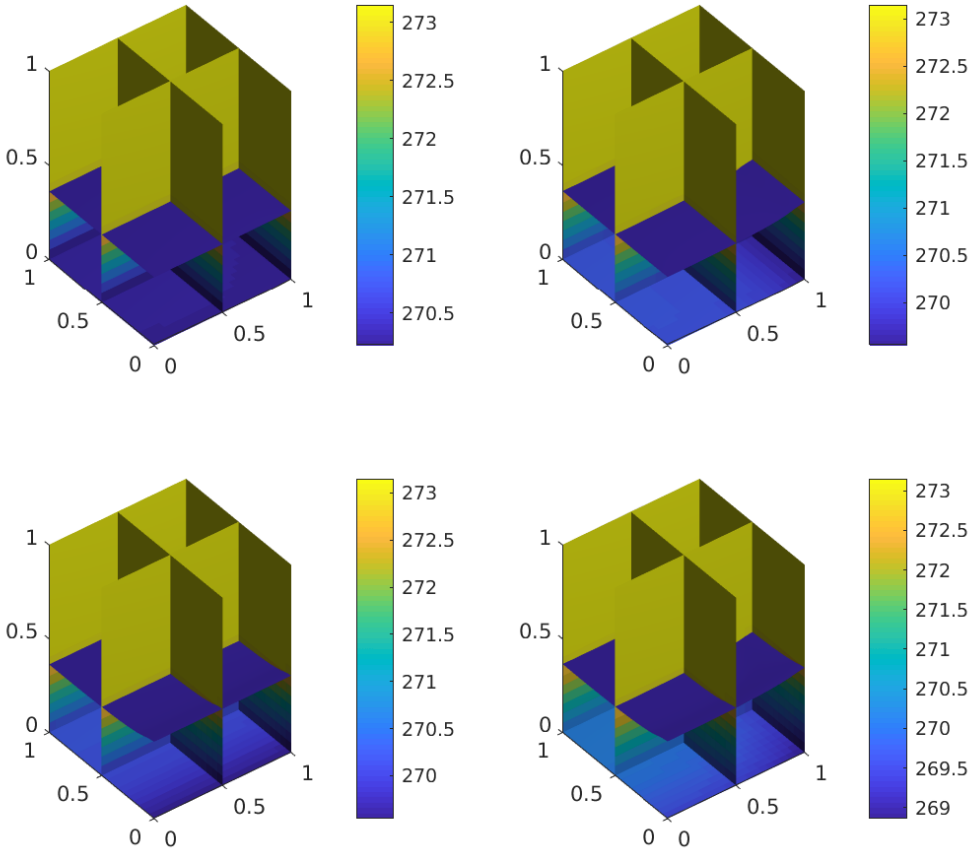

Figure A.2: $k_{shelf} = 0.76, k_{side} = 1, \tau = 3$

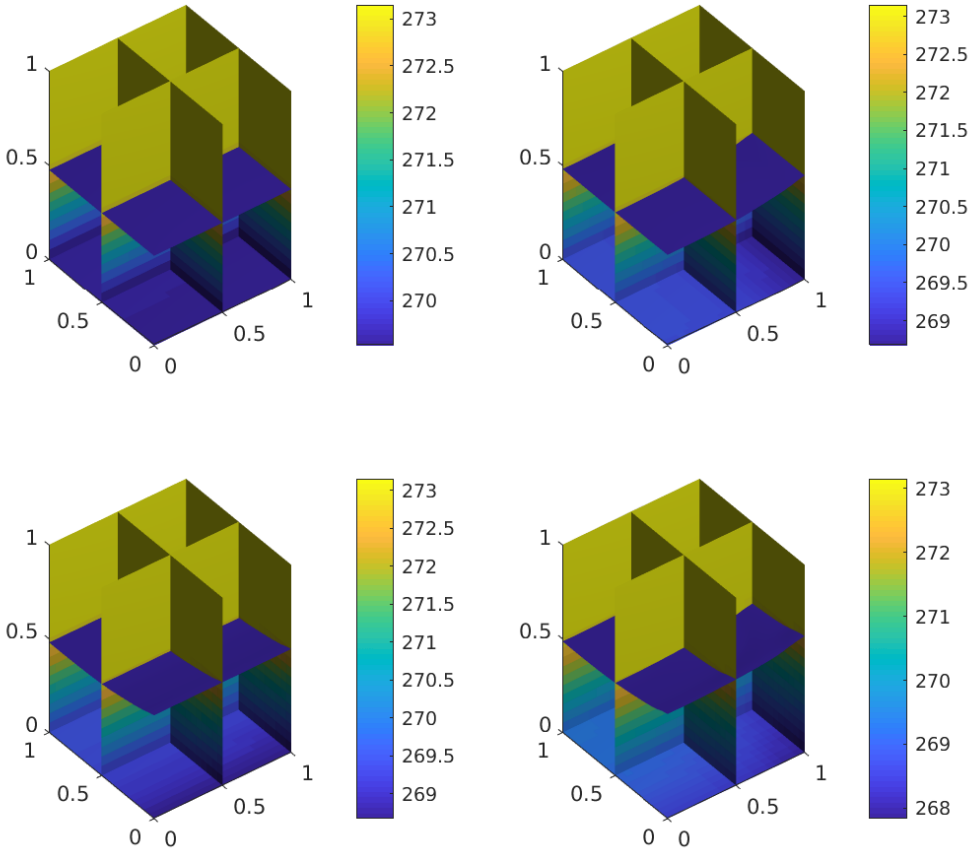

Figure A.3: $k_{shelf} = 0.76, k_{side} = 1, \tau = 5$

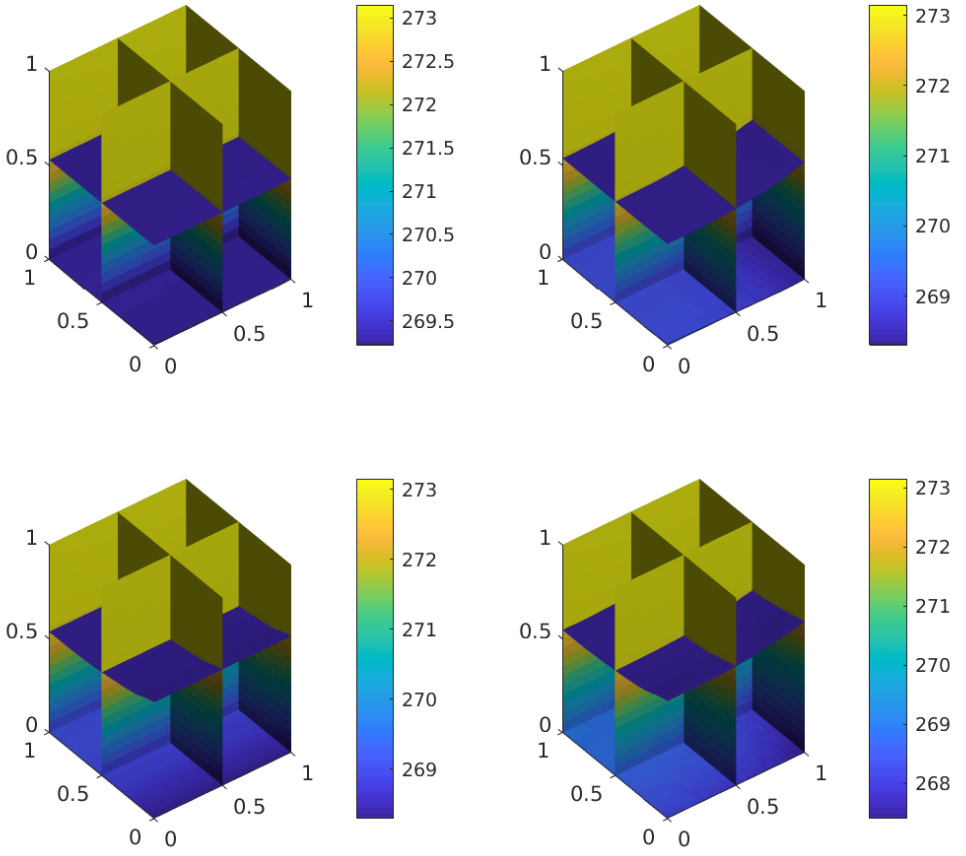

Figure A.4: $k_{shelf} = 0.76, k_{side} = 1, \tau = 6$

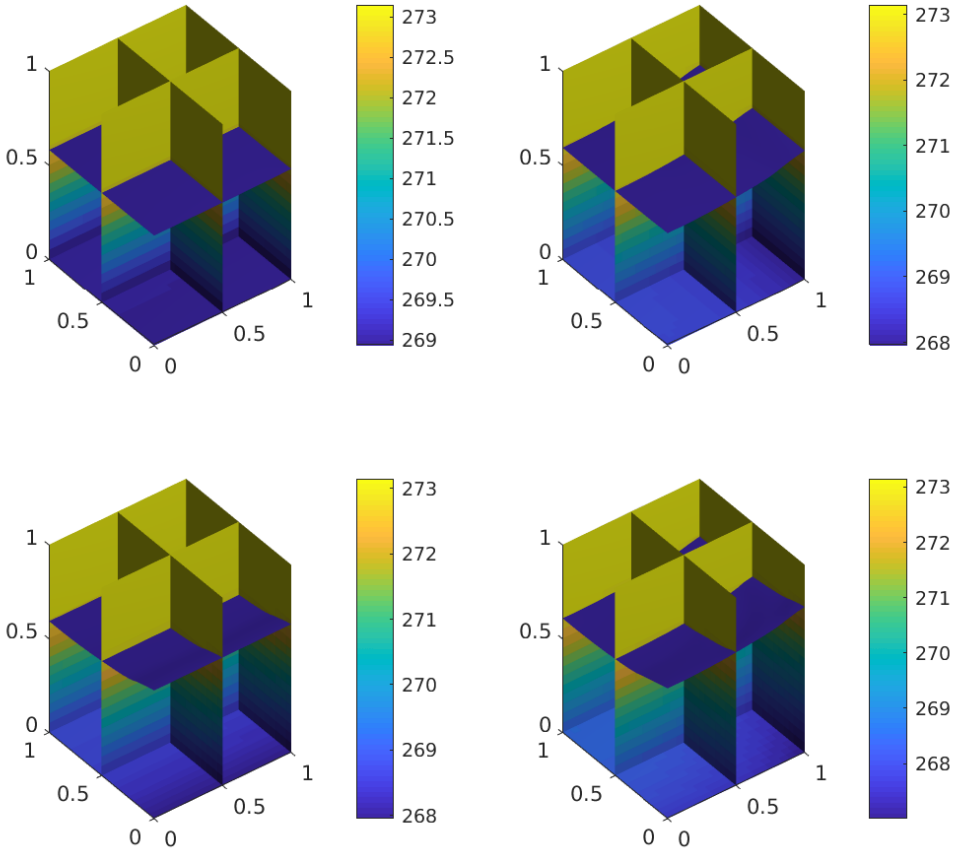

Figure A.5: $k_{shelf} = 0.76, k_{side} = 1, \tau = 7$

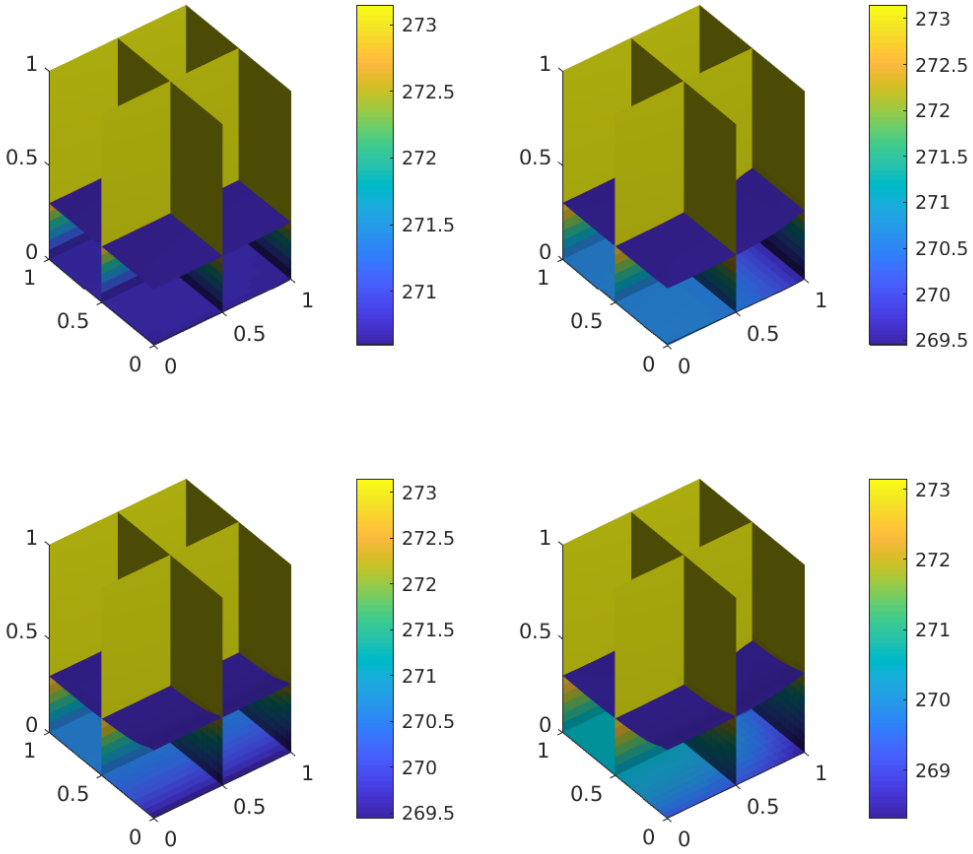

Figure A.6: $k_{shelf} = 0.76, k_{side} = 0.5, \tau = 2$

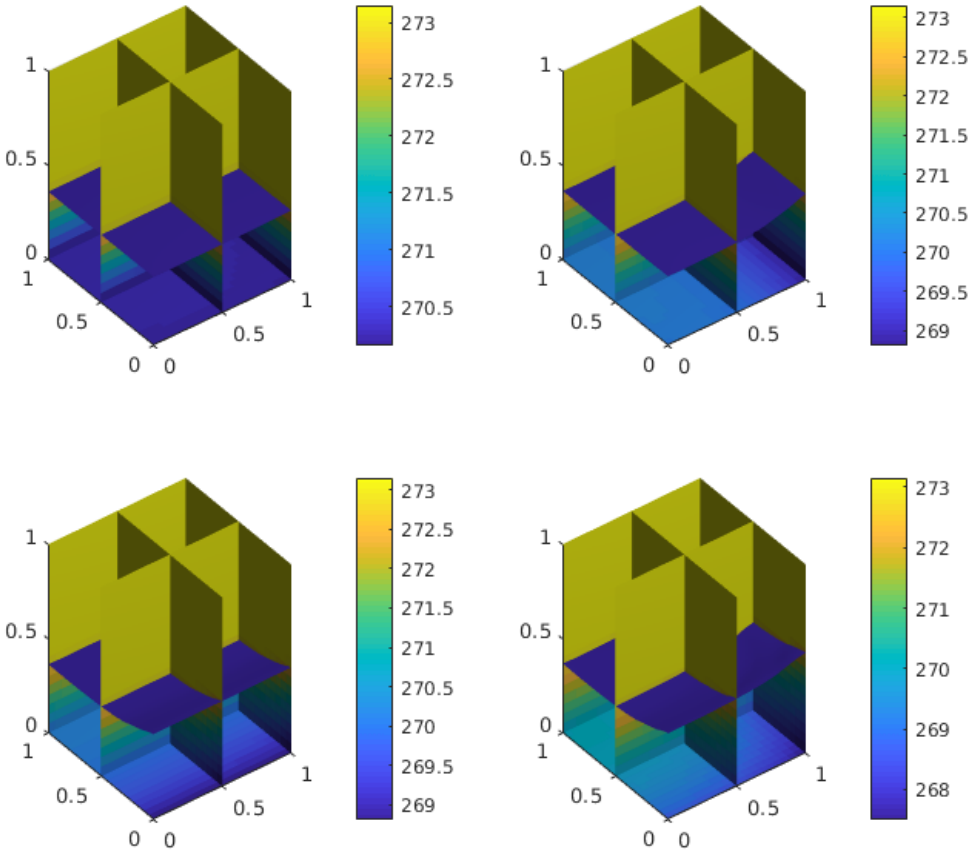

Figure A.7: $k_{shelf} = 0.76, k_{side} = 0.5, \tau = 3$

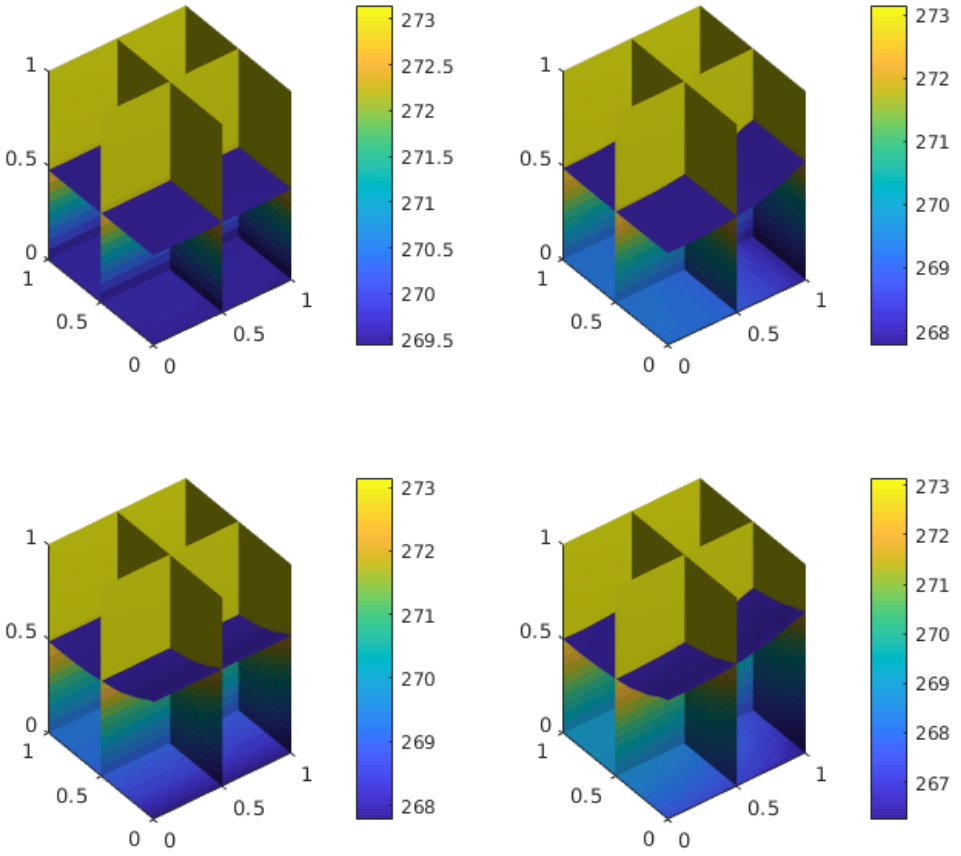

Figure A.8: $k_{shelf} = 0.76, k_{side} = 0.5, \tau = 5$

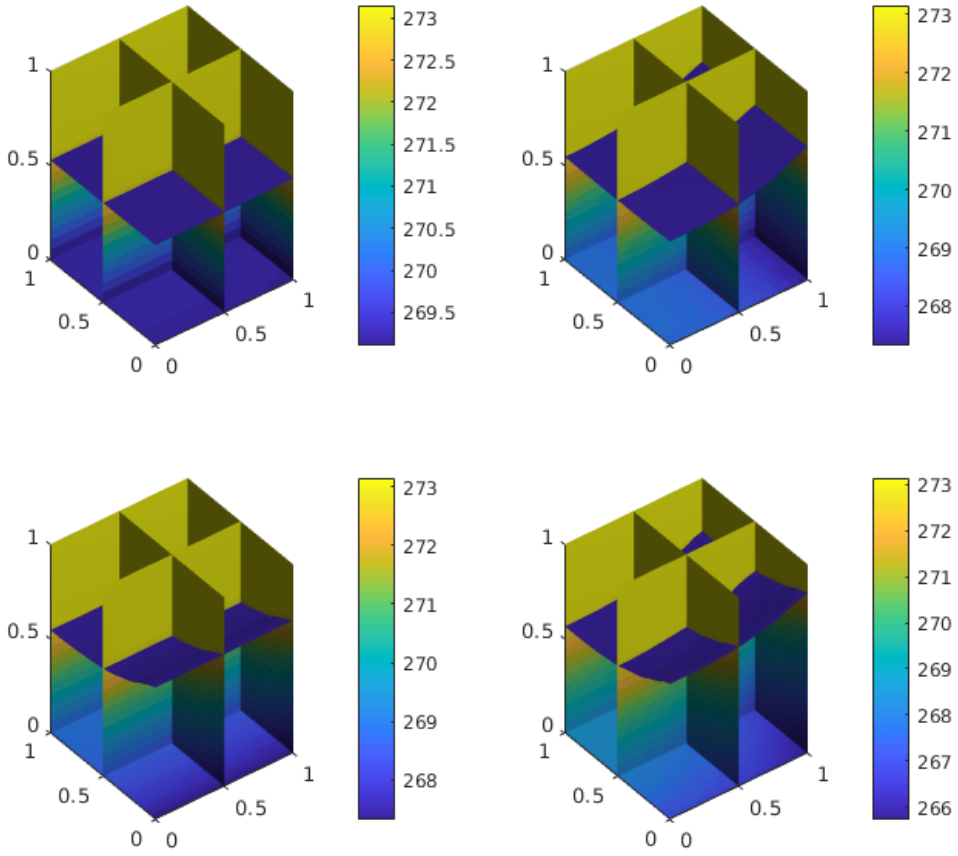

Figure A.9: $k_{shelf} = 0.76, k_{side} = 0.5, \tau = 6$

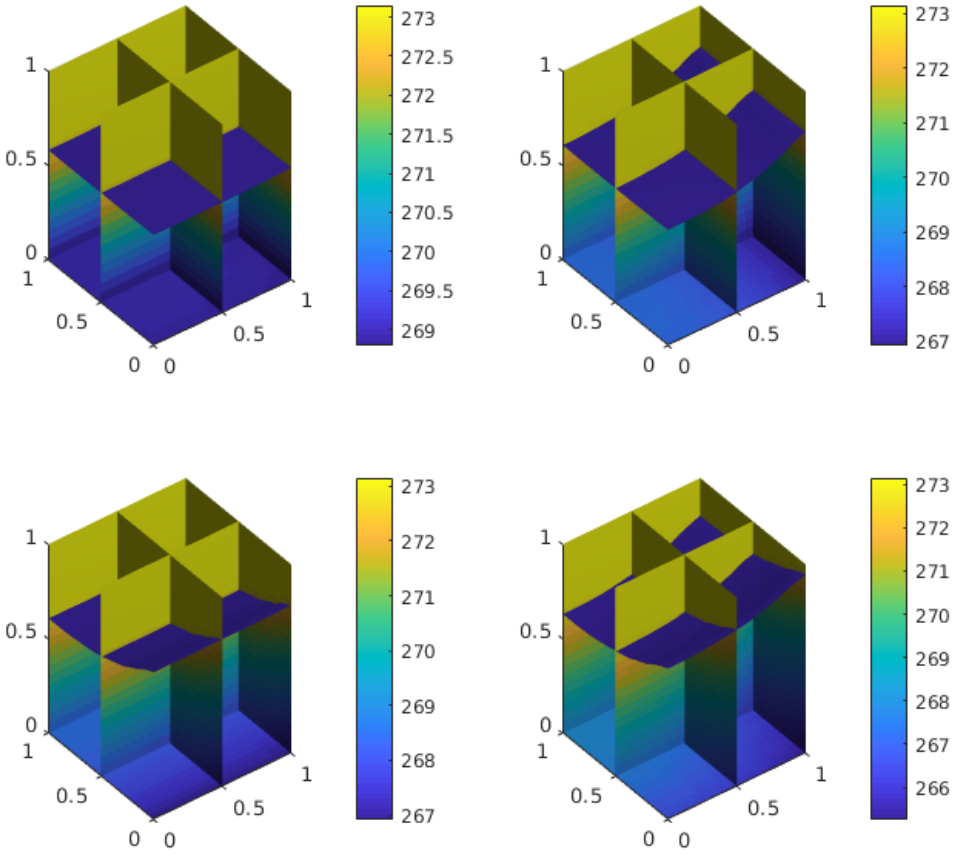

Figure A.10: $k_{shelf} = 0.76, k_{side} = 0.5, \tau = 7$

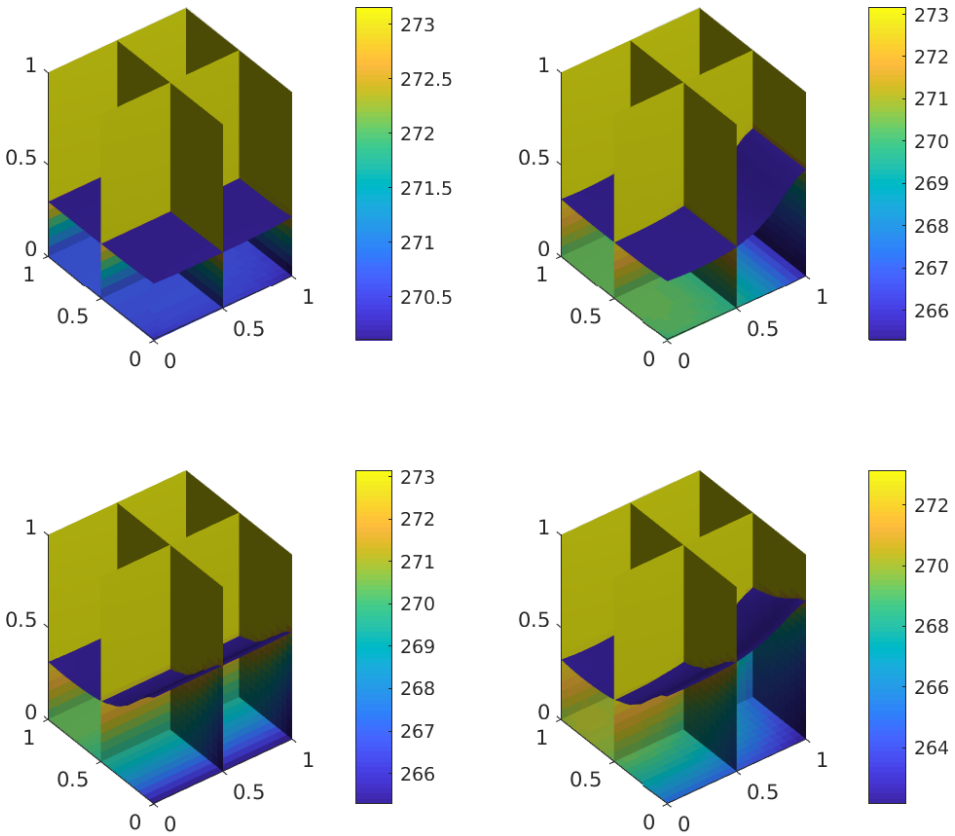

Figure A.11: $k_{shelf} = 0.76, k_{side} = 0.1, \tau = 2$

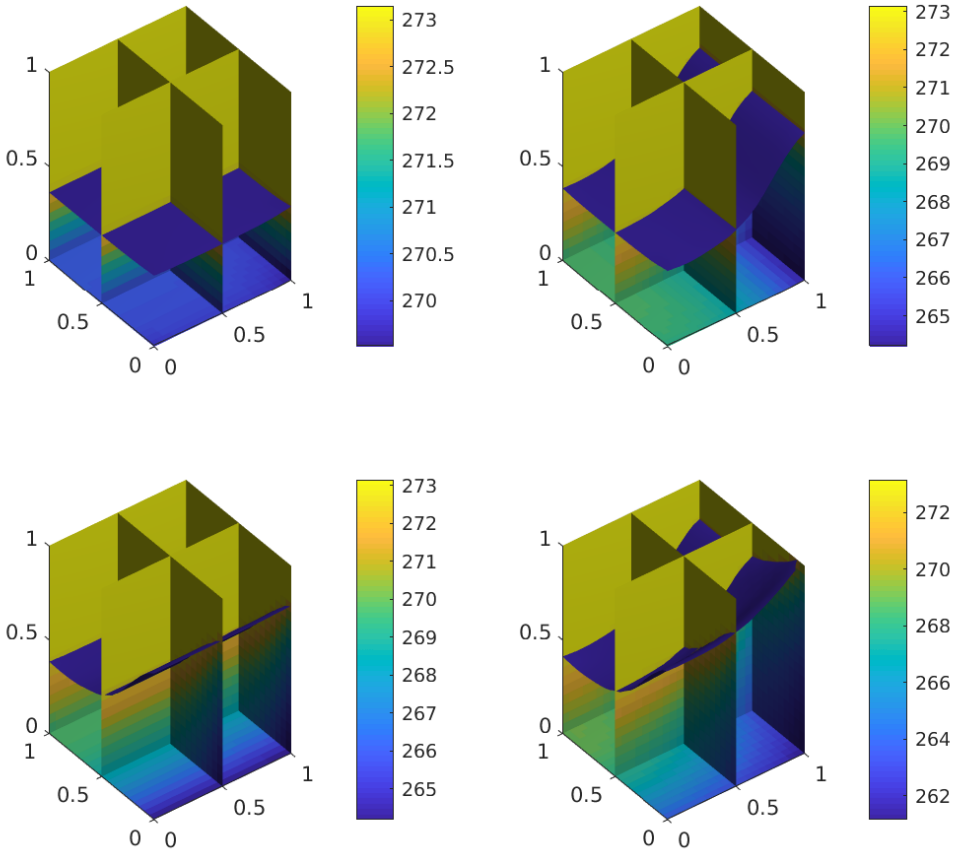

Figure A.12: $k_{shelf} = 0.76, k_{side} = 0.1, \tau = 3$

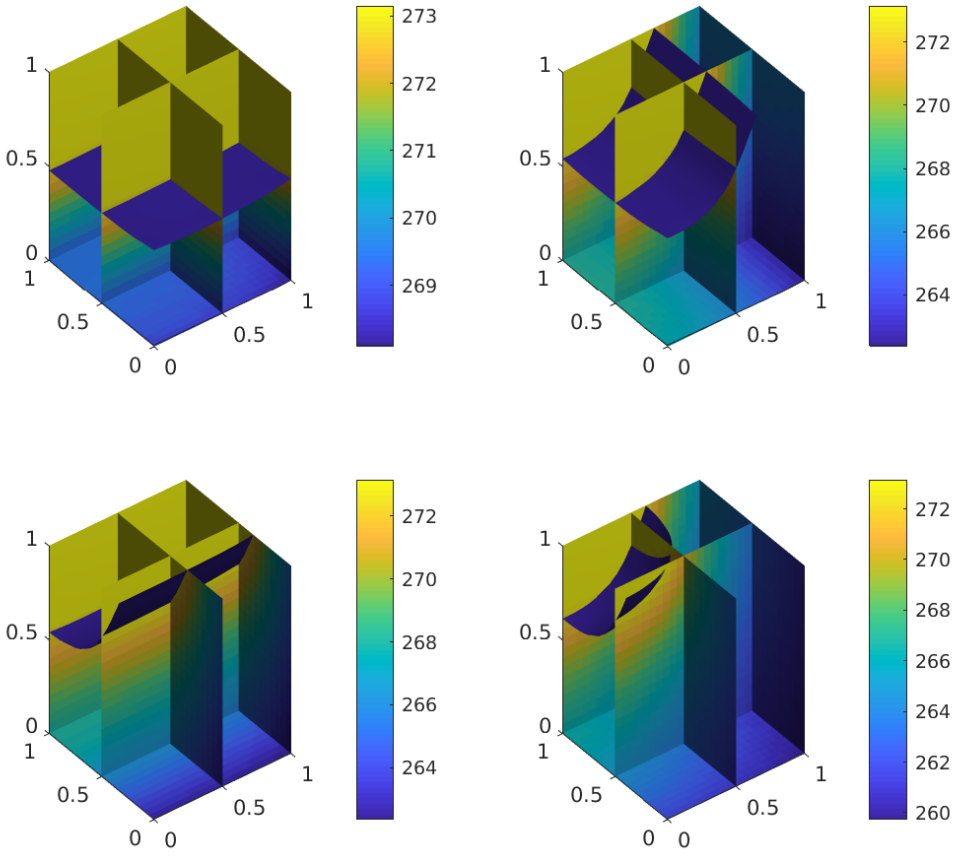

Figure A.13: $k_{shelf} = 0.76, k_{side} = 0.1, \tau = 5$

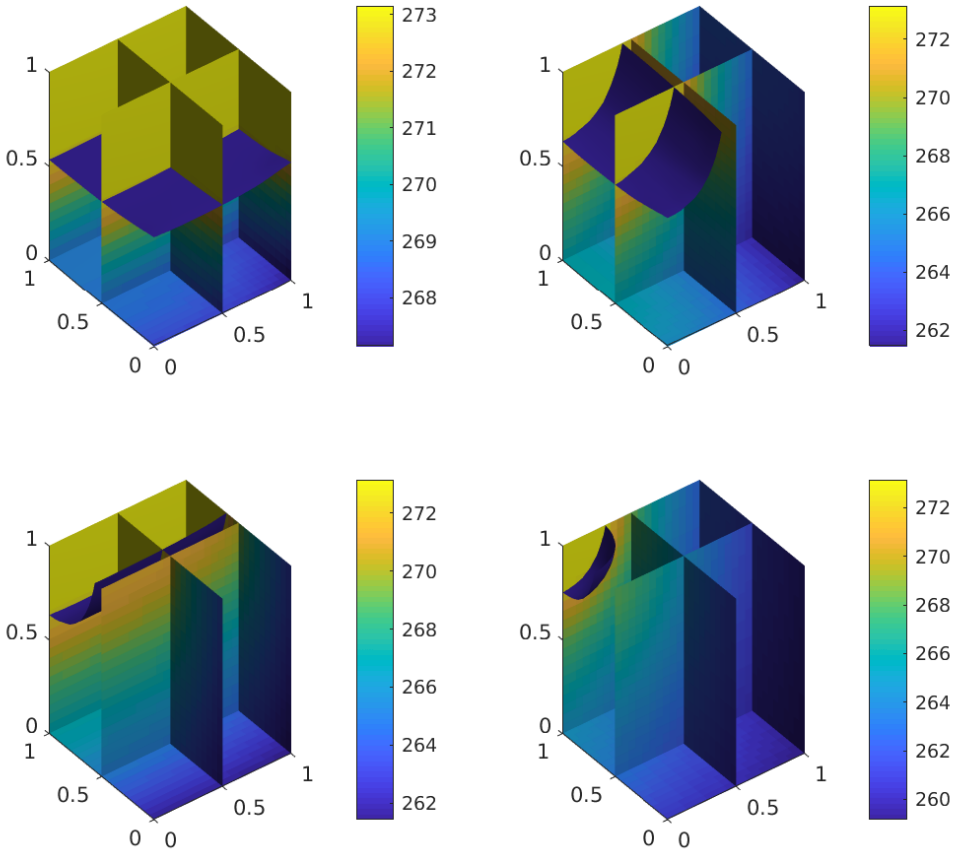

Figure A.14: $k_{shelf} = 0.76, k_{side} = 0.1, \tau = 6$

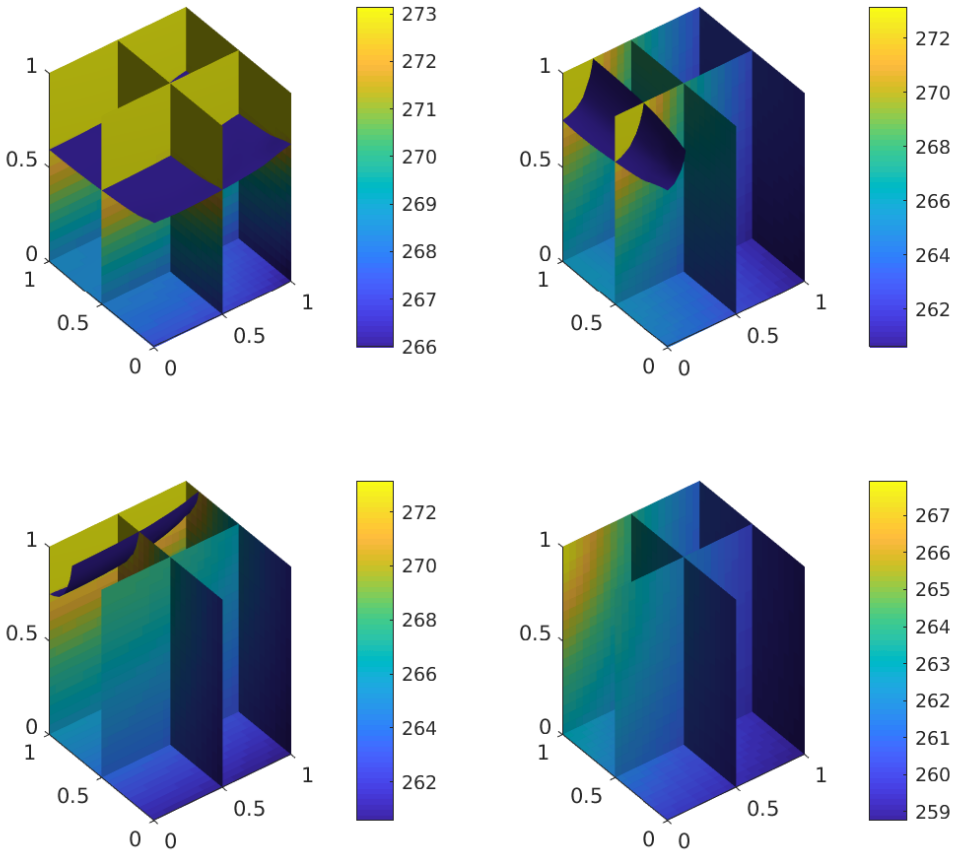

Figure A.15: $k_{shelf} = 0.76, k_{side} = 0.1, \tau = 7$

References

[1] Antonello A Barresi, Sabrina Ghio, Davide Fissore, and Roberto Pisano. Freeze drying of pharmaceutical excipients close to collapse temperature: Influence of the process conditions on process time and product quality. *Drying Technology*, 27(6):805–816, 2009.

[2] Pe L Te Brian. A finite-difference method of high-order accuracy for the solution of three-dimensional transient heat conduction problems. *AIChE Journal*, 7(3):367–370, 1961.

[3] Yiding Cao, Amir Faghri, and Won Soon Chang. A numerical analysis of stefan problems for generalized multi-dimensional phase-change structures using the enthalpy transforming model. *International journal of heat and mass transfer*, 32(7):1289–1298, 1989.

[4] S Chen, B Merriman, S Osher, and P Smereka. A simple level set method for solving stefan problems. *Journal of Computational Physics*, 135(1):8–29, 1997.

[5] David Layne Chopp. Computing minimal surfaces via level set curvature flow. 106(1):77–91, 1991.

[6] S.R. Coriell, G.B. McFadden, W.F. Mitchell, B.T. Murray, J.B. Andrews, and Y. Arikawa. Effect of flow due to density change on eutectic growth. *Journal of Crystal Growth*, 224(1âĂŞ2):145 – 154, 2001.

[7] John Crank. *Free and Moving Boundary Problems*. Oxford University Press, Oxford, 1984.

[8] Jim Douglas. Alternating direction methods for three space variables. *Numerische Mathematik*, 4(1):41–63, 1962.

[9] Jim Douglas and James E Gunn. A general formulation of alternating direction methods. *Numerische Mathematik*, 6(1):428–453, 1964.

[10] Jim Douglas and Henry H Rachford. On the numerical solution of heat conduction problems in two and three space variables. *Transactions of the American mathematical Society*, 82(2):421–439, 1956.

[11] Jim Douglas, Jr. On the numerical integration of $\frac{\partial^2 u}{\partial x^2} + \frac{\partial^2 u}{\partial y^2} = \frac{\partial u}{\partial t}$ by implicit methods. *Journal of the society for industrial and applied mathematics*, 3(1):42–65, 1955.

[12] JR Ehlert and TF Smith. View factors for perpendicular and parallel rectangular plates. *Journal of thermophysics and heat transfer*, 7(1):173–175, 1993.

[13] Felix Franks. Freeze-drying of bioproducts: putting principles into practice. *European Journal of Pharmaceutics and Biopharmaceutics*, 45(3):221–229, 1998.

[14] Arnab Ganguly, Steven L Nail, and Alina Alexeenko. Experimental determination of the key heat transfer mechanisms in pharmaceutical freeze-drying. *Journal of pharmaceutical sciences*, 102(5):1610–1625, 2013.

[15] Cheng Gao and Yansheng Wang. A general formulation of peaceman and rachford adi method for the n-dimensional heat diffusion equation. *International communications in heat and mass transfer*, 23(6):845–854, 1996.

[16] Guang-Hua Gao and Hai-Wei Sun. Three-point combined compact alternating direction implicit difference schemes for two-dimensional time-fractional advection-diffusion equations. *Communications in Computational Physics*, 17(2):487âĂŞ509, 2015.

[17] R Geidobler and G Winter. Controlled ice nucleation in the field of freeze-drying: fundamentals and technology review. *European Journal of Pharmaceutics and Biopharmaceutics*, 85(2):214–222, 2013.

[18] Ki-Young Hwang. Effects of density change and natural convection on the solidification process of a pure metal. *Journal of Materials Processing Technology*, 71(3):466 – 476, 1997.

[19] Nikolaj Nikolaevič Janenko. *The method of fractional steps*. Springer, 1971.

[20] Nikolaj Nikolaevič Janenko. *The method of fractional steps*. Springer, 1971.

[21] Guang-Shan Jiang and Danping Peng. Weighted eno schemes for hamilton–jacobi equations. *SIAM Journal on Scientific computing*, 21(6):2126–2143, 2000.

[22] Guang-Shan Jiang and Chi-Wang Shu. Efficient implementation of weighted eno schemes. *Journal of computational physics*, 126(1):202–228, 1996.

[23] Sandip Khairnar, Rajesh Kini, Mallinath Harwalkar, SR Chaudhari, et al. A review on freeze drying process of pharmaceuticals. *International Journal of Research in Pharmacy & Science*, 4(1), 2014.

[24] Alex K Konstantinidis, Wei Kuu, Lori Otten, Steven L Nail, and Robert R Sever. Controlled nucleation in freeze-drying: Effects on pore size in the dried product layer, mass transfer resistance, and primary drying rate. *Journal of pharmaceutical sciences*, 100(8):3453–3470, 2011.

[25] Y. P. Lee and S. T. Ro. Approximate determination of the shape of solidified materials with either shrinkage or expansion. *KSME Journal*, 9(4):502–505, 1995.

[26] A. I. Liapis and R. Bruttini. Freeze-drying of pharmaceutical crystalline and amorphous solutes in vials: Dynamic multi-dimensional models of the primary and secondary drying stages and qualitative features of the moving interface. *Drying Technology*, 13(1-2):43–72, 1995.

[27] Xu-Dong Liu, Stanley Osher, and Tony Chan. Weighted essentially non-oscillatory schemes. *Journal of computational physics*, 115(1):200–212, 1994.

[28] Ravi Malladi, James A Sethian, and Baba C Vemuri. Evolutionary fronts for topology-independent shape modeling and recovery. In *European conference on Computer vision*, pages 1–13. Springer, 1994.

[29] G.B. McFadden and S.R. Coriell. The effect of fluid flow due to the crystal-melt density change on the growth of a parabolic isothermal dendrite. *Journal of Crystal Growth*, 74(3):507 – 512, 1986.

[30] Andrew Ronald Mitchell and David Francis Griffiths. *The finite difference method in partial differential equations*. Number BOOK. John Wiley, 1980.

[31] Michael F Modest. *Radiative heat transfer*. Academic press, 2013.

[32] Kyuya Nakagawa, Aurélie Hottot, Séverine Vessot, and Julien Andrieu. Influence of controlled nucleation by ultrasounds on ice morphology of frozen formulations for pharmaceutical proteins freeze-drying. *Chemical Engineering and Processing: Process Intensification*, 45(9):783–791, 2006.

[33] Stanley Osher. A level set formulation for the solution of the dirichlet problem for hamilton–jacobi equations. *SIAM Journal on Mathematical Analysis*, 24(5):1145–1152, 1993.

[34] Stanley Osher and Ronald Fedkiw. *Level set methods and dynamic implicit surfaces*, volume 153. Springer Science & Business Media, 2006.

[35] Stanley Osher and James A Sethian. Fronts propagating with curvature-dependent speed: algorithms based on hamilton-jacobi formulations. *Journal of computational physics*, 79(1):12–49, 1988.

[36] Sajal M Patel, Chandan Bhugra, and Michael J Pikal. Reduced pressure ice fog technique for controlled ice nucleation during freeze-drying. *Aaps Pharmscitech*, 10(4):1406, 2009.

[37] Donald W Peaceman and Henry H Rachford, Jr. The numerical solution of parabolic and elliptic differential equations. *Journal of the Society for industrial and Applied Mathematics*, 3(1):28–41, 1955.

[38] Michael J Pikal and Saroj Shah. The collapse temperature in freeze drying: Dependence on measurement methodology and rate of water removal from the glassy phase. *International Journal of Pharmaceutics*, 62(2-3):165–186, 1990.

[39] G Poots. On the application of integral-methods to the solution of problems involving the solidification of liquids initially at fusion temperature. *International Journal of Heat and Mass Transfer*, 5(6):525–531, 1962.

[40] Dejan S Pržić, Nenad Lj Ružić, and Slobodan D Petrović. Lyophilization: The process and industrial use. *Hemijska industrija*, 58(12):552–562, 2004.

[41] M. Raessi and J. Mostaghimi. Three-dimensional modelling of density variation due to phase change in complex free surface flows. *Numerical Heat Transfer, Part B: Fundamentals*, 47(6):507–531, 2005.

[42] Kirby Rajeev and Subir Das. A numerical study for inward solidification of a liquid contained in cylindrical and spherical vessel. *Thermal Science*, 14(2):365–372, 2010.

[43] Shailaja Rambhatla and Michael J Pikal. Heat and mass transfer scale-up issues during freeze-drying, i: atypical radiation and the edge vial effect. *Aaps Pharmscitech*, 4(2):22–31, 2003.

[44] Valeria Rasetto, Daniele L Marchisio, Davide Fissore, and Antonello A Barresi. On the use of a dual-scale model to improve understanding of a pharmaceutical freeze-drying process. *Journal of pharmaceutical sciences*, 99(10):4337–4350, 2010.

[45] DS Riley, FT Smith, and G Poots. The inward solidification of spheres and circular cylinders. *International Journal of Heat and Mass Transfer*, 17(12):1507–1516, 1974.

[46] Mónica Rosa, João M Tiago, Satish K Singh, Vítor Geraldes, and Miguel A Rodrigues. Improving heat transfer at the bottom of vials for consistent freeze drying with unidirectional structured ice. *AAPS PharmSciTech*, 17(5):1049–1059, 2016.

[47] Elisabeth Rouy and Agnès Tourin. A viscosity solutions approach to shape-from-shading. *SIAM Journal on Numerical Analysis*, 29(3):867–884, 1992.

[48] Stefan Schneid and Henning Gieseler. Evaluation of a new wireless temperature remote interrogation system (tempris) to measure product temperature during freeze drying. *Aaps PharmSciTech*, 9(3):729–739, 2008.

[49] Bernadette Scutellà, Artemio Plana-Fattori, Stéphanie Passot, E Bourlès, Fernanda Fonseca, Denis Flick, and Ioan-Cristian Trelea. 3d mathematical modelling to understand atypical heat transfer observed in vial freeze-drying. *Applied Thermal Engineering*, 126:226–236, 2017.

[50] James A Sethian and Peter Smereka. Level set methods for fluid interfaces. *Annual review of fluid mechanics*, 35(1):341–372, 2003.

[51] James A Sethian and John Straint. Crystal growth and dendritic solidification. *Journal of Computational Physics*, 98(2):231–253, 1992.

[52] James Albert Sethian. *Level set methods and fast marching methods: evolving interfaces in computational geometry, fluid mechanics, computer vision, and materials science*, volume 3. Cambridge university press, 1999.

[53] P. Sheehan and A. I. Liapis. Modeling of the primary and secondary drying stages of the freeze drying of pharmaceutical products in vials: Numerical results obtained from the solution of a dynamic and spatially multi-dimensional lyophilization model for different operational policies. *Biotechnology and Bioengineering*, 60(6):712–728, 1998.

[54] Chi-Wang Shu and Stanley Osher. Efficient implementation of essentially non-oscillatory shock-capturing schemes. *Journal of computational physics*, 77(2):439–471, 1988.

[55] Soham Shukla. Freeze drying process: A review. *International journal of pharmaceutical sciences and research*, 2(12):3061, 2011.

[56] Ying Sun and Christoph Beckermann. Phase-field simulation of solidification with density change. *ASME International Mechanical Engineering Congress and Exposition,Heat Transfer*, 3:519–525, 2004.

[57] Mark Sussman, Peter Smereka, and Stanley Osher. A level set approach for computing solutions to incompressible two-phase flow. *Journal of Computational physics*, 114(1):146–159, 1994.

[58] Liapis A. I. Marchello J. M. Tang, M. M. A multi-dimensional model describing the lyophilization of a pharmaceutical product in a vial. *In: A. S.Mujumadar (ed.), Proceedings of the 5th International Drying Symposium*, 1:57–65, 1986.

[59] Xiaolin Charlie Tang and Michael J Pikal. Design of freeze-drying processes for pharmaceuticals: practical advice. *Pharmaceutical research*, 21(2):191–200, 2004.

[60] L. N. TAO. On solidification problems including the density jump at the moving boundary. *The Quarterly Journal of Mechanics and Applied Mathematics*, 32(2):175, 1979.

[61] Luh C Tao. Generalized numerical solutions of freezing a saturated liquid in cylinders and spheres. *AIChE Journal*, 13(1):165–169, 1967.

[62] Domingo A. Tarzia. Exact solution for a stefan problem with convective boundary condition and density jump. *PAMM*, 7(1):1040307–1040308, 2007.

[63] James William Thomas. *Numerical partial differential equations: finite difference methods*, volume 22. Springer Science & Business Media, 2013.

[64] M Tziannaros and FT Smith. Numerical and analytical study of bladder-collapse flow. *International Journal of Differential Equations*, 2012, 2012.

[65] Marios Tziannaros, Stephen E Glavin, and Frank T Smith. Three-dimensional effects in the lower urinary tract. *The IMA Journal of Applied Mathematics*, 78(4):729–749, 2013.

[66] Salvatore A Velardi and Antonello A Barresi. Development of simplified models for the freeze-drying process and investigation of the optimal operating conditions. *Chemical Engineering Research and Design*, 86(1):9–22, 2008.

[67] VR Voller and M Cross. Estimating the solidification/melting times of cylindrically symmetric regions. *International Journal of Heat and Mass Transfer*, 24(9):1457–1462, 1981.

[68] Pengde Wang and Chengming Huang. Split-step alternating direction implicit difference scheme for the fractional schrödinger equation in two

dimensions. *Computers & Mathematics with Applications*, 71(5):1114–1128, 2016.

[69] Jennifer Zhao, Weizhong Dai, and Tianchan Niu. Fourth-order compact schemes of a heat conduction problem with neumann boundary conditions. *Numerical Methods for Partial Differential Equations: An International Journal*, 23(5):949–959, 2007.

[70] Jennifer Zhao, Weizhong Dai, and Suyang Zhang. Fourth-order compact schemes for solving multidimensional heat problems with neumann boundary conditions. *Numerical Methods for Partial Differential Equations: An International Journal*, 24(1):165–178, 2008.